The Corrosion of Ni-Cr-Mo Alloys in Aprotic Organic Solvents

PhD Dissertation

Presented to

The Faculty of The School of Engineering and Applied Science

University of Virginia

In Partial Fulfillment

Of the Requirements for the Degree of

Doctor of Philosophy in Materials Science and Engineering

By

Pedro Atz Dick

Date:

May 20th, 2022

Members of the doctoral committee:

Name	**Role**	**Department**
Dr. Elizabeth J. Opila	Committee Chair	Materials Science and Engineering
Dr. Robert G. Kelly	Dissertation Advisor	Materials Science and Engineering
Dr. John R. Scully	Committee Member	Materials Science and Engineering
Dr. Giovanni Zangari	Committee Member	Materials Science and Engineering
Dr. Gary Koenig	Committee Member	Chemical Engineering

Abstract

The synthesis of chemicals and pharmaceuticals often requires a series of intermediate steps involving reactions in aprotic organic solvents. Many of these solutions can be aggressive towards the metallic materials that constitute the reaction vessels used, so often corrosion-resistant alloys of the Ni-Cr-Mo family are employed. Ni-Cr-Mo alloys are known to exhibit outstanding corrosion resistance in reducing and oxidizing aqueous solutions because of their passive oxide film. However, the application of passive alloys in non-aqueous solvents raises additional concerns due to: i) limited availability of passivating species; ii) different behavior of aggressive halides and acids as a result of the physicochemical properties of the solvent. Due to the scarcity of data on corrosion in organic solvents, the selection of materials for such applications is often based on the literature on aqueous corrosion. The aim of this work is to investigate the corrosion of Ni-Cr-Mo alloys in aprotic organic solvents and to explain the effect of variables such as solvent chemical properties, residual water, alloy chemical composition, and the presence of chlorides and organic oxidants. Ultimately, this work will provide fundamental understanding of the passivity of Ni-based alloys in organic solvents, assisting the selection of materials for non-aqueous applications.

Table of Contents

List of Figures

List of Tables

Chapter 1 : Introduction and scope of work

Introduction

Passivity of corrosion-resistant alloys

A variety of processes in the chemical and pharmaceutical industries take place in environments that are aggressive towards most engineering materials. To avoid degradation of the vessels and tools exposed to such environments and to minimize contamination of the products, often corrosion-resistant alloys are utilized. Corrosion-resistant alloy (CRA) is a designation used for a wide range of nickel-based solid solution alloys that present higher corrosion resistance than most stainless steels. Because nickel can be heavily alloyed, large amounts of elements can be dissolved into nickel to tailor the alloy to a specific application, while keeping a face-centered cubic structure [1]. Ni-Mo alloys (Hastelloy B family) can withstand highly reducing solutions – solutions where the hydrogen evolution reaction (HER) is the main cathodic reaction – such as concentrated HCl. However, Ni-Mo alloys have poor corrosion resistance in oxidizing solutions – solutions with oxidizing species of higher potential than HER. In that case, Ni-Cr-Mo alloys (Hastelloy C family) are preferred due to their ability to form a passive Cr-rich oxide layer that protects the bulk from oxidizing species. Amongst the alloys in the Hastelloy C family, Hastelloy C-22 (59Ni-22Cr-13Mo-3W-3Fe) is one of the most widely used, due to its low corrosion rate in a wide range of oxidizing and reducing solutions as a result of its equilibrated concentration of Cr and Mo [2].

Many authors have studied the nature of the passive film that grants Ni-Cr-Mo alloys their remarkable corrosion resistance, pointing to a synergistic action of Cr and Mo in enhancing passivity. It has been shown that a higher concentration of Cr enables the formation of a Cr-rich inner oxide layer that acts as a barrier. The exact effect of Mo is not so well understood. Some studies have reported that Mo preferentially locates in surface defects, slowing anodic dissolution because of its higher metal-metal bond strength [3]. Others proposed that active sites are rapidly covered with Mo oxy-hydroxides, inhibiting localized corrosion [4]. It has also been hypothesized that a layer of MoO_4^{2-} is formed at the outer part of the passive film, forming a cation selective layer and protecting the inner regions from aggressive anions such as Cl^- [5]. The addition of W to Ni-Cr-Mo alloys has similar effects as addition of Mo – W is also reported to segregate to outer regions of the oxide layer and inhibit localized corrosion [6]. More recent studies have presented additional positive effects of Mo and W on the mechanism of passivation [7].

The formation and preservation of a passive oxide layer is fundamental for the maintenance of low corrosion rates in Ni-Cr-Mo alloys. Passivation is believed to take place initially by formation of adsorbed hydrated complexes on the surface of the metal, which enable the formation of a hydroxide phase that deprotonates to form an insoluble surface oxide film [8]. The passive layer is a product of the reaction of the alloy with the corrosive environment and, thus, depends on the composition of both. Halide anions such as Cl^- and F^- are known to cause degradation of the passive oxide, although the exact mechanism is still debated. Water and hydroxide anion (OH^-), on the other hand, are important reactants in passivation and repassivation processes, which is the reason why application of passive alloys in nonaqueous solutions can be problematic.

Properties of organic solvents

The influence of the solvent in which a reaction takes place is sometimes disregarded. However, solvents can vary greatly in physical and chemical properties, drastically affecting reactions. One of the important physical properties of the solvent is its polarity, which is correlated to the solvent's relative permittivity, ε_r. If the ε_r of a solvent is high, it weakens the electrostatic force between two separate charges, and the solvent is more polar. Solvents of high ε_r have a higher chance of dissolving an electrolyte and are, thus, preferred in electrochemical measurements. Among other important chemical properties of a solvent are its acidity and its basicity. Acidity and basicity can be measured by the experimental scales of acceptor number (AN) and donor number (DN), respectively [9]. The lower the AN, the less acidic the solvent is, which means it is a weak proton donor, a weak hydrogen bond donor, and it solvates weakly to small anions (Cl^-, F^-, OH^-, etc.). The lower the DN, the less basic the solvent is, which means it is a weak proton acceptor, a weak hydrogen bond acceptor and it solvates weakly small cations (K^+, Na^+, etc.). Table 1.1 shows the ε_r, AN and DN for a series of solvents. The tendency of a solvent to solvate a species is described by its Gibbs free energy of solvation. As an example, Figure 1.1 shows that there is a first order relation between the Gibbs free energy of solvation for Cl^- and the AN of the solvent – the lower the AN of a solvent is, the higher is the Gibbs free energy of solvation for Cl^-.

Water has high ε_r and moderate acidity and basicity. Thus, in water, many cations and anions are solvated and many electrolytes are highly soluble. However, because water tends to form three-dimensional networks (as a result of its strong hydrogen bonding), large molecules and ions are often difficult to dissolve. Therefore, aprotic dipolar solvents (high ε_r, low AN) are frequently used in the chemical industry, because they are nonstructured and can dissolve large, hydrophobic molecules and ions. A popular example of that class of solvents is acetonitrile (ACN). ACN is a dipolar aprotic protophobic (high ε_r, low AN, low DN) solvent, which means it is a polar solvent of weak acidity and weak basicity.

Table 1.1: Properties of solvents of electrochemical interest [9].

Solvent[a]	*DN*	*AN*	pK_{SH}	ε_r	Solvent	*DN*	*AN*	pK_{SH}	ε_r
(48) 1,2-Dichloroethane (DCE)	0	16.7		10.4	(6) Methanol (MeOH)	(19)	41.3	17.2	32.7
(42) Hexane	(0)	0.0		1.88	(3) Formic acid	(19)	83.6	6.2	58.5_{16}
(43) Benzene	0.1	8.2		2.27	(13) Tetrahydrofuran (THF)	20.0	8.0		7.6
(45) Nitromethane (NM)	2.7	20.5		36.7	(4) Acetic acid (HOAc)	(20)	52.9	14.45	6.2
(46) Nitrobenzene (NB)	4.4	14.8		34.8	(15) 1,2-Dimethoxyethane (DME)	23.9	10.2		7.2
(5) Acetic anhydride	10.5	—	14.5	20.7_{19}	(28) Formamide (FA)	(24)	39.8	16.8_{20}	111.0
(24) Benzonitrile	12.0	—		25.2	(30) *N,N*-Dimethylformamide (DMF)	26.6	16.0	29.4	36.7
(20) Acetonitrile (AN)	14.1	18.9	33.3	35.9	(35) *N*-Methyl-2-pyrrolidinone (NMP)	27.3	13.3	25.6	32.2
(39) Sulfolane (TMS)	14.8	—	25.5	43.3	(32) *N,N*-Dimethylacetamide (DMA)	27.8	13.6	23.9	37.8
(14) 1,4-Dioxane	14.8	10.8		2.21	(36) Tetramethylurea (TMU)	29.6			23.6
(50) Propylene carbonate (PC)	15.1	18.3		66.1	(38) Dimethyl sulfoxide (DMSO)	29.8	19.3	33.3	46.5
Diethyl carbonate (DEC)	16.0	—		2.8	(27) Pyridine (Py)	33.1	14.2		12.9
(51) Ethylene carbonate (EC)	16.4	—		89.6	(34) Hexamethylphosphoric triamide (HMPA)	38.8	10.6	20.6	29.6
(52) Methyl acetate (MA)	16.5	10.7		6.7	(7) Ethanol (EtOH)	(32?)	37.9	19.1	24.6
(23) Butyronitrile (BuN)	16.6	—		20.3	(8) 1-Propanol (1-PrOH)		37.3	19.4	20.5
(17) Acetone (Ac)	17.0	12.5	32.5	20.7	(9) 2-Propanol (2-PrOH)	(36?)	33.6	21.1	19.9
(53) Ethyl acetate	17.1	9.3	22.8	6.0	(29) *N*-Methylformamide (NMF)	(49?)	32.1	10.74	182.4
(49) γ-Butyrolactone (γ-BL)	(18)	17.3		39	Trifluoroacetic acid		105.3		8.55
(1) Water	18(G)–33(L)[b]	54.8	14.0	78.4					

Donor number (*DN*), acceptor number (*AN*) and autoprotolysis constants (pK_{SH}) (with relative permittivities (ε_r)).

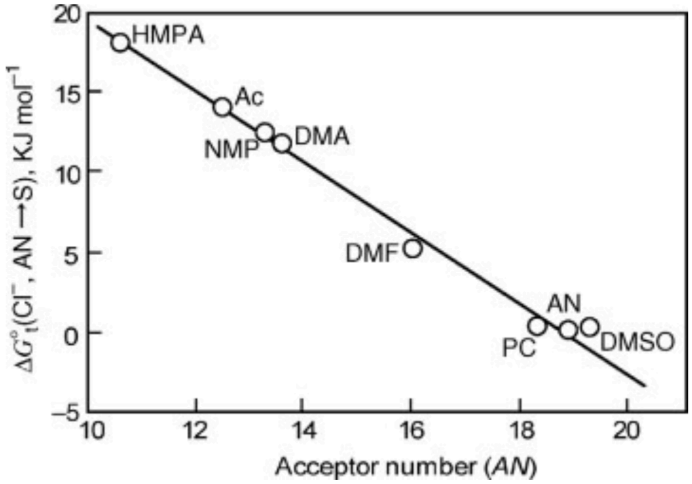

Figure 1.1: Difference in Gibbs free energy of solvation with respect to acetonitrile for Cl^- in various solvents [9]

Corrosion in organic solvents

The different properties of organic solvents and the variety of solvents of industrial interest has motivated significant research on corrosion in organic solvents. The mechanisms by which metals can stay passive in solution are: (i) maintenance of the air-formed film, (ii) formation of a salt film, (iii) chemisorption of the solvent, and (iv) oxide/oxyhydroxide formation [10]. Unlike water, many organic solvents are not able to provide oxygen atoms necessary for mechanism (iv). In addition to that, in water-organic solvent mixtures, different solvents can compete for adsorption sites in mechanism (iii) and their proportion can change the solubility of salts involved in mechanism (ii). Therefore, most studies on corrosion in organic solvents have specifically looked at the influence of the water-organic solvent proportion on passivation mechanisms.

Of the studies carried in aprotic organic solvents, the majority has utilized iron [11–18], a few have utilized nickel [11,12,19,20] and little work has been done with alloys [12,21,22]. Generally speaking, authors have observed that, in neutral organic solutions, metals tend to remain passive by the mechanisms (i)-(iii), and addition of water is deleterious to passivity by locally acting as an acid, and interfering with passivation mechanisms [10]. The effect of water in acidified organic solutions is opposite – it promotes passivation by means of mechanism (iv). As an example, Aramaki et al. studied the active corrosion of iron in ACN with 100–350 ppm water containing carboxylic acids, finding that corrosion currents increased with acidity[16]. Safonov and Haruyama [17] observed that iron is able to passivate in acidified solutions of DMF and DMSO with more than 1% water in weight and passivation potential became lower with increasing water content. A study by Farina et al. obtained similar results in ACN [14]. For nickel in DMSO containing 1 M H_2SO_4, Schwabe and Berthold observed anodic passivation when above 2% water by weight was present [11]. Conversely, in an investigation of the passivation of nickel in 0.1 N H_2SO_4 solutions of aprotic solvents, Ercolano et al. found that 11% water (by weight) was necessary for passivation in ACN, whereas no passivation was observed in DMF up to 35% water [19].

Few studies have examined the effect of Cl^- on corrosion in aprotic solvents. Schwabe and Berthold reported that HCl had no significant effect on corrosion of nickel and iron in anhydrous acidic DMSO and DMF, only when significant water was present [11]. On the other hand, Kikuchi and Aramaki found that the addition of $FeCl_3$ markedly stimulated the anodic dissolution of iron in ACN [13].

Although the existing literature on corrosion in organic solvents has provided fundamental understanding of many passivation phenomena, it is still of little use in industrial applications because most studies were done with pure metals. Only a few authors have studied the corrosion of alloys that are currently used in chemical processing environments. In a conference paper [21], Ramgopal reported that C-22 exhibited active dissolution in 1.92 M HBr/ACN solutions up to 17% water in volume, above which an active-passive transition was found. Another example is the work by Schindelholz et al.[22], explained in more detail on the next topic. Still, it can be said that there is a gap in the literature on corrosion in organic solvents regarding alloys that find application in engineering.

Case study on corrosion of C-22 in pharmaceutical solution

In a recent study by Schindelholz et al, the corrosion of C-22 parts in a reaction vessel in contact with a pharmaceutical liquor at room temperature was investigated [22]. The process utilized an ACN/EtOH solution containing 2,3-dichloro-5,6-dicyano-1,4-benzoquinone (DDQ) and HCl (produced by a homogeneous reaction between EtOH and $EtAlCl_2$). The corrosion rates observed were surprisingly high for C-22 at room temperature – above 20 mm/y in first hours of exposure (Figure 1.2). In contrast, most of the literature on the aqueous corrosion of C-22 reports corrosion rates lower than 0.2 mm/y at room temperature and significantly high corrosion rates are only obtained in boiling concentrated acids with addition of oxidants [2]. The high corrosion rates observed by Schindelholz et al. were attributed to the effect of HCl on developing transpassive dissolution of C-22 coupled with the oxidizing power of DDQ.

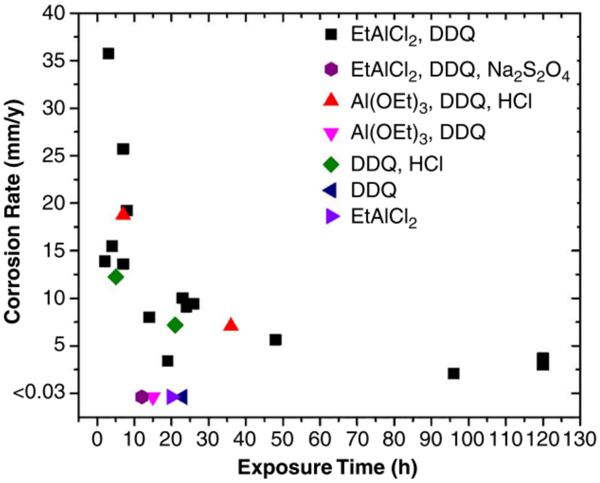

Figure 1.2: Corrosion rates derived from C-22 mass loss experiments in ACN/EtOH solution variants [22].

Although the study identified the main actors in the corrosion problem, a detailed understanding of the mechanisms has not been achieved and the reasons why the observed behavior differs so profoundly from the remaining literature have not been found yet. It is still not known why transpassive dissolution was observed at HCl concentrations in which C-22 is known to be passive in aqueous solutions and why DDQ is such a strong oxidant in combination with HCl. Additionally, it is not known to what extent the properties of the solvent – and the absence of water – play a role in important aspects of this problem, e.g. passivity and equilibrium of species.

Scope of work

The aim of this work was to explain the mechanisms responsible for corrosion and passivation of C-22 and other Ni-Cr-Mo alloys in aprotic solvents. The effect of important variables such as acidity, chlorides, oxidants, and water concentration were studied in order to understand the factors that govern passivity and passivity breakdown in organic solvents. Figure 1.3 is a scheme representing some of the variables involved in this corrosion system and how they can potentially influence corrosion. The chapters in this work were organized as individual studies, and their objectives are listed below.

- ***Chapter 2: The influence of acidity, chlorides and a high-potential quinone on the corrosion of Hastelloy C-22 in non-aqueous solutions.*** The objective of this study was to identify the main factors influencing the anodic and cathodic kinetics of corrosion of C-22 in ACN solutions containing chlorides and DDQ.

- ***Chapter 3: The influence of water concentration and solvent properties on the corrosion of C-22 in aprotic solvents containing HCl.*** The objective of this study was to understand to what extent the corrosion of C-22 in ACN-HCl is determined by the properties of the solvent and what is the effect of residual water on the anodic kinetics.

- ***Chapter 4: The localized corrosion of C-22 in neutral aprotic solvents containing chloride.*** After evidence of localized corrosion in Chapter 2 and 3, this study was aimed at understanding why C-22 can easily undergo pitting in neutral aprotic solvents containing small concentrations of chloride, and whether this process is similar to pitting in aqueous solutions. The effect of water and choice of solvent, as well as chloride concentration were assessed, and the validity of aqueous models for pitting corrosion was discussed.

- ***Chapter 5: The influence of alloy composition on the passivity of Ni-Cr-Mo alloys in acetonitrile containing HCl.*** The objective of this study was to verify whether other alloy compositions are more suited for applications in aprotic solvents. The effect of solution water concentration and of Cr and Mo bulk alloy concentrations on passivity were studied.

- ***Chapter 6: Characterization of passive films formed in acetonitrile.*** After evidence in earlier chapters showing that passive films formed in low water concentrations are less protective than typical passive oxides formed in water, the last study of this series was aimed at understanding the kinetics of growth and the chemical properties of films formed in ACN with various water concentrations. The possible influences of the film composition on corrosion performance were discussed.

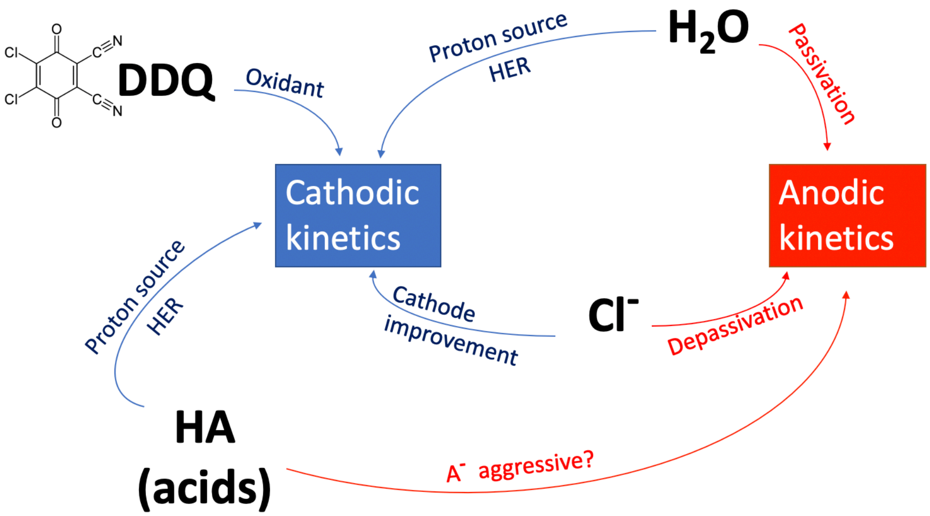

Figure 1.3: A schematic representation of the scope of the project

Chapter 2 : The Influence of Acidity, Chlorides and a High-Potential Quinone on the Corrosion of Hastelloy C-22 in Nonaqueous Solutions

(*This chapter was published as an article in the Journal of Electrochemical Society and it is shown in its original form. DOI: 10.1149/1945-7111/abcc37*)

P. Atz Dick *, M. J. Beekwilder, R. G. Kelly **,z

Department of Materials Science and Engineering, University of Virginia, Charlottesville, Virginia 22903, USA

* Electrochemical Society Student Member
** Electrochemical Society Active Member
[z] E-mail: rgk6y@virginia.edu

Abstract

The corrosion of Hastelloy C-22 at room temperature in acetonitrile (ACN) solutions containing various concentrations of tetrabutylammonium chloride (Bu_4NCl), HCl and 2,3-dichloro-5,6-dicyano-1,4-benzoquinone (DDQ) was investigated, mimicking aggressive environments used in the synthesis of pharmaceuticals. In the absence of sources of Cl^-, C-22 is passive in ACN. In neutral ACN containing Bu_4NCl, C-22 undergoes pitting upon anodic polarization. C-22 presents an active-passive transition in ACN with 5 mM HCl. In HCl concentrations above 5 mM, C-22 is completely active and i_{corr} increases with HCl concentration. Comparing with the literature in aqueous corrosion of C-22, the breakdown of passivity in ACN takes place at much lower chloride additions. The corrosion in ACN/HCl/DDQ solutions can achieve surprisingly high rates, as seen in electrochemical tests (i_{corr} = 6.5 mA cm^{-2}) and mass loss tests (penetration rate > 10 mm y^{-1}), due to the oxidizing power of DDQ. In equimolar concentration, HCl and DDQ have a synergistic effect on the elevation of the cathodic kinetics of C-22 corrosion, due to the effects of acidity on the reduction of DDQ.

Introduction

A variety of processes in the chemical and pharmaceutical industries takes place in environments that are aggressive towards most engineering materials. In order to avoid degradation of the vessels and tools exposed to such environments and to minimize contamination of the products, often highly corrosion-resistant nickel-based alloys are utilized [1]. Because the solutions utilized in synthesis processes can vary greatly in solvent type and chemical composition, the alloys exposed need to be able to endure a wide range of aggressive environments. Hastelloy C-22 (59Ni-22Cr-13Mo-3W-3Fe) is often well-suited for such applications due to its low corrosion rate in both oxidizing and reducing solutions [2].

The remarkable corrosion resistance of C-22 and other Ni-Cr-Mo-(W) alloys is a consequence of the formation of a Cr-rich passive oxide film that protects the bulk from the corrosive environment. The exact composition of the oxide film and the influence of each alloying element on its protective properties in aqueous solutions have been the subject of many studies [7]. Because the protection of passive alloys is conditional on the formation and preservation of the passive film, their application in organic solvents brings additional concerns. Firstly, unlike water, many organic solvents are not able to provide hydroxyl anions necessary for passive layer formation. Secondly, the behavior of aggressive species can differ greatly as a consequence of the range of physicochemical properties offered by organic solvents. Aprotic solvents such as acetonitrile (ACN), for example, have weaker acceptor and donor properties than water, which results in weaker solvation of small halide anions and weaker dissociation of acids [9].

The mechanisms by which metals stay passive in organic solvents are usually divided in four types: (*i*) preservation of air-formed film; (*ii*) salt film formation; (*iii*) chemisorption of the solvent; and (*iv*) oxide/oxyhydroxide formation. Most of the corrosion studies carried in aprotic organic solvents have utilized pure metals, such as iron [11–18] and nickel [11,12,19,20]. Generally speaking, authors have observed that, in neutral anhydrous organic solutions, metals tend to remain passive by mechanisms *i – iii*, and addition of water is deleterious to passivity by locally acting as an acid, and interfering with passivation mechanisms [10]. On the other hand, studies have shown the opposite behavior in acidified anhydrous aprotic solvents. In such cases, nickel and iron corrode actively but can passivate by mechanism *iv* if water is added above a threshold, usually in the order of a few percent in weight [11,14,19]. Few studies have examined the effect of Cl^- on corrosion in aprotic solvents. Schwabe and Berthold reported that HCl had no significant effect on corrosion of nickel and iron in anhydrous acidic dimethyl sulfoxide (DMSO) and N,N-dimethylformamide (DMF), only when significant water was present to provide passivation [11]. On the other hand, Kikuchi and Aramaki found that the addition of $FeCl_3$ markedly stimulated the anodic dissolution of iron [13]. Although the fundamentals of passivation in organic solvents have been described, little is known of the performance of popular engineering alloys in organic solvents and the influence of environment-specific aggressive species. Shifler et al. reported that 304 stainless steel was able to remain passive in anhydrous propylene carbonate by maintaining its air-formed oxide layer (mechanism *i*). Once the oxide was removed, repassivation could take place by either salt film formation or solvent adsorption, depending on the potential [23].

Of the myriad of species present in processes involving aprotic solvents, quinones deserve attention due to their redox-active behavior and their usefulness in biologic processes, as well as in the energy, pharmaceutical and chemical industries [24]. Although many studies have been dedicated to understanding the redox behavior of quinones, few studies have reported its effect on corrosion of metals. Some authors have suggested the use of quinones of low reduction potential as corrosion inhibitors [25]. Other studies with similar quinones, in contrast, have shown that the addition of quinones can increase the corrosion of aluminum in aqueous acidic solutions [26] and the corrosion of steel in black liquor [27]. More recently, Schindelholz et al. observed that C-22 corroded at surprisingly high rates (circa 20 mm y^{-1}) at room temperature in a pharmaceutical liquor containing 2,3-dichloro-5,6-dicyano-1,4-benzoquinone (DDQ) and HCl in acetonitrile [22]. Although the study identified the main actors in the corrosion problem, a detailed understanding of the mechanisms has not been achieved and the reasons why the observed behavior differs so profoundly from the literature in aqueous solutions have not been found yet.

In the present work, we studied the corrosion of C-22 at room temperature in a series of acetonitrile-based solutions of varying acidity, chloride concentration, and DDQ concentration, utilizing electrochemical, characterization and exposure techniques. The aim is to understand the fundamental aspects of the influence of acids, chloride, and DDQ on the corrosion of passive alloys in acetonitrile, ultimately providing useful insight on materials selection for nonaqueous applications.

Experimental

Materials and specimen preparation

The material used in this study consisted of Ni-Cr-Mo-W Hastelloy C-22 (UNS N06022) sheets with 3.5 mm of thickness, supplied by Haynes International, USA. The nominal chemical composition of alloy C-22 is shown in Table 2.1. For exposure tests, rectangular specimens of approximated dimensions 10 x 10 mm were cut using a SiC abrasive disc, and then drilled to allow use of a PTFE string to suspend the specimens in solution. For electrochemical tests, a water abrasive jet was used to machine round specimens of diameter 15 mm. Unless otherwise noted, all specimens were prepared by grinding to P4000 grit sand paper in water. For mass loss tests, all sides of the specimens were ground, whereas for electrochemical tests only the one side exposed to the solution was ground.

Table 2.1: Nominal chemical composition of alloy C-22 (UNS N06022).

Element	Cr	Mo	W	Fe	Ni
Mass fraction (wt%)	22	13	3	3	Bal.

Reagents and solutions

Anhydrous acetonitrile (99.8%, Sigma), 2,3-dichloro-5,6-dicyano-1,4-benzoquinone (98 %, Aldrich), ferrocene (≥ 98 %, Aldrich), tetrabutylammonium hexafluorophosphate (≥ 98 %, Fluka), tetrabutylammonium chloride (≥ 97 %, Aldrich), silver nitrate (99.9999 %, Aldrich), and hydrogen chloride in methanol (1.25 M, Sigma-Aldrich) were used as received. All reagents were stored in a desiccator at all times to avoid moisture uptake.

Solutions used in mass loss and electrochemical tests were prepared by drying solid reagents in closed flasks under 99.999 % N_2 overnight, then adding solvents and liquid reagents with glass syringes. A positive pressure difference between the flasks and the external atmosphere was maintained using a pass-through bubbler filled with mineral oil to ensure that air would not penetrate into the system during the tests. All solutions were used immediately after their preparation. As measured by Karl Fischer coulometric titration, this protocol resulted in a final typical water concentration of circa 100 –150 ppm.

Exposure tests

Exposure tests were performed in closed flasks filled with circa 50 mL of solution under N_2 atmosphere, one specimen at a time. Solutions were stirred with a magnetic stirrer at 60 rpm to avoid excessive concentration gradients. The measurements of mass loss and calculations of corrosion rates were carried out in accordance with ASTM G1 and G102 [28,29]. Before weighing, specimens were sonicated in ethanol and dried with hot air.

Electrochemical tests

For all electrochemical tests, the working electrode was either a Pt disc of 1.6 mm diameter (BASi) or a C-22 specimen enclosed in a PTFE holder with an exposed area of 0.785 cm^2. In all cases the counter electrode was a coiled Pt wire of length 20 cm and diameter 0.25 mm. The reference electrode consisted of a silver wire submerged in a glass tube fitted with a porous glass Vycor tip containing a solution of 0.01 M $AgNO_3$ + 0.1 M Bu_4NPF_6 in acetonitrile, which was replaced before each test. The potential of the reference electrode was determined by comparison with the half-wave potential of the ferrocene/ferrocenium redox pair in acetonitrile (Fc/Fc$^+$). Cyclic voltammetry using a Pt working electrode (BASi) at 100 mV s^{-1} was periodically performed to test the reference electrode, yielding a stable potential of -98 ± 1.8 mV vs Fc/Fc$^+$. Therefore, when referring to potential values, we use the Fc/Fc$^+$ potential as a reference, but values can be converted to the standard hydrogen electrode (SHE) scale by adding 624 mV [30].

Electrochemical measurements were performed with a Bio-Logic SP-150 potentiostat (Bio-Logic USA). All experiments were conducted at room temperature, in a closed vessel under N_2 atmosphere. After placing the electrodes and purging the cell vessel with N_2, the test solution was transferred into the vessel using a double-tipped needle. After the electrodes were immersed, open circuit potential (OCP) was measured for 60 min, which was enough to observe a stable behavior, unless otherwise noted. After the OCP period, the solution resistance (R_S) was determined by electrochemical impedance spectroscopy in the high frequency range (typically above 10 kHz). Potentiodynamic polarization (PDP) scans were performed either as single sweeps or as series of cycles, with scan rates of 1 or 100 mV s^{-1}. PDP was carried with automatic compensation of 85% of ohmic drop in the solution, considering the R_S obtained before beginning the scan.

Electrochemical impedance spectroscopy (EIS) was performed using an excitation signal with amplitude 10 mV around the open circuit potential over a frequency range from 100 kHz to 10 mHz. Unless otherwise noted, all solutions contained 0.1 M Bu_4NPF_6 as supporting electrolyte.

Characterization

When of interest, specimens were examined after corrosion tests using scanning electron microscopy (FEI Quanta 650), after rinsing with isopropanol to remove corrosion products.

Results

In this study exposure tests, potentiodynamic polarization, cyclic voltammetry, and electrochemical impedance spectroscopy were utilized to investigate the effects of chloride, acidity and quinones on the corrosion of C-22 in acetonitrile. Due to the large number of variables which behavior can differ from aqueous solutions, the results are organized by types of solutions – and not by analytical technique. We start with the simplest case (C-22 in neutral acetonitrile), after which the complexity is increased by the addition of HCl and, later, DDQ. Finally, cyclic voltammetry with a Pt electrode was utilized to provide further insight of the electrochemical phenomena observed in corrosion tests. The choice of concentrations for HCl and DDQ was based on information of solutions utilized in synthesis processes of the pharmaceutical industry [22].

C-22 in neutral ACN solutions

In order to understand the effects of HCl on the corrosion of C-22 in an aprotic solvent such as acetonitrile, we first need to define the behavior of C-22 in the solvent. Figure 2.1a shows anodic voltammograms on C-22 and on Pt in ACN with Bu_4NPF_6 supporting electrolyte. Pt was used as a model of inert electrode in order to provide information on electrochemical reactions that do not involve the electrode material. C-22 is passive up to circa 1.1 V vs Fc/Fc^+, where the anodic current starts increasing and eventually becomes more than one order of magnitude greater than that on Pt at the same potential. This difference indicates that the rise in anodic current is mainly due to the transpassive oxidation of C-22 and not to the oxidation of the solvent or electrolyte. These results agree with reports that ACN/Bu_4NPF_6 electrolytes offer a wide electrochemical window – roughly from -2.7 to +2.9 V vs SCE or -3.1 to 2.5 V vs Fc/Fc^+ [30,31]. Because the potentials of interest were far from the limits of the electrochemical window in all tests, oxidation of the solvent and of the electrolyte will both be ignored for ACN-Bu_4NPF_6 mixtures in this study. After reversing the direction of the scan, a small negative hysteresis is observed, followed by an increase in open circuit potential (OCP) for both Pt and C-22. When the potential is scanned to 1.5 V vs Fc/Fc^+ on C-22 and held for 4 h, no signs of localized corrosion are seen in subsequent optical micrography (Figure 2.1b). However, after the 4-h potential hold, a semi-transparent film is observed on the surface of C-22. This film could not be removed by rinsing with organic solvents, but was effectively dissolved with 20% nitric acid. After removing the film, the morphology of the surface is more easily observed, showing uniform crystallographic etching.

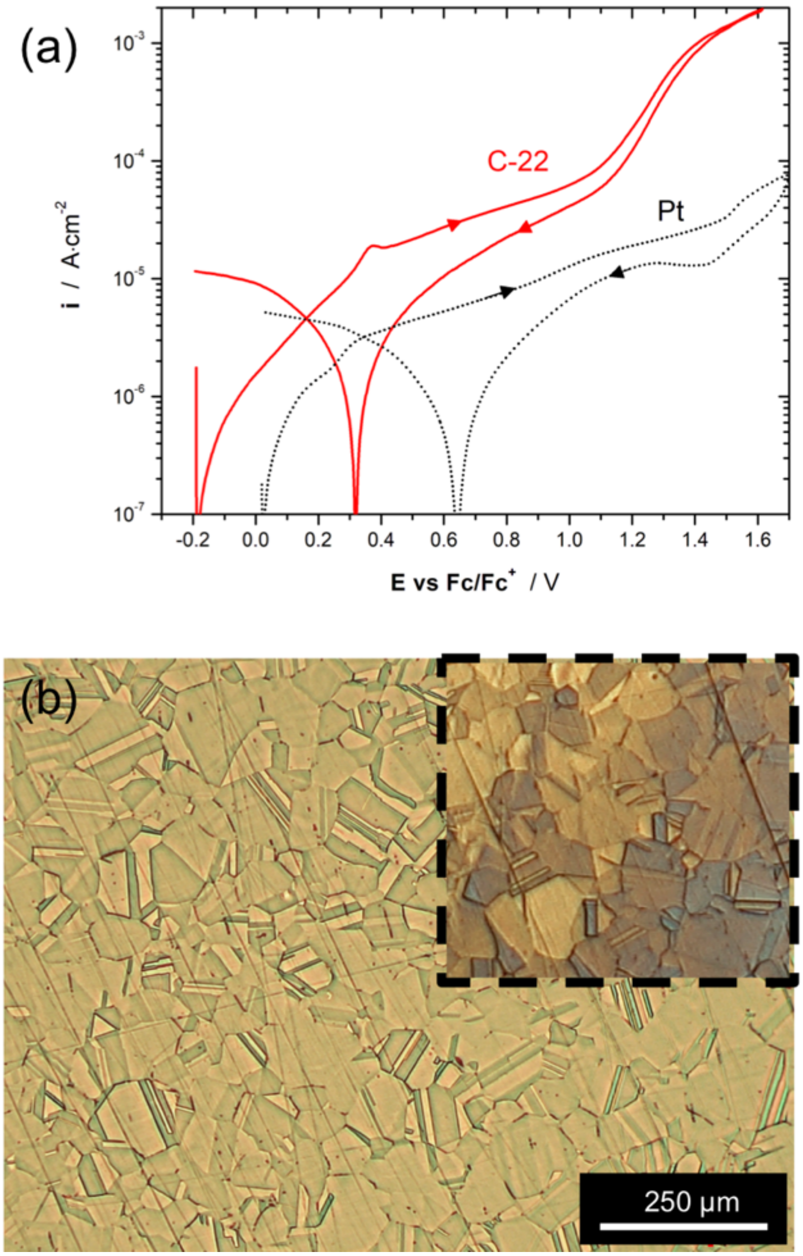

Figure 2.1: (a) Potentiodynamic polarization at 1 mV s^{-1} with C-22 or Pt in ACN / 0.1 M Bu_4NPF_6 solution; (b) optical micrograph of C-22 surface after potentiostatic polarization at 1.5 V vs Fc/Fc$^+$ for 4 h. Inset shows surface before removal of film formed on the surface. Potential values in the Fc/Fc$^+$ scale can be converted to the SHE scale by adding 0.624 V [30].

Figure 2.2 shows PDP results on C-22 in ACN + 140 mM Bu_4NCl solution. It should be noted that this solution did not contain Bu_4NPF_6. Thus, the main difference between this solution and the one used in Figure 2.1 is the presence of Cl^- instead of PF_6^- anions. In this case, C-22 exhibits passivity only up to -0.1 V vs Fc/Fc^+, where anodic current density increases suddenly (E_{pit}). The current density continues to increase even after reversal of sweep direction, but eventually repassivates at -0.78 V vs Fc/Fc^+ (E_{rep}), presenting a wide positive hysteresis typical of localized corrosion. This figure also shows a PDP scan on Pt in a similar solution, where no increase in current is observed in the same range of potentials. Above 0.22 V, however, anodic current density starts to rise, possibly as a result of oxidation of the electrolyte. The SEM micrographs with C-22 specimens obtained after PDP (Figure 2.2b) reveal a corrosion morphology replete with small pits, with diameter below circa 0.5 μm. These pits appear to be aligned with the scratches introduced during specimen preparation.

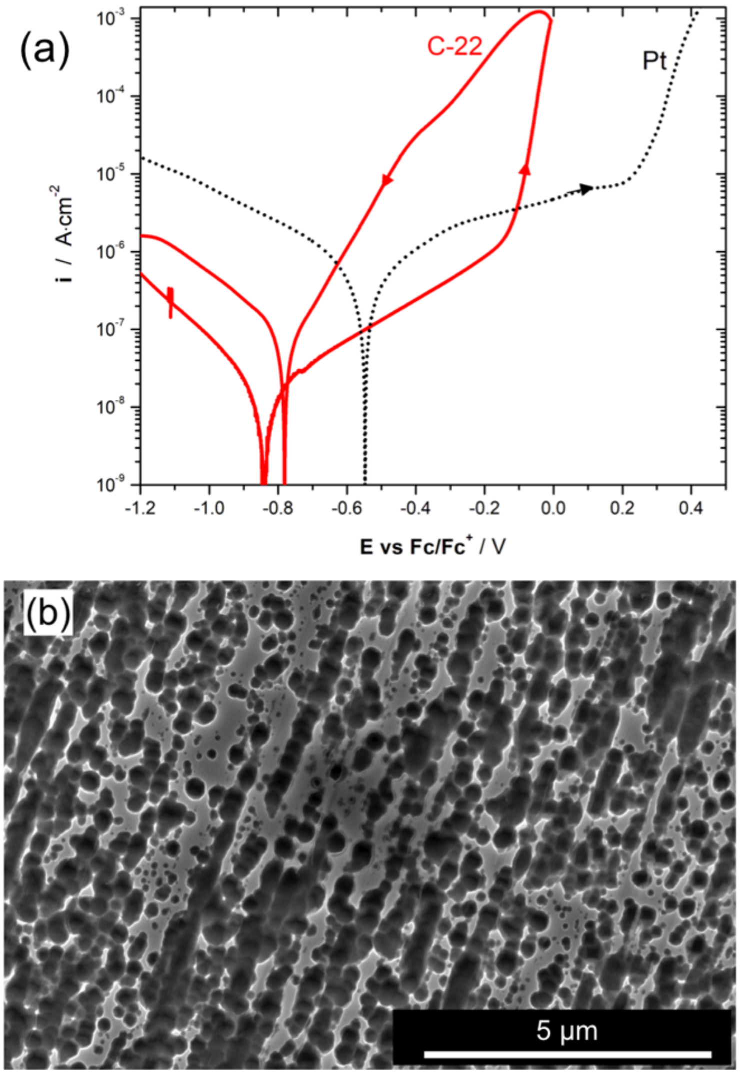

Figure 2.2: (a) Potentiodynamic polarization at 1 mV s^{-1} with C-22 or Pt in ACN / 0.14 M Bu_4NCl solution; (b) scanning electron micrograph of C-22 surface after potentiodynamic polarization. Potential values in the Fc/Fc^{+} scale can be converted to the SHE scale by adding 0.624 V [30].

C-22 in ACN-HCl solutions

Figure 2.3a shows a series of voltammograms for C-22 exposed to different ACN-HCl solutions, performed in a similar manner as in Figure 2.1 and Figure 2.2. The data corresponding to the negative sweep in 28 mM and 140 mM HCl were omitted due to their similarity with their respective positive sweeps. Comparing the anodic branches for different concentrations, there is a clear influence of HCl on the active-passive behavior of C-22. A concentration as low as 5 mM HCl is sufficient to cause activation of C-22 at relatively small overpotentials. Comparing the results in 5 and 28 mM HCl solutions, there is no significant difference in anodic currents up to -0.1 V vs Fc/Fc^+, both exhibiting a Tafel slope of circa 100 mV per decade. In 140 mM HCl, however, the anodic branch is steeper (Tafel slope of circa 58 mV per decade). No active-passive transition is observed in 28 mM or in 140 mM HCl. Although the potential was not scanned to high overpotentials such as those in 5 mM HCl, it is unlikely that passivation would take place in these conditions due to the high anodic current densities and clear active behavior. Passivation is observed only in 5 mM HCl, with a short range between 0.70 and 0.95 V vs Fc/Fc^+. This region is followed by a rise in anodic current density, which starts at lower potentials and is more intense than in the transpassive dissolution observed in the absence of HCl. The lack of positive hysteresis after reversing the scan direction indicates that the rise in current density is not a consequence of localized corrosion. As in the solution without HCl, in 5 mM HCl C-22 presents a more passive behavior in the negative sweep.

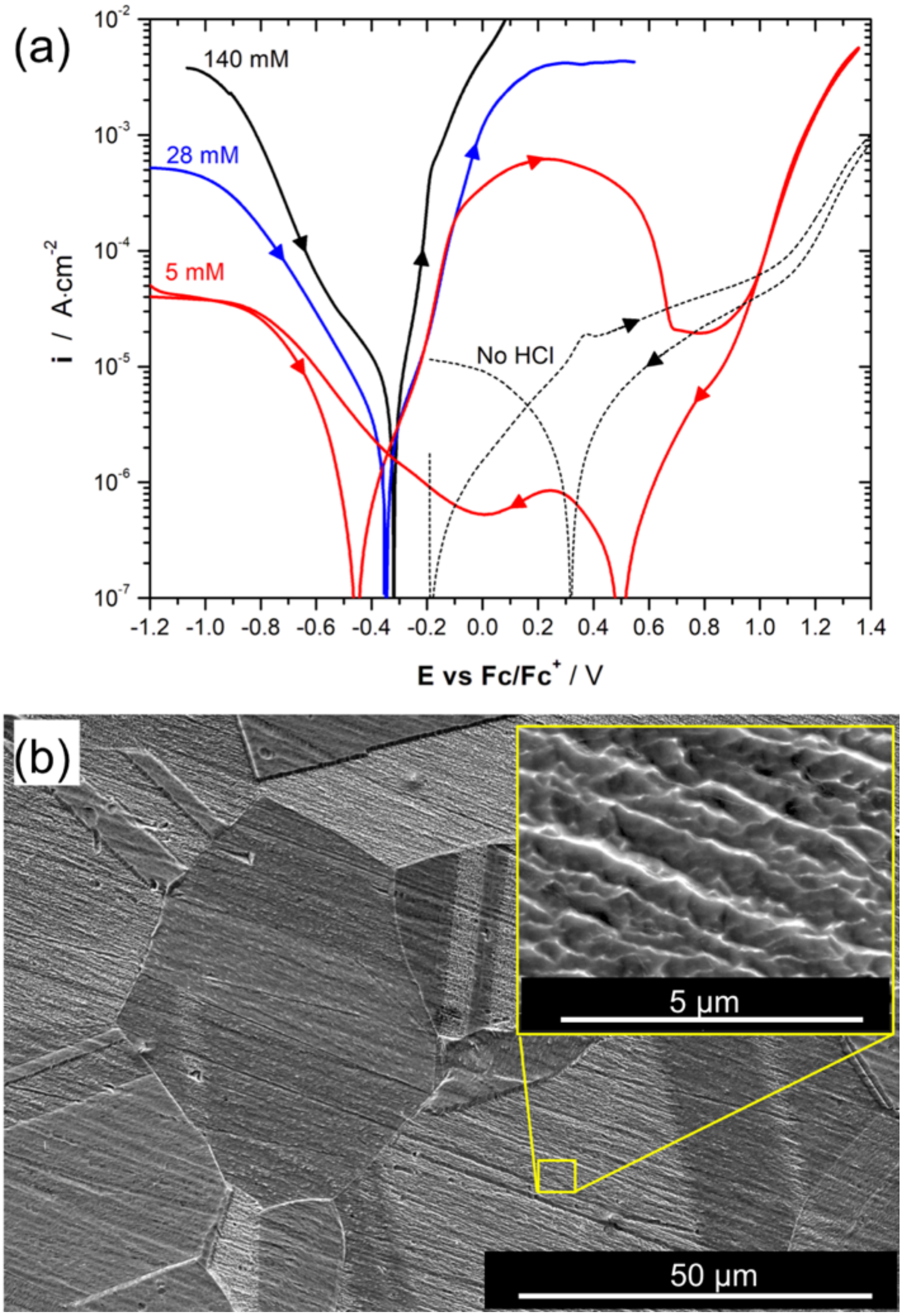

Figure 2.3: (a) Potentiodynamic polarization at 1 mV s^{-1} in various concentrations of HCl in ACN, with supporting electrolyte 0.1 M Bu_4NPF_6; (b) scanning electron micrograph of C-22 surface after PDP in 140 mM HCl. Potential values in the Fc/Fc^+ scale can be converted to the SHE scale by adding 0.624 V [30].

The cathodic branches of these voltammograms are marked by the increase in current density with the increase in HCl concentration. They can be roughly divided in two regions: a region at lower potentials, where the current density is independent of potential and seems limited by diffusion; and a region near OCP, where the current densities are lower and seem controlled by charge transfer. With an increase in HCl concentration, the point of transition between these two regions shifts to lower potentials and the current density in the diffusion-limited region becomes higher. Also, the increase in HCl concentration seems to increase the OCP observed in the positive sweep. Still, the OCP is lower in all HCl solutions than in the absence of HCl, consistent with the large differences in anodic kinetics caused by HCl addition. Figure 2.3b shows the C-22 surface after PDP in 140 mM HCl. Differently from the PDP in Bu_4NCl (Figure 2.2b), the corrosion morphology in this case is generalized, and depth of attack varies with crystallographic orientation. No signs of pitting or crevice corrosion were observed.

Figure 2.4 and Figure 2.5 show, respectively, corrosion potential (E_{corr}) and EIS measurements in various HCl concentrations. The period marked as "EIS" in each curve in Figure 2.4 represents the time of acquisition of EIS spectra such as the ones shown in Figure 2.5. Each E_{corr} transient can be divided in two parts. The first part, in the beginning of the measurement, is marked by a rapid rise of E_{corr}, which slows down until reaching a peak. After that peak, the E_{corr} starts to decrease at a slow rate – the decrease in potential is not shown in 5 mM because it requires longer immersion times (up to 2.5 h). At short times, both the initial values and the rate of change in E_{corr} increase with HCl concentration. Moreover, the time to reach the peak E_{corr} becomes shorter with increasing HCl concentration. Some difference is observed between the final E_{corr} values and the crossover potentials in PDP (Figure 2.3), especially in 5 mM HCl, where the influence of the initially cathodic polarization in the PDP seems greater.

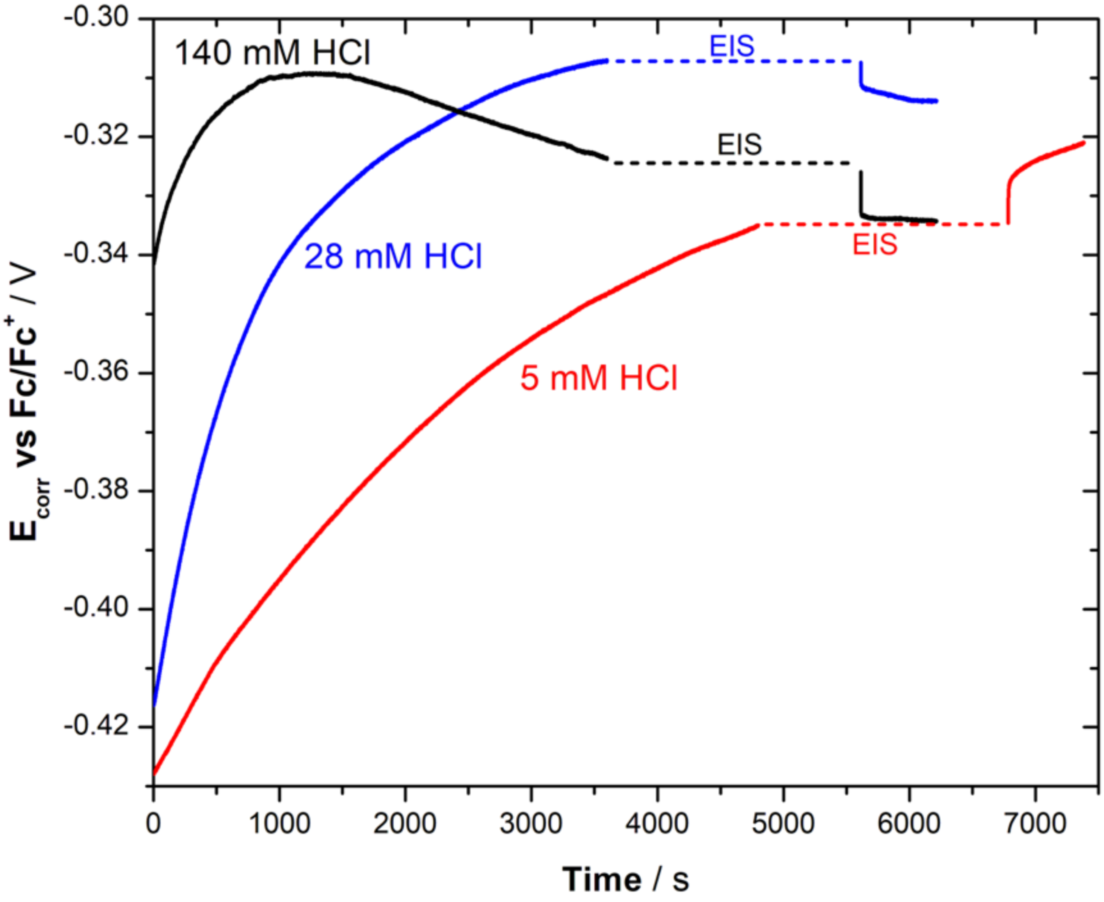

Figure 2.4: Corrosion potential transients measured in various concentrations of HCl in ACN. Supporting electrolyte: 0.1 M Bu_4NPF_6. Potential values in the Fc/Fc$^+$ scale can be converted to the SHE scale by adding 0.624 V [30].

Figure 2.5 shows the impedance spectra measured for the same HCl concentrations used in Figure 2.3a and 4, acquired after 1 hour of exposure or more. For each HCl concentration, frequency was scanned from 10^5 Hz to 10^{-2} Hz, and then back to 10^5 Hz. This 35-min cyclic pattern was used to identify the occurrence of non-steady state behavior in the impedance data. Although the data points acquired at low frequencies may resemble an inductive behavior in some cases, this possibility can be discarded by the analysis of the reverse part of scan. Clearly, even after 1 hour at E_{corr}, the polarization resistance (R_P) changes over the time of acquisition of each cycle. The R_P were estimated by fitting the spectra with the 3-element equivalent circuit shown as an inset in Figure 2.5, which has been employed by other authors in the description of corrosion of C-22 in aqueous HCl [32] as well as many other systems. In order to capture the initial and final values of R_P, the lowest decade of frequencies in each sweep was ignored in fitting. These results are summarized in Table 2.2. Although in 5 mM HCl R_P increased with time by 9%, in 28 and in 140 mM HCl R_P decreased by 28 and 43%, respectively. Thus, the increase in HCl concentration not only provokes a faster change in R_P, but also decreases R_P.

Table 2.2: Data obtained from EIS and potentiodynamic polarizations with varying HCl concentration.

HCl concentration	**$R_{P(\text{initial})}$ / Ohm cm^2**	**$R_{P(\text{final})}$ / Ohm cm^2**	**B / mV**	**i_{corr} / mA cm^{-2}**	**Penetration rate / mm y^{-1}**
5 mM	$32.3 \cdot 10^3$	$35.4 \cdot 10^3$	46.1 ± 5.2	$1.30 \cdot 10^{-3}$	$1.14 \cdot 10^{-2}$
28 mM	$24.4 \cdot 10^3$	$17.6 \cdot 10^3$	29.2 ± 2.3	$1.66 \cdot 10^{-3}$	$1.45 \cdot 10^{-2}$
140 mM	$6.06 \cdot 10^3$	$3.45 \cdot 10^3$	20.2 ± 3.4	$5.86 \cdot 10^{-3}$	$5.13 \cdot 10^{-2}$

The corrosion current density (i_{corr}) can be calculated using the Stern-Geary equation [33]:

$$i_{corr} = \frac{B}{R_P} \qquad (1),$$

where B is the Stern-Geary coefficient, which can be derived from the Tafel slopes b_a and b_c as follows:

$$B = \frac{b_a b_c}{2.303(b_a + b_c)} \qquad (2)$$

The Tafel slopes were obtained from the polarization curves shown in Figure 2.3a at a distance between 100 and 200 mV from the point of zero current of each curve, where a straight line was usually visible on both cathodic and anodic branches. The calculations of B and average i_{corr} (calculated with the final R_P of each EIS cycle) show that corrosion current density increases with HCl concentration (Table 2.2). Using the information provided by E_{corr} transients in Figure 2.4 and the variation in R_P shown in Figure 2.5, it becomes clear that R_P increases if E_{corr} is ascending, and R_P decreases if E_{corr} is descending.

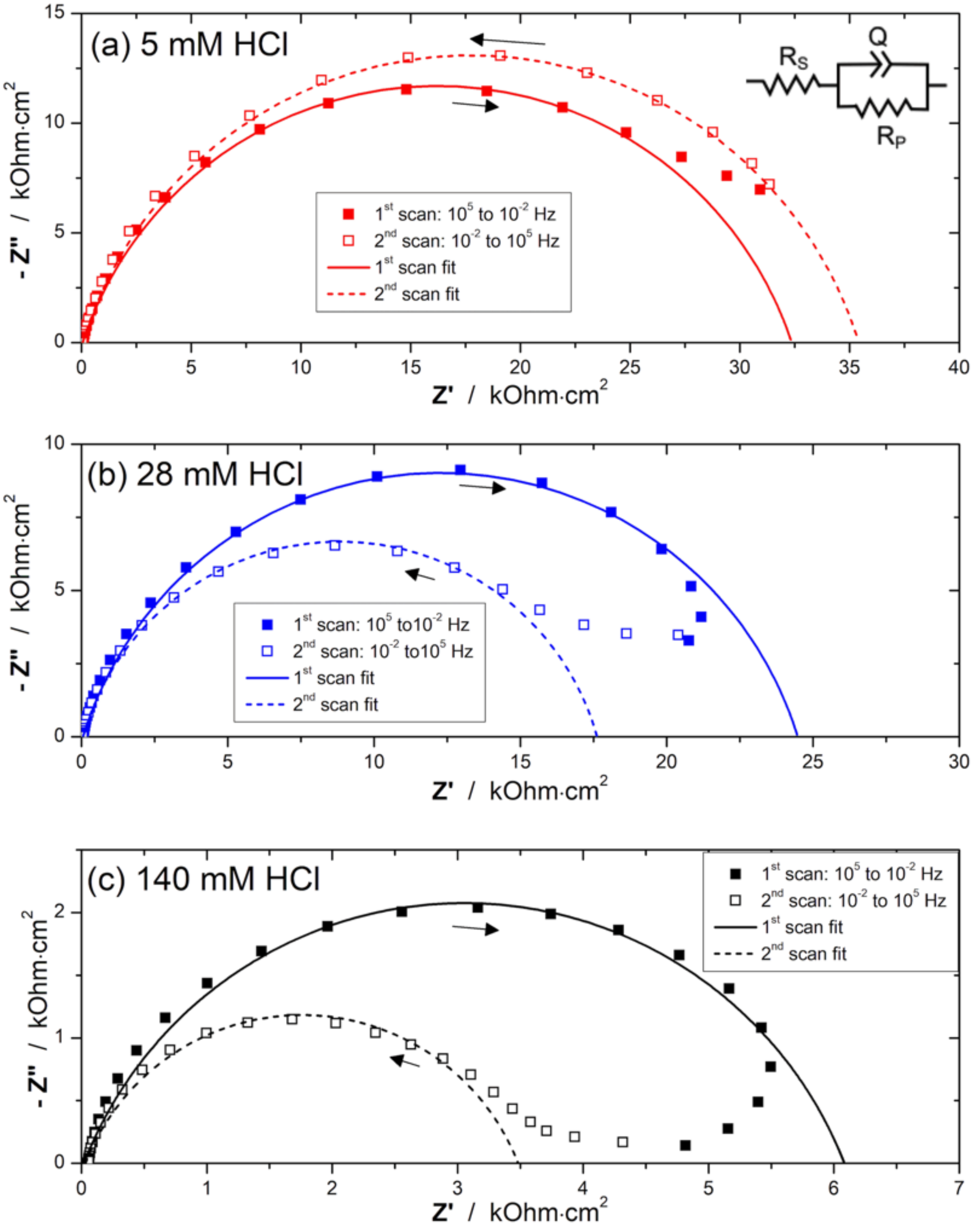

Figure 2.5: Electrochemical impedance spectra of C-22 in various concentrations of HCl in ACN. Supporting electrolyte: 0.1 M Bu_4NPF_6.

C-22 in ACN-HCl-DDQ solutions

The influence of DDQ on the corrosion of C-22 in ACN was initially investigated with exposure tests. Corrosion rates calculated form 24-h mass loss are shown in Fig. 6 for various solution compositions. Figure 2.6a shows corrosion rates in 140 mM HCl with different additions of DDQ, with an auxiliary axis for the E_{corr} measured in some of the solutions. For a fixed HCl concentration, corrosion rate increases logarithmically with DDQ molarity, reaching values above 10 $mm \cdot y^{-1}$ (millimeters per year) in 140 mM DDQ + 140 mM HCl. E_{corr} also increases, although the quantitative trend is not clear without more data points. Figure 2.6b shows corrosion rates and E_{corr} measurements for a fixed DDQ concentration of 140 mM, with various HCl additions up to equimolar concentration (the data points at the highest concentration in Figure 2.6a and b correspond to the same solution). In this case, corrosion rate increases linearly with HCl concentration, and E_{corr} decreases.

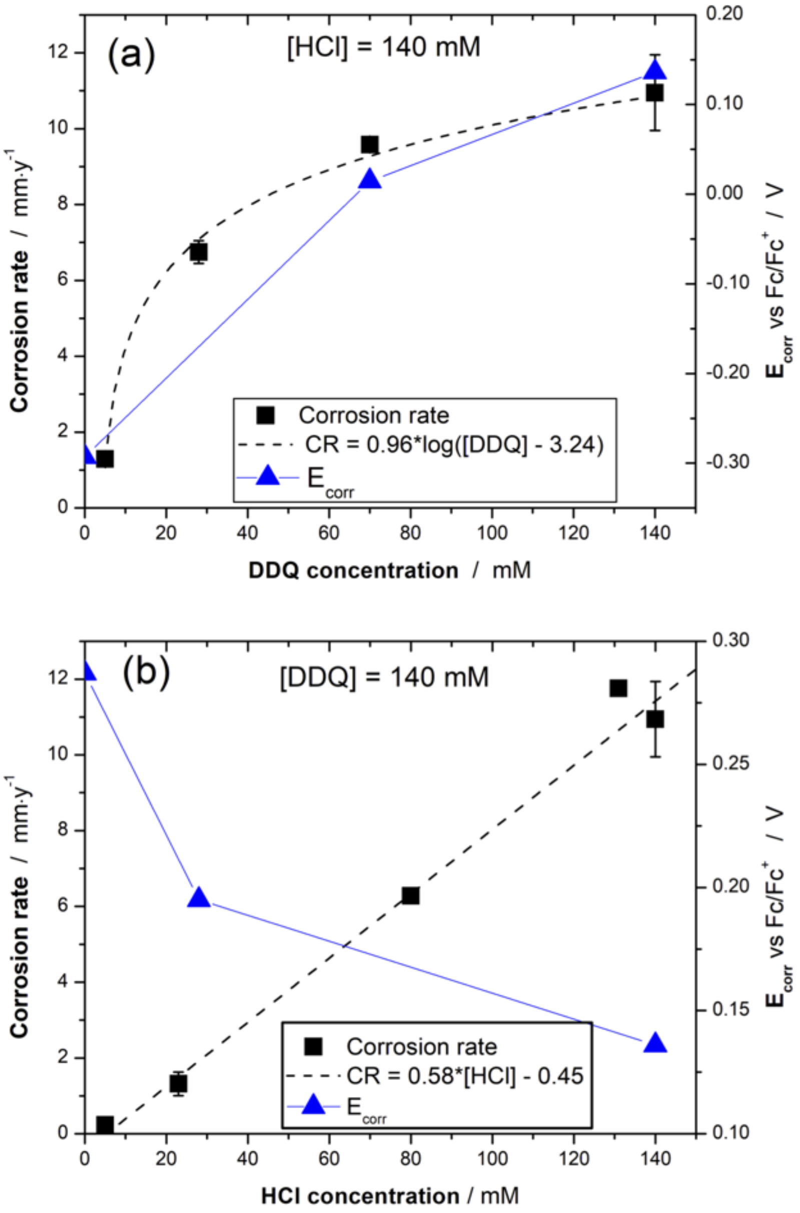

Figure 2.6: Corrosion rates calculated from mass loss and E_{corr} (measured after 1h) for fixed [HCl] = 140 mM with varying [DDQ] (a); for fixed [DDQ] = 140 mM with varying [HCl] (b). Potential values in the Fc/Fc^{+} scale can be converted to the SHE scale by adding 0.624 V [30].

The morphology of the corrosion of C-22 in HCl-DDQ solutions can be observed in the scanning electron micrographs in Figure 2.7. Figure 2.7a and 7b show the surface after 24 h of exposure to 23 mM HCl + 140 mM DDQ. In this condition the corrosion is uniform over the entire specimen, but the final surface is highly porous, which gives the specimen an opaque appearance. Although some grains are more deeply attacked (Figure 2.7b), presumably as a consequence of their crystallographic orientation, the shape of the pores is random and crystallographic etching is not observed in this case. When HCl concentration is increased to 140 mM HCl + 140 mM DDQ (Figure 2.7c and Figure 2.7d), corrosion is more intense, as seen in mass loss results (Figure 2.6). The surface is covered with crystallographic pits randomly distributed throughout the specimen. Contrarily to the specimens exposed to low HCl concentration solutions, the areas that show a more porous appearance here are actually composed of small crystallographic pits (< 1 µm). Some of the pits grow to larger diameters (> 50 µm), maintaining a proportional increase in depth.

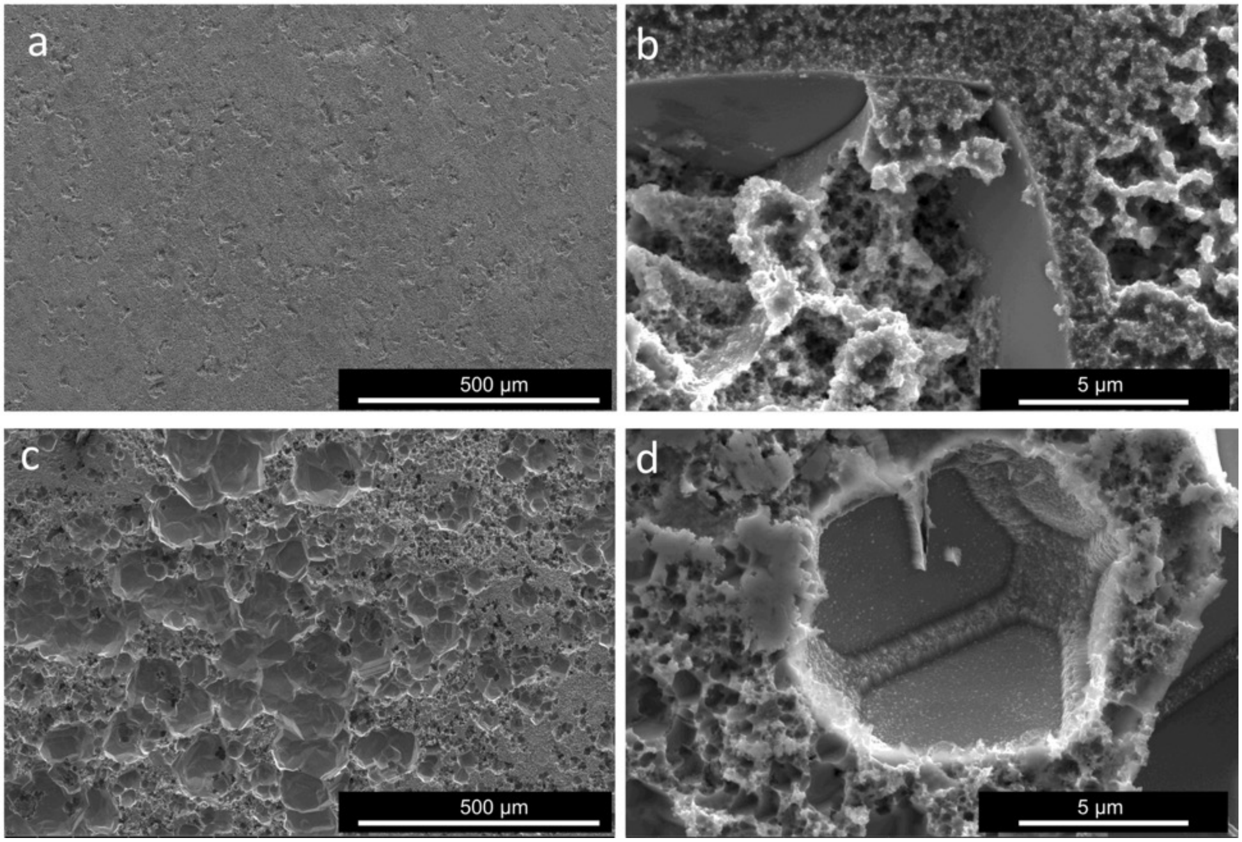

Figure 2.7: Scanning electron micrographs of C-22 specimens exposed for 24 h to 23 mM HCl + 140 mM DDQ (a, b) and 140 mM HCl + 140 mM DDQ (c, d).

Potentiodynamic polarization curves were generated in 140 mM HCl, 140 mM DDQ and 140 mM HCl + 140 mM DDQ, with C-22 (Figure 2.8a) and with Pt (Figure 2.8b**)**. The curves in Figure 2.8a are overlaid with data from the exposure tests in Figure 2.6, shown here as points of coordinates [*x,y*], where *x* is E_{corr}

(measured or interpolated) and y is i_{corr} (calculated from mass loss). The cathodic currents for the PDP in 140 mM DDQ are significantly higher than in 140 mM HCl for potentials above -0.8 V vs Fc/Fc$^+$. The anodic branch of the curve shows that, in DDQ, C-22 does not display an active behavior such as that seen in HCl, and OCP is circa 600 mV higher. When both DDQ and HCl are added to the solution, the corrosion behavior changes markedly. The cathodic currents are surprisingly high even at low polarizations, with values almost two orders of magnitude greater than those in 140 mM DDQ. The cathodic current appears to transition into a diffusion-limited regime at more negative polarizations, although part of the curvature could be a result of ohmic drop in the solution, considering IR correction was limited to 85%. Although the decrease in E_{corr} seen in Figure 2.6b is a net result of HCl addition, the PDP results show that HCl and DDQ have a synergistic effect on the intensification of cathodic currents. The anodic branch of the PDP in HCl + DDQ exhibits active behavior, but it is shifted to more anodic potentials in comparison to that in pure HCl. Nevertheless, corrosion rate in this case is much stronger, as shown in exposure tests.

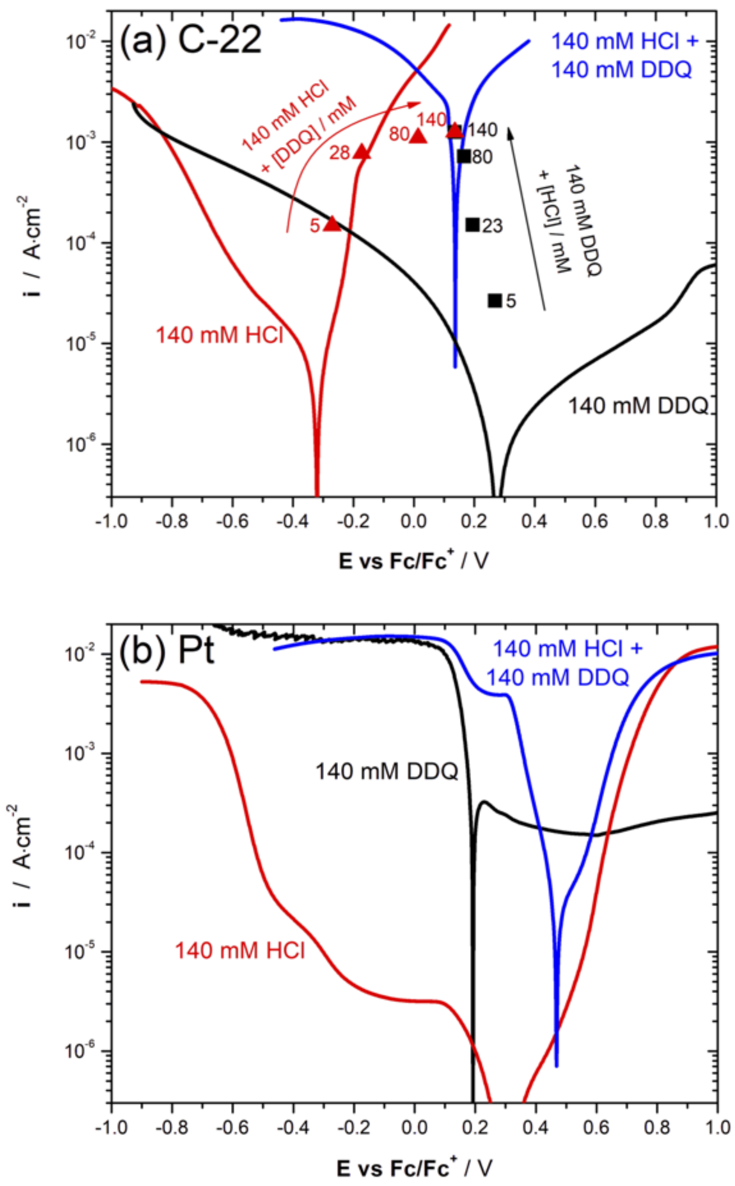

Figure 2.8: Potentiodynamic polarization scans for C-22 in 140 mM HCl, 140 mM DDQ or 140 mM HCl + 140 mM DDQ in ACN (supporting electrolyte: 0.1 M Bu_4NPF_6) and average [E_{corr}, i_{corr}] points extracted from exposure tests; **(b)** PDP results for Pt in similar solutions. Potential values in the Fc/Fc$^+$ scale can be converted to the SHE scale by adding 0.624 V [30].

The data points from exposure tests are shown in two different patterns in Figure 2.8a: black squares, for the increasing additions of HCl to a fixed concentration of 140 mM DDQ; red triangles, for the increasing additions of DDQ to a fixed concentration of 140 mM HCl. The black squares are distributed as a straight line between the points representing [E_{corr}, i_{corr}] for the PDP in 140 mM DDQ and in 140 mM DDQ + 140 mM HCl. This indicates a gradual activation of C-22 and augmentation of cathodic currents with HCl addition. The red triangles, in contrast, do not form a straight line. The addition of DDQ to 140 mM HCl provides, at first, significant increase of corrosion current density, roughly following the anodic line in 140 mM HCl. This indicates that low additions of DDQ primarily enhance cathodic kinetics. At concentrations above 28 mM, however, the larger anodic shifts in E_{corr} (or lower increase in i_{corr}) indicate a breach with the anodic behavior in HCl. There appears to be simultaneous enhancement of cathodic processes and hindering of anodic processes, as seen in the positive shift of the anodic branch with little increase in i_{corr}. The results from exposure tests were expected to underestimate instantaneous corrosion rates due to the 24-h period of exposure, during which aging of the solution can happen. Nevertheless, there appears to be a reasonably good agreement between PDP and exposure test results.

The PDP results on Pt (Figure 2.8b) are shown in the same scale of Figure 2.8a, for comparison. In HCl, the anodic branch of Pt is shifted to higher potentials in comparison to that of C-22 and the OCP is around 0.46 V vs Fc/Fc$^+$. Comparing the anodic branches in HCl and in HCl + DDQ, it is clear that the anodic inhibition observed at high DDQ concentrations does not occur for Pt. Near the OCP, the cathodic branch in HCl shows a low-current diffusion-limited region, but at lower potentials it appears to follow a similar behavior to that seen on C-22. The cathodic branches for DDQ and HCl + DDQ both appear to be in a diffusion-limited regime below 0.1 V vs Fc/Fc$^+$, a behavior that was observed on C-22 only below circa -0.3 V vs Fc/Fc$^+$ and only when both HCl and DDQ were present. It should be noted that the cathodic branch of Pt in HCl + DDQ has a 'wave' representing another diffusion-limited region closer to OCP. While the cathodic current in DDQ is diffusion-limited even near the OCP, in HCl + DDQ there is a region under charge transfer control with Tafel slope b_c = 72 mV/dec extending down to 160 mV below OCP.

Figure 2.9 shows the electrochemical impedance spectra obtained in solutions of the same concentration as the ones used for PDP in Figure 2.8. In 140 mM DDQ, R_P increases substantially during the measurement. Because the change in E_{corr} was less than 1 mV during the EIS measurement period, contributions of drifting are negligible. In a 140 mM DDQ solution, R_P is greater than in 140 mM HCl, which agrees with PDP results which show that C-22 has a passive behavior in DDQ. When both HCl and DDQ are present in solution, the impedance spectrum can be fitted using an equivalent circuit with three time constants, as shown in Fig. 9b. Due to the lower magnitude of R_1, R_2 and R_3 in comparison with the solution resistance (R_S), the impedance is mostly resistive; the spectrum presents small change of phase angle, and is more affected by noise than in other cases. Although the exact meaning of each time constant is not clear, we assume that $R_P = R_1 + R_2 + R_3$ for the estimation of corrosion currents. Thus, R_P is three orders of magnitude lower than in DDQ or in HCl. Again, equation 1 can be used to calculate i_{corr}, along with B from

PDP curves (B_{PDP}) and R_P. These results are summarized in Table 2.3. As shown in exposure tests, the calculated i_{corr} has the highest values in the presence of equimolar HCl and DDQ. Alternatively, for 140 mM HCl + 140 mM DDQ, R_P from EIS results and 24-h average i_{corr} from exposure tests can be used to estimate an average B for the 24 h of exposure (B_{ML}). B_{ML} is almost five times smaller than B_{PDP}, due to the lower average i_{corr} used in the calculation.

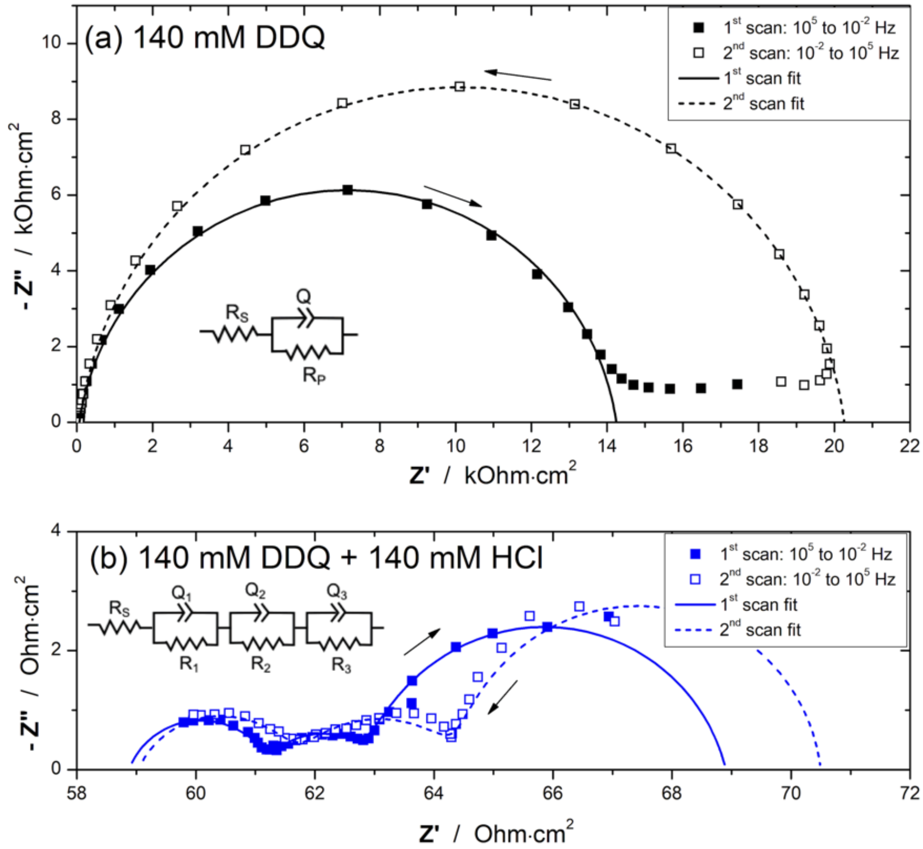

Figure 2.9: Electrochemical impedance spectra of C-22 in 140 mM DDQ (a) and in 140 mM DDQ + 140 mM HCl in ACN (b). Supporting electrolyte: 0.1 M Bu_4NPF_6.

Table 2.3: Electrochemical data derived from EIS, PDP and mass loss tests.

Solution	**R_P / Ohm cm^2**	**B_{PDP} / mV**	**i_{corr} / mA cm^{-2}**	**i_{corr} (ML) / mA cm^{-2}**	**B_{ML} / mV**
140 mM DDQ	$14.2 \cdot 10^3$	55.6	$3.90 \cdot 10^{-3}$	–	–
140 mM DDQ + 140 mM HCl	12.0	78.4	6.53	1.25	15.0

Cyclic voltammetry on Pt

In order to better understand the electrochemistry of DDQ and HCl in acetonitrile, cyclic voltammetry scans were performed at 100 mVs^{-1} using a Pt working electrode (Figure 2.10), after measuring the open circuit potential (OCP_{Pt}, marked by a dashed line) until stability was observed. The solutions utilized were of the same concentrations as those used for PDP tests in Figure 2.8b. In HCl (Figure 2.10a), OCP_{Pt} has the lowest value (+72 mV vs Fc/Fc$^+$). The main features in this curve are the reduction wave with a peak at -0.810 V vs Fc/Fc$^+$ and the oxidation wave with a peak at 0.981V vs Fc/Fc$^+$. The small reduction wave at 0.448 V vs Fc/Fc$^+$ was only observed at faster scan rates (50 mV s^{-1} and above), and only after the potential was scanned to sufficiently high values for the oxidation wave to occur previously. The voltammogram in the DDQ solution (Figure 2.10b) shows typical features of quinone electrochemistry: two distinct pairs of reduction/oxidation events (labeled 1 and 2), with half-wave potential $E_{1/2}$= 0.105 V and $E_{1/2}$= -0.818 V vs Fc/Fc$^+$. OCP_{Pt} in the DDQ solution was approximately 140 mV higher than in HCl.

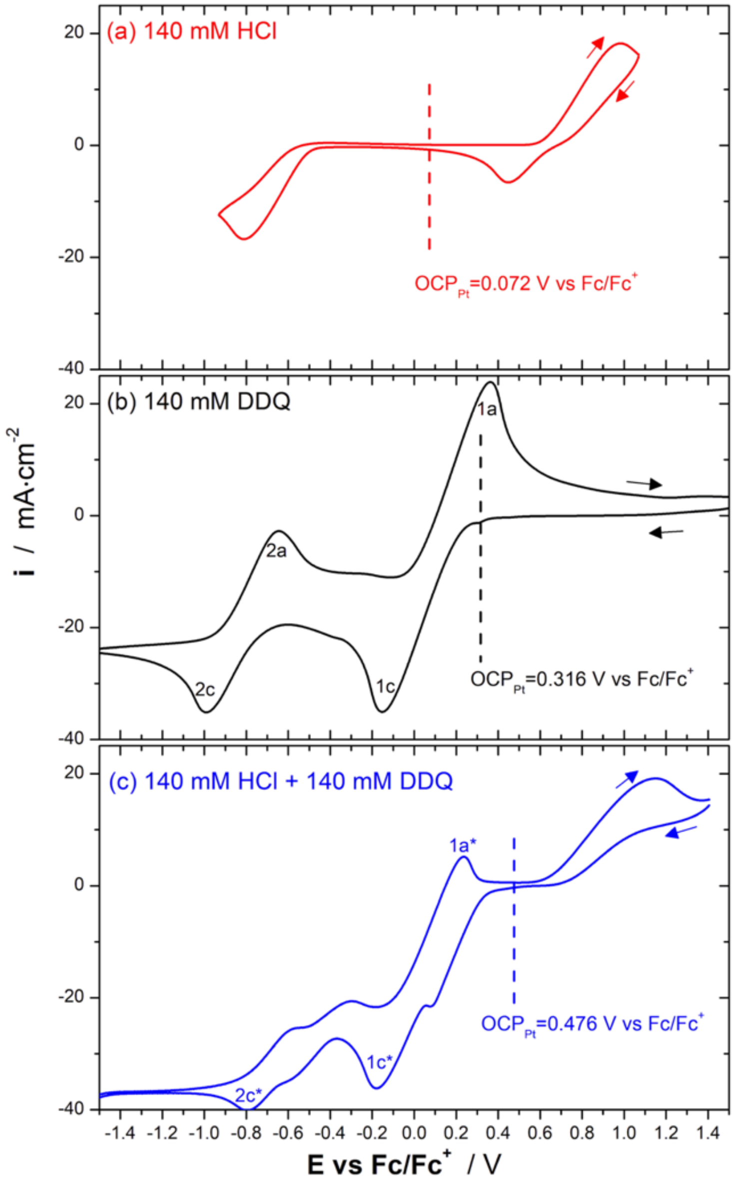

Figure 2.10: Cyclic voltammetry at 100 mVs^{-1} with Pt working electrode in 140 mM HCl (a), 140 mM DDQ (b), and 140 mM HCl +140 mM DDQ (c). Supporting electrolyte: 0.1 M Bu_4NPF_6. Potential values in the Fc/Fc$^+$ scale can be converted to the SHE scale by adding 0.624 V [30].

When both DDQ and HCl are present in solution, OCP_{Pt} is the highest, at 0.476 V vs Fc/Fc$^+$. Also, the CV shows distinct cathodic features. The cathodic wave 1c* in DDQ + HCl is at the exact same position as 1c in DDQ (-0.152 V vs Fc/Fc$^+$), with slight increase of peak current. However, this cathodic wave is preceded by a pre-wave (or shoulder). At lower potentials, there is another cathodic wave (2c*), which also appears to be preceded by a pre-wave, and is shifted to higher potentials in comparison with 2c in DDQ. The oxidation waves below OCP_{Pt} in DDQ + HCl are diminished in comparison with the DDQ solution, especially 1a*. The oxidation wave above OCP_{Pt} starts at the same potential (approximately 0.58 V) as that seen in HCl, although the peak current is only reached at higher potentials (1.148 V vs Fc/Fc^+).

Discussion

C-22 is passive in neutral Cl^--free ACN

The PDP results obtained in ACN (Figure 2.1a) are useful in providing a baseline for comparison with more complex solutions. The fact that passivity is maintained up to a polarization of 1.2 V above the open circuit potential suggests that C-22 should resist chloride-free ACN solutions even in the presence of strong oxidants. Because there is no evidence of spontaneous dissolution of the air-formed oxide film or of formation of an anodic film in solution, this initial passive condition is likely a result of the protection offered by the air-formed film. This behavior is similar to that described for 304 stainless steel in anhydrous propylene carbonate [23].

Under strong anodic polarization (above 1.05 V vs Fc/Fc^+), the rise of current density is similar to that observed in transpassive dissolution in aqueous solutions, indicating that the initial passive film is dissolved, at least to some extent. Because there is no similar rise of current density on Pt, we can infer that the increase in current density exhibited on C-22 is truly due to the oxidation of the metal and not of the electrolyte or solvent. Still, the enhanced passivity observed after decreasing the anodic polarization is an indication that residual water enables repassivation of C-22 and further oxide growth. Indeed, after holding the potential in the transpassive region for 4 h, C-22 presented a semi-transparent film on the surface, which could only be removed with concentrated nitric acid. This film was probably not the result of oxidation/polymerization of the solvent (or impurities) on the surface of the electrode, as indicated by the low anodic currents observed on Pt under the same potential range. Because this film is not uniform and the current density was stable during the potential hold, we can infer that this is not the result of precipitation of a salt. As suggested previously, residual water could enable oxide growth with different colors resulting from the varying thickness. After removal of the film, only crystallographic attack is observed, with no signs of localized corrosion (Figure 2.1b).

Low concentrations of Cl^- can cause pitting of C-22 in neutral ACN

When 140 mM Bu_4NCl is used as an electrolyte (Figure 2.2), C-22 undergoes pitting slightly above -0.1 V vs Fc/Fc^+. The repassivation potential is only about 100 mV above the OCP, indicating a high susceptibility to pitting. Inspection of the surface of C-22 by SEM after the PDP reveals that localized corrosion propagates by the widespread nucleation of small pits, without signs of crevice formation. These results contrast markedly with the literature on the corrosion of C-22 in aqueous solutions, where stable localized corrosion is usually not observed unless a crevice is formed, even at temperatures above 60 ˚C and Cl^- concentration in the order of several molar [34,35].

The literature on corrosion in aprotic solvents lacks studies in Cl^--containing solutions. Schwabe and Berthold reported pitting of pure Fe and Ni in DMSO and DMF containing H_2SO_4 + HCl only when water concentration was between 2–50% to allow previous passivation [11]. In the present study, the protection before pitting is more likely to be a result of the air-formed film because a low and nearly potential-independent anodic current density is observed at potentials below the pitting potential (-0.1 V vs Fc/Fc^+). Although the results in Bu_4NCl shown here are limited, we can infer that the passive film of C-22 has a much higher susceptibility to pitting in neutral Cl^--containing acetonitrile than in Cl^--rich aqueous solutions.

Addition of low concentrations of HCl can activate C-22 surface

The PDP results in varying HCl concentration (Figure 2.3a) have shown a profound influence of HCl on the anodic kinetics of the corrosion of C-22 in acetonitrile at low (mM) concentrations in stark contrast to the excellent resistance to HCl in aqueous solutions at high (M) concentrations [36]. Concentrations of HCl as low as 5 mM in ACN are sufficient to cause activation of the C-22 surface. For additions of 28 mM or more, C-22 exhibits a completely active behavior, without any signs of passivation. The absence of hysteresis upon reversal of scan direction (omitted in Figure 2.3a for clarity) indicates an essentially uniform corrosion process, without formation of surface films. C-22 presented an active-passive transition and a narrow region of passivity between 0.65 V and 0.80 V vs Fc/Fc^+ only at the lowest HCl concentration used (5 mM). The subsequent rise in anodic current density initially resembles the transpassive dissolution process observed in the absence of HCl, with a similar enhancement of passivation as a net result of the anodic polarization. Nevertheless, in HCl, this rise in current density occurs at a lower potential (0.8 V vs Fc/Fc^+), at which a similar increase in current density is seen in potentiodynamic tests using Pt (Figure 2.8b and Figure 2.10). Thus, the increase in current density observed above 0.8 V vs Fc/Fc^+ on C-22 in HCl solutions could be at least partially due to the oxidation of Cl^- from HCl. Analogously to the anodic oxidation of water in aqueous solutions, this could lead to local acidification of the electrode surface and enhancement of dissolution.

The literature on corrosion of C-22 in aqueous HCl provides markedly different results than observed here with ACN. In PDP experiments in various HCl concentrations, Mishra et al. [36,37] observed complete passivity at 1.4 M, an active-passive transition at 6 M, but complete activation occurred only above 9 M. In linear polarization resistance measurements in 6 M HCl, R_P was above 1000 Ohm cm^2 [36], in the same order of magnitude as R_P observed for ACN/140 mM HCl in this study. Therefore, the HCl concentration necessary for active corrosion of C-22 in acetonitrile is orders of magnitude lower than in water, which suggests a strong influence of the solvent.

Effects of solvent properties on acidity

The chemical differences between water and acetonitrile can be explained from the point of view of the donor-acceptor approach developed by Gutmann [38]. As listed in Table 2.4, acetonitrile has a lower donor number (DN) than water, which means that it has weaker donor properties. Thus, the solvent does not easily accept protons and CH_3CNH^+ is rather unstable. Therefore, HCl undergoes little dissociation and behaves like a weak acid, which results in a significantly higher pK_a in acetonitrile than in water. In essence, HCl will dissociate far less in ACN than in water; in ACN, it is essentially all present in the molecular form.

Table 2.4: Solvent properties and dissociation constant of HCl for acetonitrile and water [9].

Solvent	**DN**	**AN**	**pK_a(HCl)**
Water	33	54.8	-3.7
Acetonitrile	14.1	18.9	8.9

Although residual water might play a role as oxidant under small cathodic polarizations, the fact that diffusion-limited cathodic currents increase and cathodic Tafel lines shift to higher potentials with increasing HCl concentration (Figure 2.3a) suggests that hydrogen evolution reaction (HER) is the main cathodic reaction available in ACN-HCl solutions. In acidic aprotic solvents, hydrogen is most commonly produced by either reduction of solvated protons or direct reduction of the acid (reactions I and II, respectively):

$$2H^+ + 2e^- \longrightarrow H_2 \quad \text{(I)}$$

$$2HCl + 2e^- \rightarrow H_2 + 2Cl^- \quad \text{(II)}$$

HER through reaction I requires a previous chemical step of formation of the solvated proton (CH_3CNH^+), which only happens significantly for strong acids in acetonitrile, such as trifluoromethanesulfonic (pK_a=2.6) [39]. By comparing the pK_a of HCl with those of acids which reduction in acetonitrile has been described in the literature [39], we can infer that its reduction probably takes place through reaction II.

It has been experimentally shown that the inflection point in reduction waves for acids in acetonitrile decreases linearly with increasing pK_a [39]. Similarly, other works have correlated increase in pK_a with decrease in standard potential for acid reduction [40,41]. Thus, the lower DN of ACN makes acids weaker oxidizers. The activation of C-22 with low HCl additions may, however, be linked to other factors, particularly Cl^- attack.

Effects of solvent properties on chloride solvation

Acetonitrile differs from water not only in donor, but also in acceptor behavior. As listed in Table 2.4, acetonitrile has a much lower acceptor number (AN) than water, which indicates that anions in acetonitrile are more weakly solvated. Gutmann et al. have shown that the free energy of solvation for Cl^- decreases linearly with decreasing AN [42]. The free energy of solvation for a species *i* in a solvent "S" can be assessed using the transfer Gibbs free energy with reference to another solvent "R", i.e., the difference between the solvation energies for the species in the two solvents:

$$\Delta G_t^0\,(i, R \rightarrow S) = G_{sv}^0(i, S) - G_{sv}^0(i, R) \quad (3)$$

To describe how the solvation energy affects the reactivity of a certain species, we can use the transfer activity coefficient, $\gamma_t(i, R \rightarrow S)$, given that:

$$\log \gamma_t(i, R \rightarrow S) = \frac{\Delta G_t^0\,(i, R \rightarrow S)}{2.303\, R\, T} \quad (4)$$

According to Izutsu [9], the transfer activity coefficient of Cl^- from water to ACN is $\gamma_t(Cl^-, H_2O \rightarrow MeCN)$ = $10^{7.4}$, which allows us to make the relation

$$\gamma_{Cl^-, MeCN} = 10^{7.4}\, \gamma_{Cl^-, H_2O} \quad (5)$$

this means that Cl^- is $10^{7.4}$ times more reactive in ACN than in water [9]. Thus, for the same concentration of free Cl^- in water and in acetonitrile, Cl^- in acetonitrile should have a much stronger tendency to engage in reactions to form products, which could lead to a more effective attack of the passive layer. The observation of localized corrosion with reasonably low concentrations of Bu_4NCl in acetonitrile might, therefore, be a consequence of a greater activity coefficient of Cl^-. However, it should be noted that the concentration of free Cl^- obtained as a result of HCl additions in acetonitrile is smaller than in water, due to the higher pK_a of HCl in acetonitrile. We can use the pK_a values informed in Table 2.4 to build the following equation

$$pK_a(HCl, H_2O) = pK_a(HCl, MeCN) - 12.6 \qquad (6)$$

Because the pK_a of HCl can be defined as

$$pK_a = -\log\left(\frac{[H^+][Cl^-]}{[HCl]}\right) \quad (7),$$

we can use eq. 6 and eq. 7 to relate the concentrations of solvated protons and chloride in water and acetonitrile for the same [HCl] as follows:

$$[H^+]_{H_2O}[Cl^-]_{H_2O} = 10^{-12.6}\,[H^+]_{MeCN}[Cl^-]_{MeCN} \quad (8)$$

With the assumption that in solution $[H^+]_{MeCN} = [Cl^-]_{MeCN}$ and $[H^+]_{H_2O} = [Cl^-]_{H_2O}$, we equate the concentrations of Cl^- in water and ACN.

$$[Cl^-]_{MeCN} = 10^{-6.3}[Cl^-]_{H_2O} \qquad (9)$$

Eq. 9 tells us that for the same [HCl], $[Cl^-]$ is about a million times smaller in acetonitrile than in water. Moreover, we can use the definition of activity $a_{Cl^-} = \gamma\,[Cl^-]$ with eq 10 and eq 6 to get to a relation between activities:

$$a_{Cl^-,MeCN} = 10^{7.4}\,\gamma_{Cl^-,H_2O}10^{-6.3}[Cl^-]_{H_2O} = 10^{1.1}\,a_{Cl^-,H_2O} \qquad (10)$$

Thus, the activity of Cl^- in acetonitrile ($a_{Cl^-,MeCN}$) is about one order of magnitude greater than the activity of chloride in water (a_{Cl^-,H_2O}), for the same HCl molarity. It should be noted that this calculation ignores the effects of impurities and the effect of hydrogen bonding between Cl^- and HCl in acetonitrile, also known as homoconjugation. Still, eq. 10 provides the rationale for the observations that HCl in ACN in this study are comparable to results in much higher concentrations of HCl in water.

As a result of the high pK_a of HCl in ACN, the concentration of free Cl^- in solution is expected to be higher in the absence of a source of protons. Thus, chloride attack in Bu_4NCl should be more intense than in the same concentration of HCl. This approach does not explain why C-22 is active in 140 mM HCl, whereas in 140 mM Bu_4NCl it is initially passive but undergoes pitting. Thus, there might be other factors in play, such as acidity, influencing the prevalence of uniform corrosion.

Transient aspects of corrosion in ACN-HCl solutions

The E_{corr} and EIS measurements (Figure 2.4 and Figure 2.5) showed that the corrosion of C-22 in ACN-HCl solutions has a transient behavior at least in the first two hours of exposure. At the start of freely corroding exposure, E_{corr} increases with HCl concentration, which agrees with the OCP seen in PDP for different HCl concentrations (Figure 2.3a). This information, along with the fact that R_P decreases with increasing HCl concentration, suggests that the main effect of HCl upon initial exposure is the enhancement of cathodic kinetics. Nevertheless, in all concentrations tested, the E_{corr} of C-22 first increases before decreasing at longer times, forming a peak. Furthermore, R_P in EIS increases when E_{corr} is moving in the anodic direction; R_P decreases when E_{corr} is moving in the cathodic direction. Although in some cases small drifts from E_{corr} can alter a given EIS spectrum due to the change in slope of the i *vs* E dependence, this effect should only account for small changes in R_P, below 7% in the worst case for this system*. Thus, the effect of drifting was not considered in the calculations, as it does not explain the magnitude of change in R_P with time, and it does not impact any of the inferences drawn. The changes in R_P observed in EIS measurements can be assumed to be true at the E_{corr}.

From the perspective of mixed potential theory, these results indicate that there is a change in anodic kinetics over time. Initially, when E_{corr} is going in the positive direction, the anodic kinetics is getting slower and R_P increases as a result; later, when E_{corr} goes in the negative direction, the opposite takes place. It is not clear what processes could lead to the observed changes of anodic kinetics. However, because the rates of change of R_P and of E_{corr} with time both increase with HCl additions, it can be assumed that HCl controls the transient behavior of anodic kinetics. A reasonable hypothesis is that corrosion is initially limited by a surface oxide. At initial exposure this oxide grows as a consequence of residual water, but oxide growth is eventually overcome by Cl^- attack, causing decrease of R_P and elevation of E_{corr}.

DDQ is a strong oxidant in the presence of HCl

The capability of DDQ as an oxidant towards C-22 was observed in various tests containing HCl. First, the addition of DDQ increases E_{corr} and corrosion rate in exposure tests (Figure 2.6). Using mixed potential theory, this can be interpreted as a consequence of the enhancement of cathodic kinetics, which requires E_{corr} and i_{corr} to increase in order to maintain conservation of charge. Furthermore, in PDP results, the

---

* For each impedance spectrum shown, the influence of drifting during EIS measurements was estimated by considering the shift in E_{corr} during the measurement and assessing the slope at different points of the voltammogram measured directly after EIS. The transient behavior of R_P determined by EIS was independent of the drift observed.

increase in i_{corr} and positive shift of E_{corr} are accompanied by much higher cathodic current densities when DDQ is added to ACN-HCl solutions.

The CV using Pt in ACN + DDQ presents two reduction waves (1c and 2c in Figure 2.8), which the literature in quinone electrochemistry commonly attributes to two consecutive steps of quinone reduction, according to the following reactions [43]:

$$DDQ + e^- \rightarrow DDQ^{\cdot -} \quad \text{(III)}$$

$$DDQ^{\cdot -} + e^- \rightarrow DDQ^{2-} \quad \text{(IV)}$$

Because reaction IV requires further reduction of an already negatively charged species, it takes place only at significantly lower potentials ($E_{1/2}$ = -0.818 V vs Fc/Fc$^+$) than reaction III ($E_{1/2}$ = 0.105 V vs Fc/Fc$^+$). The E_{corr} observed for C-22 in DDQ solutions is about 0.9 V above the $E_{1/2}$ of reaction IV, which suggests that reaction IV does not contribute to corrosion. Furthermore, the contribution of O_2 reduction as a cathodic reaction can be discarded because it takes place at very cathodic potentials in ACN, with $E_{1/2}$ = -1.08 V vs SCE on Pt [44] (-1.46 V vs Fc/Fc$^+$ [30]). In the absence of HCl, however, corrosion in DDQ is not significant, as a consequence of low anodic current densities (Figure 2.8a). When the HCl concentration is increased for a fixed DDQ concentration, corrosion rate increases linearly and E_{corr} shifts in the negative direction (Figure 2.6b). From the point of view of mixed potential theory, this result means that the main effect of HCl in ACN-HCl-DDQ solutions is the activation of the anodic reaction. Thus, we can infer that, in DDQ without HCl, the corrosion current density is low due to the preservation of the air-formed film. The activation of anodic kinetics is, however, not the only effect of HCl in ACN-HCl-DDQ solutions.

In the PDP in Figure 2.8a, the cathodic current density in HCl + DDQ is about two orders of magnitude greater than the sum of the cathodic current densities in HCl and in DDQ. A similar behavior is seen on Pt (Figure 2.8b), although in this case the difference can only be seen when the cathodic current density is below the diffusion-limited current density of DDQ reduction. Although the difference of cathodic current densities on C-22 could be partially explained by the effect of HCl on the degradation of the surface oxide and consequent improvement of the catalytic properties of the cathode, the same cannot be said of Pt. Thus, there appears to be a synergistic action of HCl and DDQ, making the solution more oxidizing when both are present. The CV on Pt in Figure 2.10 suggests changes in mechanism that could explain the synergistic effect of HCl and DDQ. In HCl + DDQ, the appearance of a reduction pre-wave prior to the wave for the first DDQ reduction step indicates that there is another reducible species in equilibrium with DDQ, which can be reduced under a lower cathodic polarization. Furthermore, on the PDP with Pt in HCl + DDQ (Figure 2.8b), there is a cathodic Tafel line at more positive potentials than that in DDQ. This line transitions into diffusion-limited regime at lower cathodic current density than that in DDQ, also indicating the existence of a stronger oxidant in solution.

Based on the classic 3 x 3 square schemes [45], Scheme 1 illustrates possible electron and proton transfer processes associated with DDQ. As explained before, the phenomena involving the first electron transfer to DDQ are more relevant to corrosion of C-22 because they take place at higher potentials. The appearance of a pre-wave before the first reduction step, thus, deserves attention. Many studies have described the appearance of a pre-wave in CV of quinones upon addition of acids to nonaqueous solvents as a result of the formation of QH^+ (protonated quinone), a species with higher electron affinity than the quinone itself [46–48]. It has also been reported that hydrogen bonding between quinones and acids can cause positive shifts in reduction waves and, in some cases, pre-waves [47]. Although the features observed in the CV are compatible with the protonation of DDQ to $DDQH^+$, the high pK_a of HCl in acetonitrile (8.9) suggests that it is unlikely to significantly donate protons. Other authors have attributed the appearance of a pre-wave to the local modification of the effective pH on the surface of the electrode [49]. This option, however, does not seem to fit our results because the appearance of a new diffusion-limited wave at slow scan rates (Figure 2.8b) indicates the formation of a reasonably stable reducible species. An exact description of the new reduction mechanism of DDQ would require further tests and it is not the focus of this study.

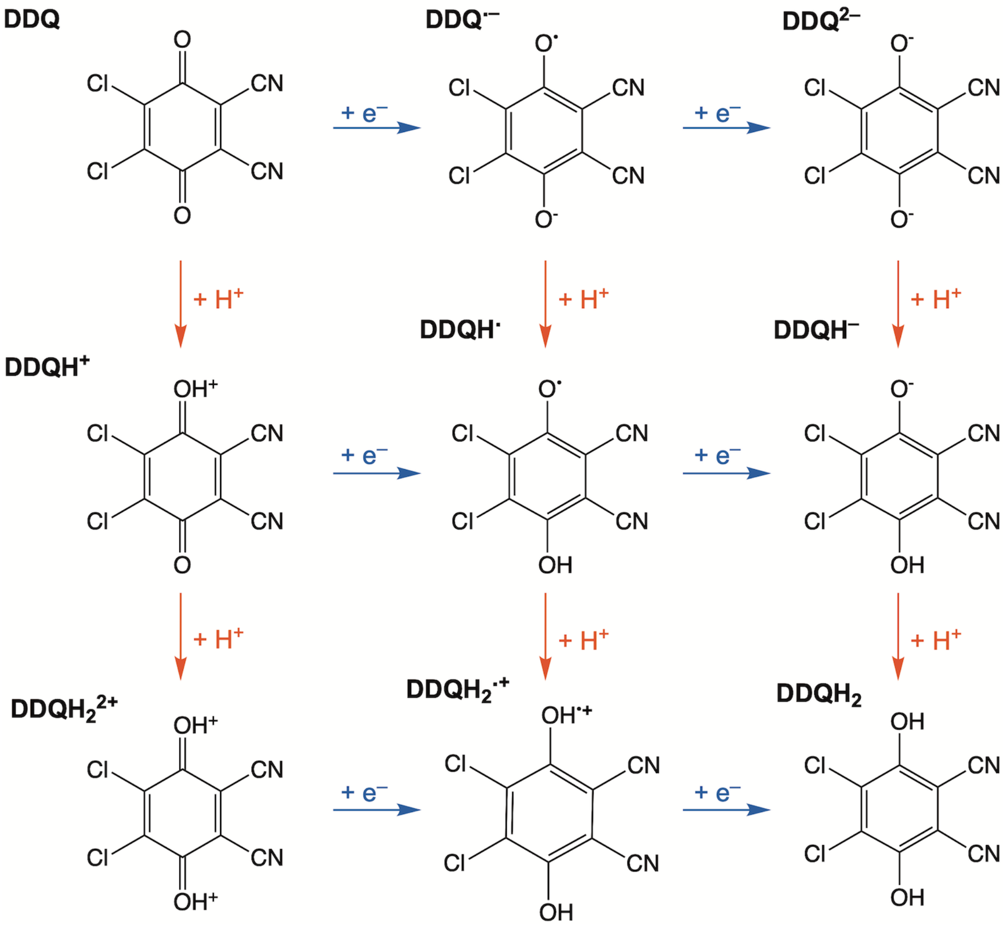

Scheme 1: Possible proton and electron transfer processes involving DDQ.

Conclusions

In order to understand the conditions for corrosion and passivation in solutions typical of organic synthesis, electrochemical techniques and exposure tests were utilized to study the corrosion of C-22 at room temperature in acetonitrile containing chloride from Bu_4NCl or HCl, and the quinone DDQ. The main findings are summarized below:

1. C-22 is passive in neutral Cl^--free acetonitrile containing residual water (100–150 ppm), probably due to the preservation of its air-formed oxide film. When Cl^- is added to the solution by using 140 mM Bu_4NCl, C-22 undergoes pitting upon anodic polarization. The greater susceptibility to pitting in acetonitrile in comparison with water may be a consequence of the weak anion solvation properties of the solvent, which cause a greater activity coefficient for Cl^-.

2. In ACN-HCl and ACN-HCl-DDQ solutions, there is a strong dependence of anodic kinetics on HCl concentration. C-22 can be activated with HCl concentrations as low as 5 mM. In 5 mM HCl, C-22 undergoes an active-passive transition upon anodic polarization. Further increase in HCl concentration results in a decrease of polarization resistance and a completely active anodic behavior. Although HCl behaves as a weak acid due to its weak dissociation in acetonitrile, the anodic behavior seen in potentiodynamic polarizations is similar to that seen in much higher concentrations of aqueous HCl. We presume this is a consequence of the intensification of Cl^- attack, as a result of the solvent's chemical properties.
3. DDQ acts as a strong oxidant towards C-22, leading to high corrosion rates in combination with HCl, as seen in electrochemical and exposure tests. In equimolar concentrations, HCl and DDQ have a synergistic effect on the intensification of cathodic kinetics of C-22 corrosion. As indicated by potentiodynamic tests on Pt, this is a consequence of the change in the mechanism of DDQ reduction in the presence of a source of protons, making the solution more oxidizing.

Acknowledgments

We acknowledge Haynes International (Ajit Mishra) for supplying the samples utilized in this study.

Chapter 3 : The influence of water concentration and solvent properties on the corrosion of C-22 in aprotic solvents containing HCl

Introduction

Ni-Cr-Mo alloys are often used in applications where engineering materials need to withstand aggressive solutions. The good corrosion resistance of these alloys can be attributed to the formation of a Cr-rich oxide on the surface, protecting the bulk material from aggressive environments, and allowing their application in a wide range of solutions and temperatures, including concentrated acids [37], oxidizing solutions, and chloride-rich solutions [2]. Due to its versatility, C-22 (UNS N06022) is often the preferred choice in situations where exceptional corrosion resistance is required.

Various synthesis processes in the chemical and pharmaceutical industries are carried out in organic solvents instead of water [50]. Water has a strong tendency to form hydrogen bonds and presents various peculiar properties as a result, including high boiling and melting points, difficulty to dissolve large molecules and ions, high heat of vaporization and surface tension, etc. Because water easily dissociates in a strong acid (H^+) and strong base (OH^-), its chemical properties are also unique. In many situations where these properties are undesirable, polar aprotic organic solvents are used as solvents, allowing a range of new properties while presenting a reasonably high polarity [9]. However, the influence of these properties on the corrosivity of solutions is vastly unknown, which presents problems for the application of well-known alloys in reaction vessels and other equipment, as well as potential impact on cost, contamination of products, and process safety.

The stability of passive alloys in organic solvents depends on the preservation of the passive film. Therefore, effects of variables that influence the dissolution or formation of a passive film, such as acidity, halide concentration, and residual water concentration, need to be understood. In nearly anhydrous acidified organic solvents, researchers have most often observed that metals dissolve under activation control [12,19,51]. This behavior is usually attributed to some combination of the following reasons: the dissolution of the air-formed oxide film because of acidity; the difficulty to form an oxide film due to lack of water; the effect of acidity on hindering other forms of passivation, such as salt film formation and solvent adsorption [51]. Under these circumstances, addition of water above a certain threshold typically enables the formation of an oxide film.

Very few studies on the effect of halides or halide-containing acids on corrosion in aprotic organic solvents can be found in the literature. Schwabe and Berthold reported that Ni and Fe did not passivate in either anhydrous dimethyl sulfoxide (DMSO) or anhydrous dimethylformamide (DMF) containing H_2SO_4 + HCl. When the water concentration was high enough to form a passive oxide, increase in HCl could cause reactivation [11]. Kikuchi and Aramaki found that addition of Cl^- (as $FeCl_3$) stimulated the anodic dissolution of Fe in anhydrous acetonitrile (ACN), but that addition of Br^- ions (from LiBr) inhibited the anodic process [13]. Ramgopal, on the other hand, reported that C-22 corroded actively in ACN containing 1.92 M HBr and 17 vol% water at 65° C [21].

Despite contributions from numerous researchers, the existing knowledge of corrosion phenomena in organic solvents is still deficient. Our previous studies have shown that C-22 has unusually high rates of uniform corrosion in ACN containing low concentrations of chlorides and oxidants at room temperature [22,52]. Clearly, the concentration of aggressive or passivating species are not the only important variables, and the choice of solvent has substantial impact on the corrosion properties of passive alloys. However, because many studies failed to correlate corrosion phenomena with solvent properties, experimental observations are often not translatable between solvents. In the present study, we investigate the corrosion of C-22 in a range of polar aprotic solvents containing HCl and various concentrations of water using electrochemical methods and discuss the influence of solvent chemical properties (donor strength and acceptor strength) on the phenomena observed.

Experimental

Specimen and solution preparation

This study utilized Ni-Cr-Mo-W Hastelloy C-22 (UNS N06022) sheet samples with 3.5 mm of thickness supplied by Haynes International, USA. The nominal chemical composition of alloy C-22 is 22 wt% Cr, 13 wt% Mo, 3 wt% W, 3 wt% Fe, and balance Ni. Round specimens of diameter 15 mm were machined with a water abrasive jet. Before electrochemical tests, the specimens were ground to P4000 grit using SiC abrasive paper in water.

Acetonitrile (99.8%, Sigma-Aldrich), N,N-dimethylformamide (99.8%, Sigma-Aldrich), N,N-dimethylacetamide (99.8%, Sigma-Aldrich), ferrocene (≥ 98%, Sigma-Aldrich), tetrabutylammonium hexafluorophosphate (≥ 98%, Sigma-Aldrich), tetrabutylammonium chloride (≥ 97%, Sigma-Aldrich), silver nitrate (99.9999 %, Aldrich), and hydrogen chloride in methanol (1.25 m, Sigma-Aldrich) were used as received. All reagents were stored in a desiccator at all times to avoid moisture uptake.

The solutions used in electrochemical tests were prepared by drying solid reagents in closed flasks under 99.999 % N_2 overnight, then adding solvents and liquid reagents with glass syringes. For experiments in which a low residual water concentration was desired (typically below 100 ppm), 4 Å molecular sieves were added to the solution at a 0.15 g per ml ratio. The residual water was determined by Karl Fischer coulometric titration before beginning each test, and water was added with a micropipette when desired. Water concentrations are reported as molarity to allow comparison across the different solvents. The authors are aware that most of the classical literature on corrosion in organic solvents reports water concentrations as mass ratios for practical reasons, so Table 3.1 provides the conversion between the different units.

Table 3.1: Conversion between molarity of water and approximate mass ratios with ACN, DMF and DMA.

H_2O molarity /M	10^{-4}	10^{-3}	10^{-2}	10^{-1}	10^{0}	10^{1}
H_2O:ACN	2.3 ppm	23 ppm	230 ppm	0.23 wt%	2.3 wt%	28 wt%
H_2O:DMF	2.0 ppm	20 ppm	200 ppm	0.20 wt%	2.0 wt%	23 wt%
H_2O:DMA	2.0 ppm	20 ppm	200 ppm	0.20 wt%	2.0 wt%	23 wt%

Electrochemical techniques

Potentiodynamic polarization (PDP) and electrochemical impedance spectroscopy (EIS) were carried out with either C-22 or Pt working electrodes. The Pt electrode was a disc of diameter 1.6 mm (BASi); the C-22 electrodes consisted of specimens exposed through an opening at the bottom of the cell, with an exposed area of 0.785 cm^2. The electrochemical cell was an air-tight flat cell composed of glass and PTFE parts. The counter electrode was a coiled Pt wire of length 20 cm and diameter 0.25 mm.

As explained in detail in a previous publication [52], the reference electrode (RE) consisted of a silver wire immersed in a solution of 0.01 M $AgNO_3$ + 0.1 M Bu_4NPF_6 in the same solvent as that of the test solution, enclosed in a glass tube with a Vycor frit. The potential of each RE was periodically determined by comparison with the half-wave potential of the ferrocene/ferrocenium redox pair in acetonitrile (Fc/Fc^+) determined by 100 mV s^{-1} cyclic voltammetry. The potentials were: -98 ± 1.8 mV vs Fc/Fc^+ for the ACN-based RE; -39 ± 2.8 mV vs Fc/Fc^+ for the DMF-based RE; and -102 ± 4.9 mV vs Fc/Fc^+ for the DMA-based RE. For the DMF- and DMA-based RE, the RE potential was assessed before each test. In order to facilitate the comparison between phenomena in different solvents, we use the Fc/Fc^+ potential as a reference in the text and in the figures. Values informed in the Fc/Fc^+ potential scale can be converted to the standard hydrogen electrode (SHE) scale by adding 624 mV [30].

Before beginning each test, the electrochemical cell was purged with N_2 gas for at least 10 min, then the solution was transferred from another N_2-pressurized flask via a double-tipped needle. Under N_2 atmosphere at room temperature, the electrochemical techniques were performed using a Bio-Logic SP-150 potentiostat (Bio-Logic USA). Before starting EIS measurements, open circuit potential (OCP) was measured for 1 h. EIS was performed using an excitation signal of amplitude 10 mV, with frequency sweeps from 100 kHz to 10 mHz and in the reverse direction, separated by 5 min at OCP. PDP was performed as a full potential cycle, with scan rate 1 mV s^{-1}. PDP was carried with automatic compensation of 85% of ohmic drop in the solution, using the solution resistance (R_S) obtained from high-frequency impedance (typically above 10 kHz).

For chronoamperometry using the scratched electrode technique, samples were polarized at the chosen potential of 0.3 V vs Fc/Fc^+ for the entire test without interruption. At this potential C-22 presents a passive region with similar current densities in the three solvents, so the behavior can be compared. After 10 min of polarization, a small port on the top of the cell was momentarily opened to insert a sharp glass scribe used to scratch the surface of the sample.

Characterization

After the PDP scans, specimens were rinsed with isopropanol and examined using scanning electron microscopy (FEI Quanta 650).

Results

PDP in neutral, chloride-free aprotic solvent solutions

To understand the passivity of C-22 in aprotic organic solvents, PDP was initially performed in the absence of chlorides. Figure 3.1 shows a series of potentiodynamic scans with either C-22 or Pt in solutions of ACN (Figure 3.1-a), DMF (Figure 3.1-b) and DMA (Figure 3.1-c) with 0.1 M Bu_4NPF_6 as a supporting electrolyte. Due to the noble properties of Pt, we can assume that the anodic current density (*i*) measured on the Pt electrode is due to reactions involving solely the solvent-electrolyte mixture, without oxidation of the electrode material. Taking the potential to achieve a current density of 10^{-4} A·cm^{-2} as a measure of the upper limit of the electrochemical window, it can be said that the DMA-based Bu_4NPF_6 electrolyte oxidizes at the lowest potential (0.867 V vs Fc/Fc$^+$), followed by DMF (1.058 V vs Fc/Fc$^+$) and ACN (1.492 V vs Fc/Fc$^+$).

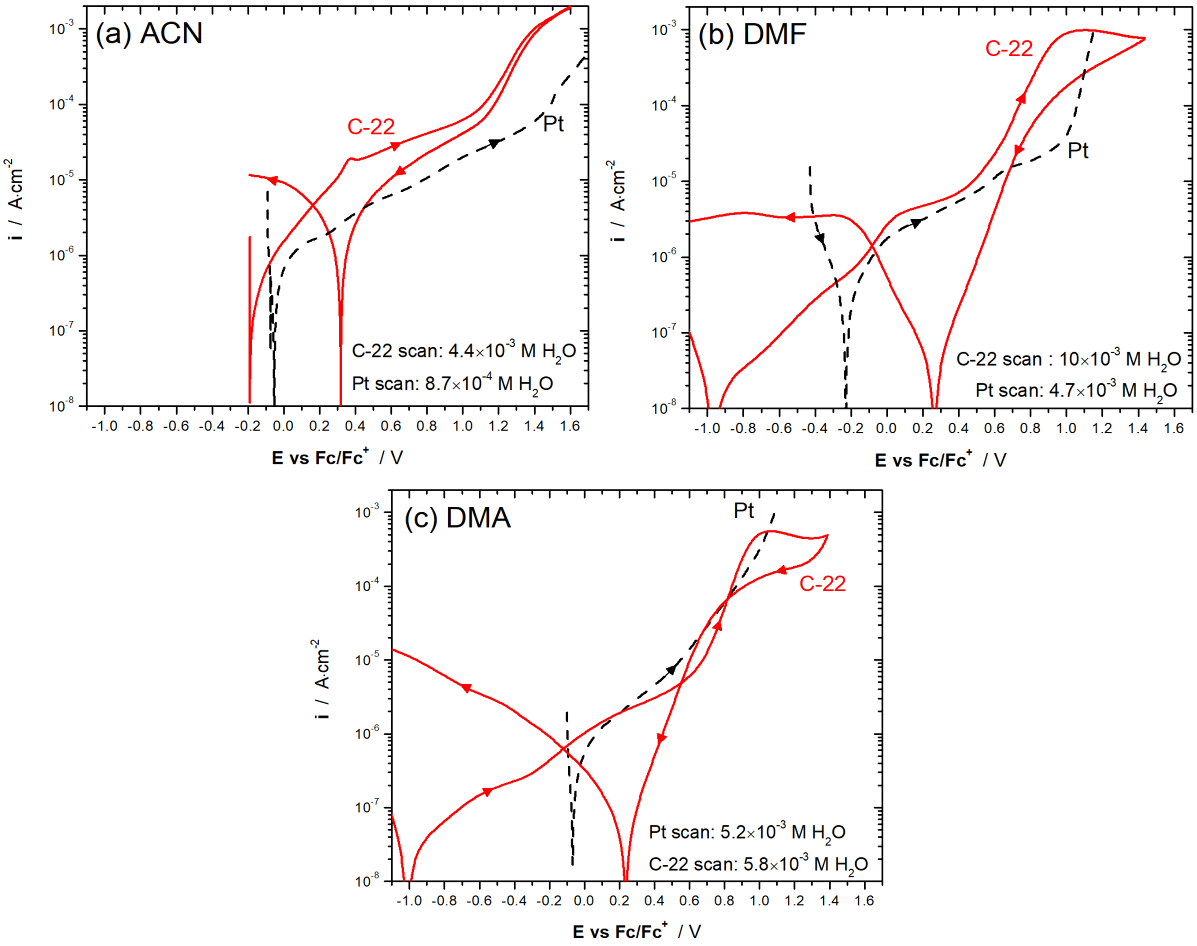

Figure 3.1: Potentiodynamic polarization scans of C-22 and Pt in (a) ACN, (b) DMF, and (c) DMA at scan rate 1 mV/s. All solutions contained 0.1 M Bu_4NPF_6 as supporting electrolyte. The concentration

In all three solvents the anodic scans on C-22 show a wide passive region with higher current densities than on Pt, eventually reaching a transpassive region and negative hysteresis upon reversal of the scan direction. The potential necessary to reach 10^{-4} A·cm^{-2} is the lowest in DMF (0.737 V), followed by DMA (0.842), and highest in ACN (1.117 V vs Fc/Fc^{+}). In DMF and in ACN, *i* on C-22 rises to values well above those on Pt, indicating that oxidation of the metal is most probably taking place. It can be said that C-22 is more easily anodically dissolved in DMF because the anodic current starts rising at lower potentials. In DMA, however, the rise in *i* on C-22 overlaps with that measured on Pt, indicating that the current measured on C-22 is, to some degree, the result of oxidation of the solvent-electrolyte mixture. A discussion including the surface alteration after prolonged periods at the transpassive region for the case of ACN can be found in a previous publication [52].

Chronoamperometry using the scratched electrode technique in neutral, chloride-free aprotic solvents

Although Figure 3.1 already shows wide passive regions in the three solvents, the ability of C-22 to form a protective oxide layer in solution is more clearly observed when the bare surface is exposed to solution, without the influence of the air-formed film. Therefore, potentiostatic chronoamperometry was carried out in combination with *in situ* scratching of the electrode's surface (Figure 3.2). The potential was held at 0.3V vs Fc/Fc+ for the entire duration of these tests. The surface was manually scratched with a glass scribe after 10 min, when the current transient was already stable.

All the current transients obtained in Figure 3.2-a show a combination of two features: a sharp current spike when the scribe touches –and scratches– the surface; and a comparatively slower elevation in current that begins either after or just before the scratch and decays slowly. The original current transients can be compared with the situations shown in Figure 3.2-b – manual stirring of the solution with a glass rod (without touching the surface of the electrode) and bubbling of N_2 gas near the C-22 surface – which also cause a rise in current with slow decay. It can be inferred that the transients in Figure 3.2-a show both the effect of exposing a small area of bare metal (the scratched area) and the stirring effect caused by the scribe's movement. Figure 3.2-c shows the current transients caused by the scratches after subtraction of their baseline and normalization of the current by the peak current value. Clearly, repassivation of the bare surface happens rapidly in all three solvents, despite the low levels of residual water.

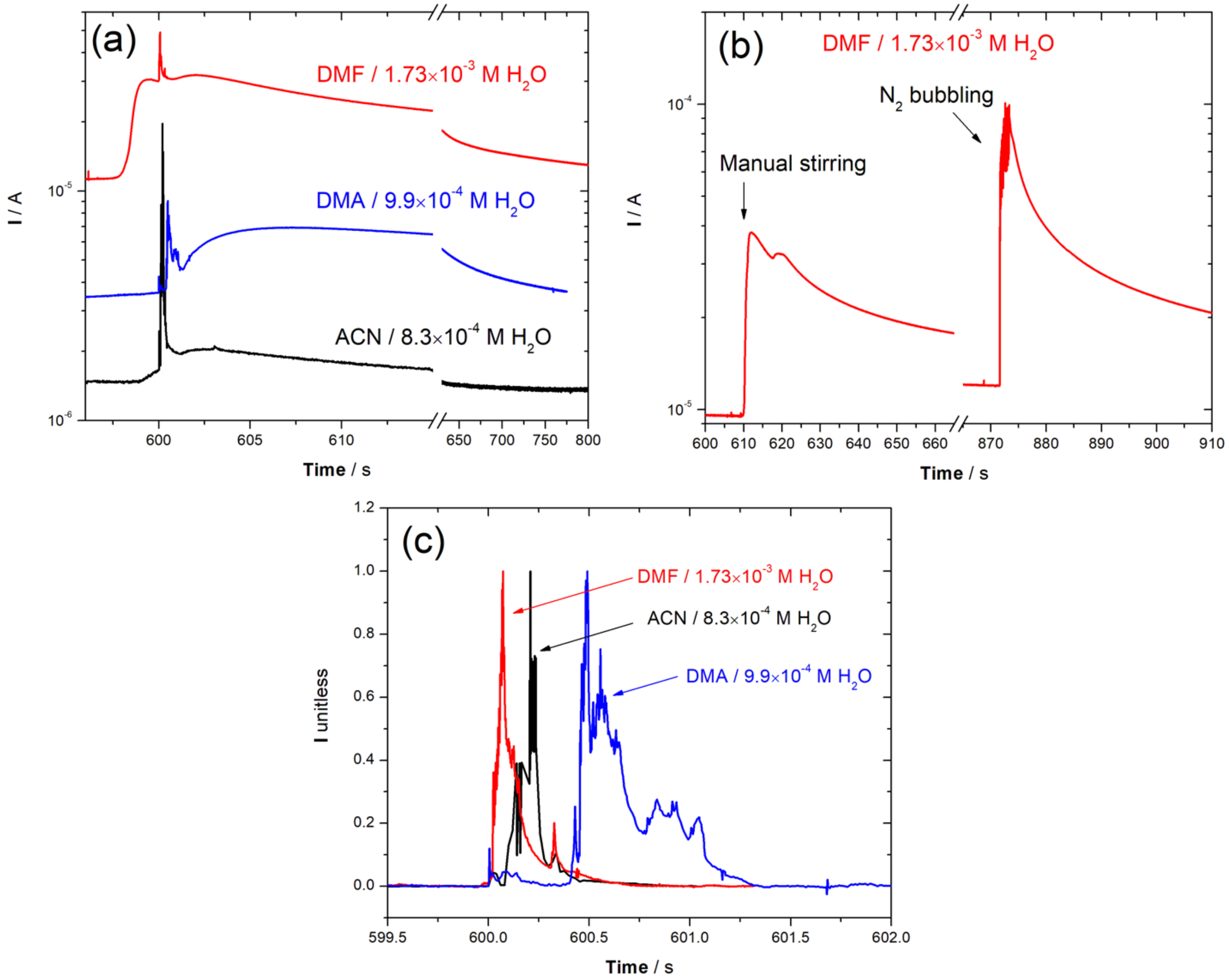

Figure 3.2: Potentiostatic chronoamperometry at 0.3 V vs Fc/Fc$^+$ using the scratched electrode technique on C-22 in aprotic solvents with low residual water concentrations: a) current transients obtained while scratching C-22. b) example of peaks produced by manual stirring and by bubbling N$_2$ near the electrode's surface. c) Same scratches shown in figure (a) after baseline subtraction and normalization of current by peak current.

PDP in aprotic solvents containing HCl

To aid the interpretation of the anodic processes occurring on C-22 in aprotic solvents, it is useful to first study what faradaic reactions take place in these solutions and how they are affected by water inside the range of potentials of interest. Figure 3.3 shows a series of anodic PDP scans with a Pt working electrode in solutions of aprotic solvents (containing 0.1 M Bu$_4$NPF$_6$ as supporting electrolyte) with or without 0.11 M HCl, and various concentrations of residual water. When HCl is not present, addition of water generally increases the anodic current density measured on Pt and provokes a negative shift of the upper limit of the electrochemical window. Particularly in DMF and in DMA, addition of water causes the emergence of a new Tafel slope (265 and 242 mV/dec in DMF and DMA, respectively, at 4.8 M H_2O), indicating a new electrochemical reaction, probably oxidation of water. In DMF, this behavior changes above 1.0 V, where curves begin to align at the same Tafel slope (93 mV/dec), suggesting that the DMF-electrolyte mixture starts to oxidize. For ACN, however, addition of water only causes a shift of the current to lower potentials without changing the Tafel slope (circa 328 mV/dec). Thus, the same oxidation reaction limits the electrochemical window at low or high concentrations of water and is facilitated by addition of water.

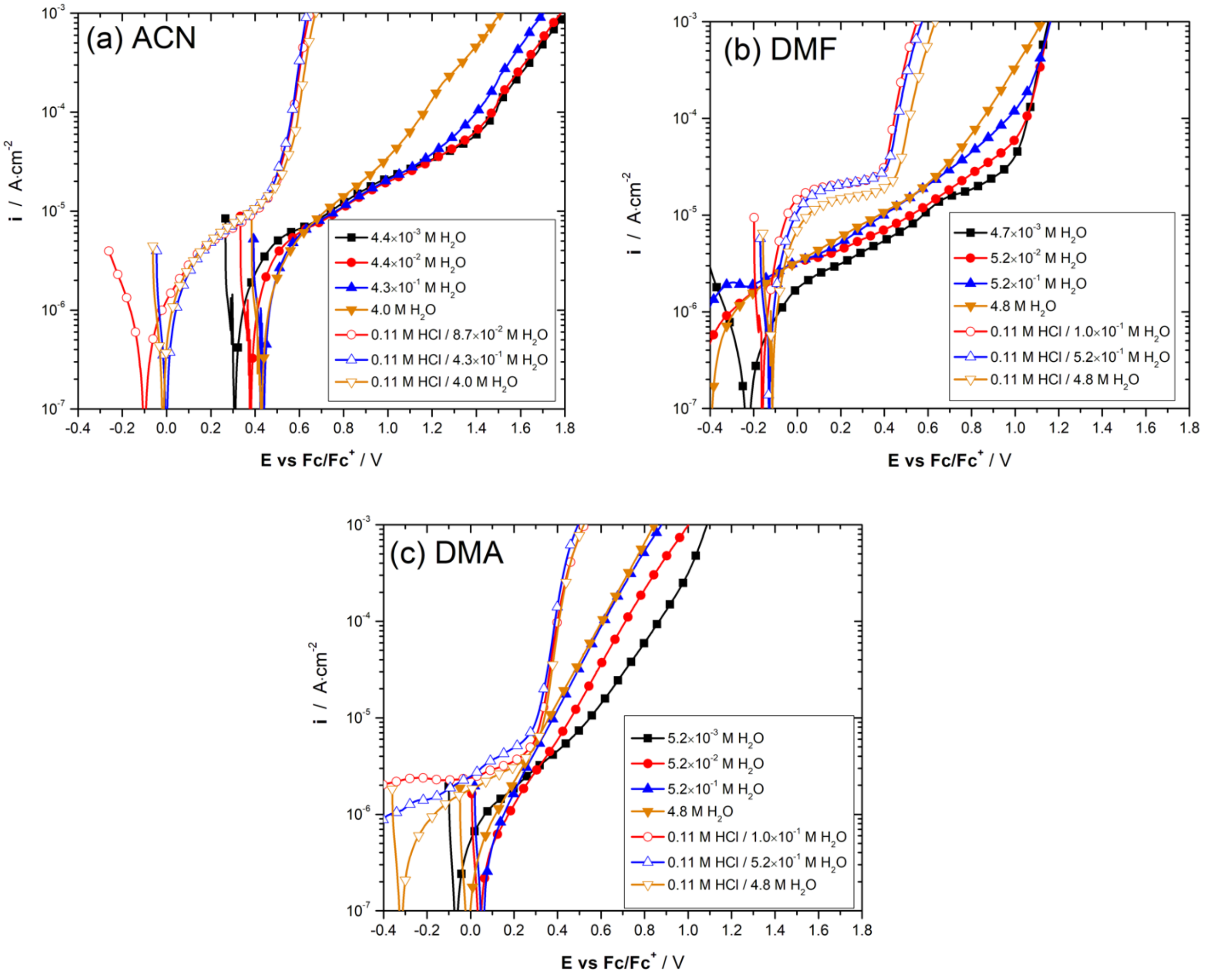

Figure 3.3: Potentiodynamic polarization scans (1 mV/s) of Pt in aprotic solvents (ACN, DMF and DMA) either with or without 0.11 M HCl, and with various water concentrations. All solutions contained 0.1 M Bu_4NPF_6 as supporting electrolyte.

When HCl is added to either of the solvents, the rise in anodic current density takes place at lower potentials, with Tafel slopes of 67, 83, and 68 mV/dec for ACN, DMF, and DMA, respectively (for H_2O concentrations between 87 and 100 mM). The earlier rise in current implies the introduction of a new electrochemical reaction involving oxidation of HCl (or Cl^-, depending on the pK_a of HCl in each solvent). Using the potential to achieve 30 $\mu A.cm^{-2}$ as a measure to compare the three solvents, it becomes evident that this process takes place at the lowest potential in DMA (0.364 V), followed by DMF (0.395 V) and ACN (0.520 V). For all three solvents, this process is little impacted by the addition of water up to 0.5 M but is slightly shifted to more anodic potentials when a concentration of circa 5 M H_2O is used. It should be noted that no corrosion of the Pt electrode was observed after any of the scans, as assessed by optical microscopy.

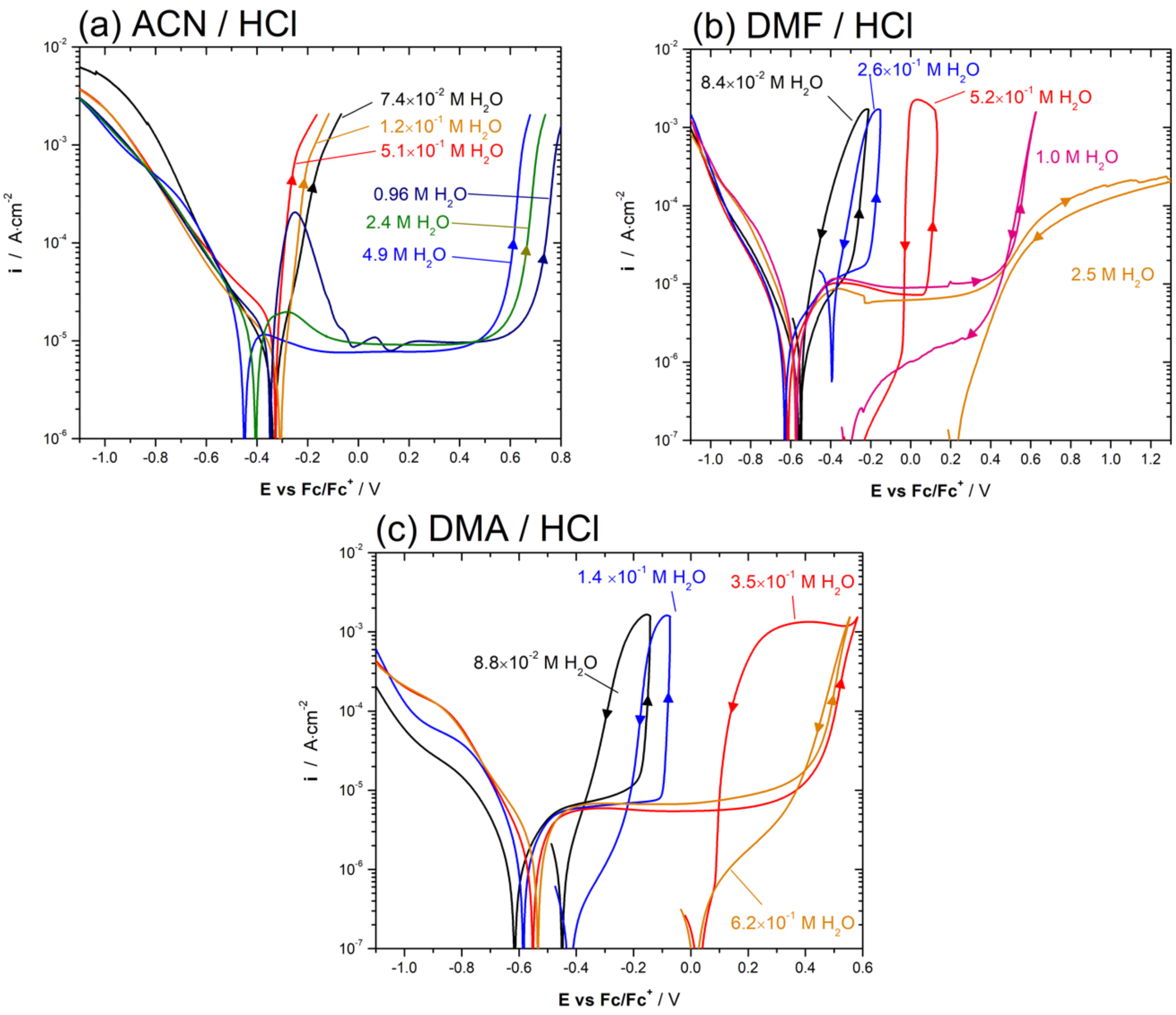

Figure 3.4: Potentiodynamic polarization scans (1 mV/s) of C-22 in aprotic solvents (ACN, DMF and DMA) with 0.11 M HCl and various water concentrations. All solutions contained 0.1 M Bu_4NPF_6 as supporting electrolyte.

Figure 3.4 shows a series of PDP scans of C-22 in aprotic solvent solutions containing 0.1M Bu_4NPF_6 as supporting electrolyte, 0.11 M HCl, and different concentrations of water. When ACN is used as a solvent (Figure 3.4-a.), C-22 undergoes active dissolution upon anodic polarization, without signs of passivation in low concentrations of residual water. As water concentration is increased up to 0.5 M, the kinetics of anodic dissolution are enhanced, as shown by a shift of the anodic branch to lower potentials. This behavior contrasts with reports in the literature that state that small additions of water to acidified organic solvents generally result in corrosion inhibition by formation of an oxide layer [10].

For a water concentration of 0.96 M, an active-passive transition is observed, and further addition of water results in decrease of height of the active nose as well as a decrease in passive current density for most potentials. This passive region extends up to circa 0.5 V vs Fc/Fc^+, where current density rises again, forming a transpassive region. This region shifts to lower potentials if water concentration is further increased, indicating an enhancement of the transpassive behavior. It should be noted that the transpassive region is situated at potentials where oxidation of the HCl solution was observed on Pt (Figure 3.3-a) and it presents a similar Tafel slope. Unlike the PDP on Pt, however, addition of water shifts the rise in current density to lower potentials. The Tafel slopes measured at this segment (67.5 mV/dec for 0.96 M, 56 mV/dec for 2.4 M, and 53.5 mV/dec for 4.9 M water) also decrease with addition of water. The effect of water on the cathodic branch is not clear, except for potentials below -0.8 V vs Fc/Fc^+, where water additions decrease the magnitude of cathodic current densities.

The reverse scan portion of the PDP in ACN was omitted for clarity because it does not present any different features from the forward scan portion. For DMF and DMA-based HCl solutions (Figure 3.4-b and Figure 3.4-c), the entire PDP cycles are shown. Both in DMF and in DMA, C-22 is initially passive upon anodic polarization, until a breakdown potential (E_{pit}) is achieved. In all cases, the scanning direction was reversed after achieving a current density of 2 $mA \cdot cm^{-2}$. Generally, if residual water concentration is low enough, the behavior is typical of localized corrosion, with a reverse scan marked by positive hysteresis followed by repassivation. As water concentration is increased, both the E_{pit} and the repassivation potential (E_{rep}) shift to higher potentials.

When water is above a critical concentration, no localized corrosion features are found, and either very small positive or completely negative hysteresis is observed in the reverse scan. This critical water concentration, above which localized corrosion is not seen in PDP, is between 0.5 and 1 M in DMF; in DMA, the same happens between 0.35 and 0.62 M H_2O. Above these values of water concentration, the behavior observed is characteristic of transpassive dissolution, and the specimens presented no sign of localized corrosion. As in ACN-HCl solutions, the transpassive region seen in DMF- and DMA-HCl solutions overlaps with the potentials where oxidation of the HCl solution was observed on Pt (Figure 3.3-b and Figure 3.3-c) and Tafel slopes are similar (74 mV/dec in DMA-HCl / 0.62 M H_2O, 74 mV/dec in DMF-HCl / 1.0 M H_2O). For DMA-HCl with 0.35 M H_2O, localized corrosion initiates on the transpassive region and the exact breakdown potential is not clear, although a large positive hysteresis is observed in the reverse scan. In a few solutions with very high water concentrations such as the case of DMF-HCl / 2.5 M H_2O, the transpassive region becomes curved, similarly to what was seen in DMF without HCl.

Scanning Electron Microscopy of corroded specimens

The specimens exposed to PDP in Figure 3.4 were examined by SEM, and images are shown in Figures Figure 3.5, Figure 3.6, and Figure 3.7. Figure 3.5 shows the typical morphology obtained when C-22 is polarized to anodic current densities of a few mA/cm^2 in ACN – HCl with water concentrations up to 0.5 M. The surface is the result of uniform corrosion, and the slight differences in depth of attack and angle of facets reveal the grain patterns. This morphology did not seem to be affected by water concentration in the range of concentrations that enabled active behavior.

When DMF was used as solvent (Figure 3.6), the morphology is completely different, showing pits surrounded by preserved areas. For the lowest water concentration of 84 mM, pit diameter is in the order of 100 nm and pits are preferentially nucleated in scratches produced during specimen preparation. Although in severely degraded areas this morphology can resemble that of uniform corrosion, this mode of corrosion is clearly distinct from that seen in ACN (Figure 3.5). When the water concentration is increased, pit size increases (diameter ≈ 0.5 μm) and the number of pits per area decreases by orders of magnitude. At 0.52 M H_2O, pit diameter is in the order of 10 μm and the bottom of pits reveals the crystal facets textured

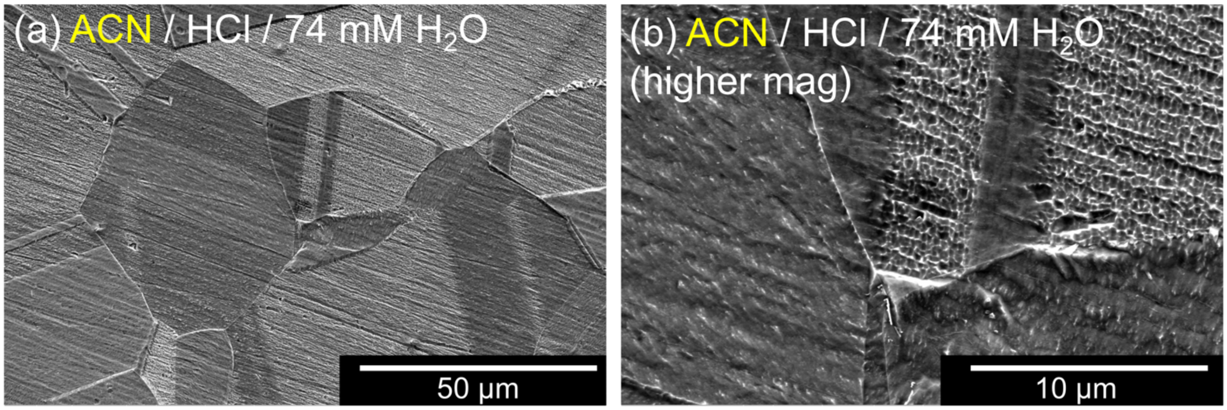

Figure 3.5: Scanning electron micrographs of C-22 after PDP in ACN / 0.11 M HCl with a low water concentration.

with spikes (Figure 3.6-c). Surprisingly, the specimen polarized in the transpassive region in DMF- HCl / 1.0 M H_2O still shows a few isolated areas where small pits could be found (Figure 3.6-d), even though no positive hysteresis was seen in PDP.

The corrosion morphology of C-22 in DMA-based HCl solutions (Figure 3.7) is similar to that in DMF solutions, and pit size and frequency of occurrence have a similar dependence on water concentration. In DMA-HCl with 0.35 M H_2O (Figure 3.7-c and d), and unusual localized corrosion morphology is observed. Pits are typically composed of a central orifice connected to surrounding deeply corroded areas. These areas propagate as a combination of deep attack (producing in an acicular appearance) and partially covered channels. When DMA-HCl solutions contained higher water concentrations than 0.35 M, no corrosion was observed.

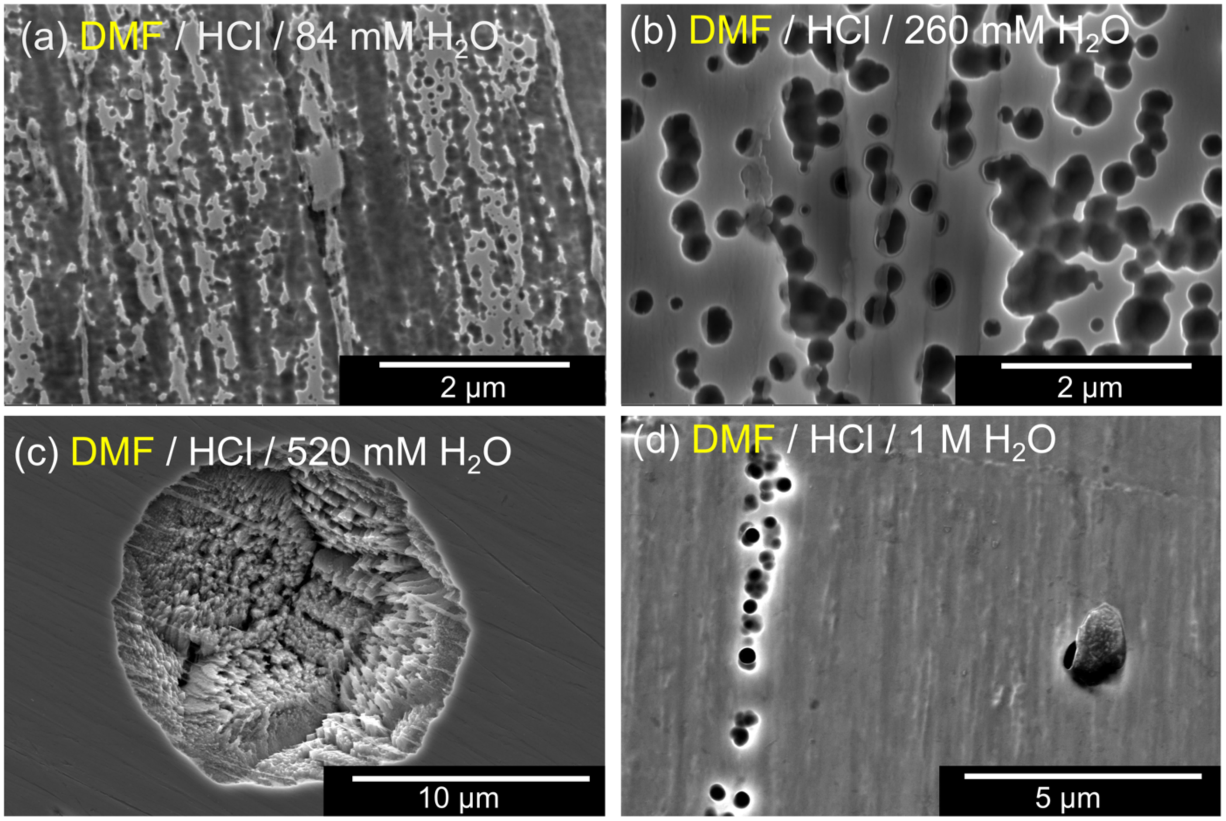

Figure 3.6: Scanning electron micrographs of C-22 after PDP in DMF / 0.11 M HCl with various water concentrations.

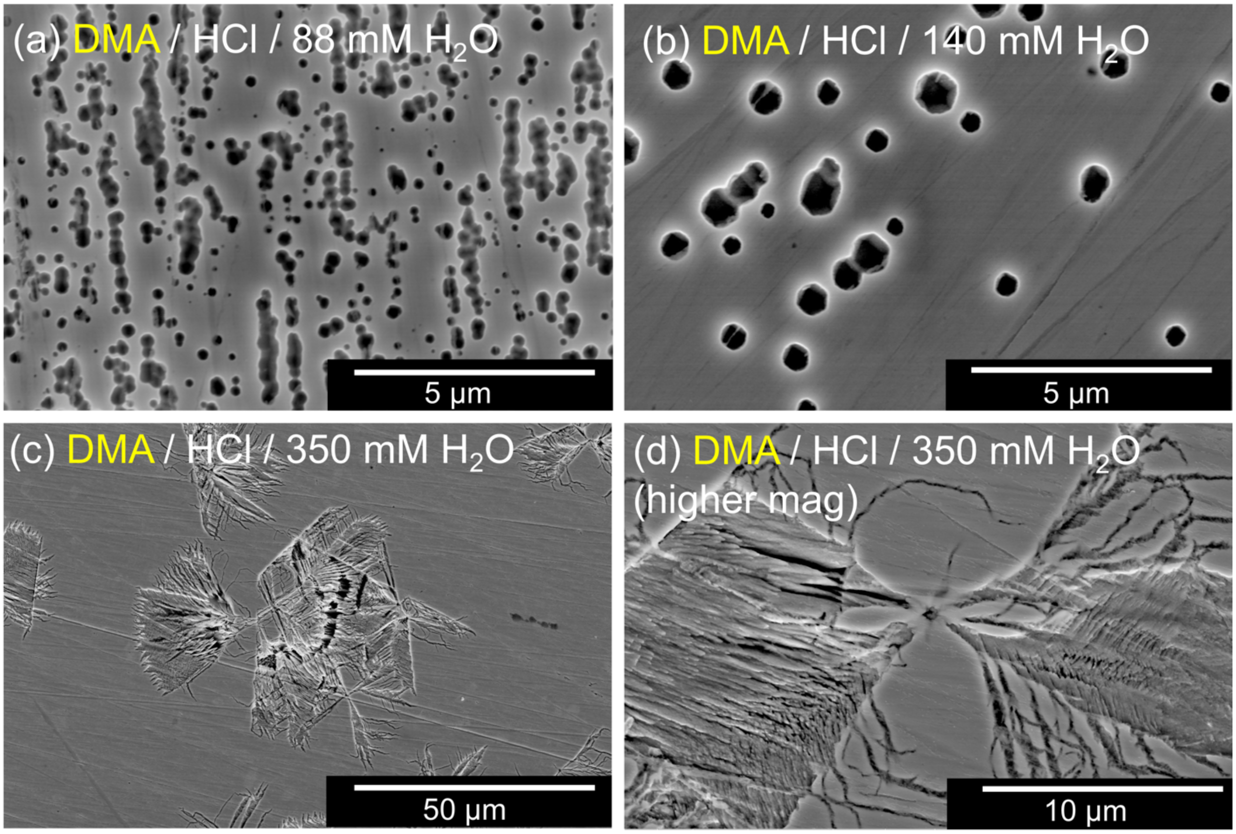

Figure 3.7: Scanning electron micrographs of C-22 after PDP in DMA / 0.11 M HCl with various water concentrations, as shown in Fig. 3c.

Electrochemical Impedance Spectroscopy

The effects of different solvents and residual water concentration on the phenomena taking place at the corrosion potential were studied by EIS (Figure 3.8), in the range of water concentrations for which water was seen to have effects on corrosion phenomena in PDP, for each solvent. In order to capture the influence of time on each spectrum, EIS was scanned as a frequency cycle, as explained in detail in a previous publication [52]. This approach allows for a more accurate and simple description of the system because it makes time-dependent distortions in the low-frequency range more evident. Finally, the spectra can be fitted by a modified Randles circuit composed of solution resistance (R_S) and a constant phase element (CPE, or Q) in parallel with polarization resistance (R_P), as previously used by other authors for C-22 in aqueous 0.1M HCl [32]. The data points which were excessively affected by the transient behavior – typically below 0.05 Hz – were not included in the fitting calculations. Thus, the fits do not assume a complete steady state and they represent a better description of the impedance spectra at the beginning and at the end of the acquisition cycle.

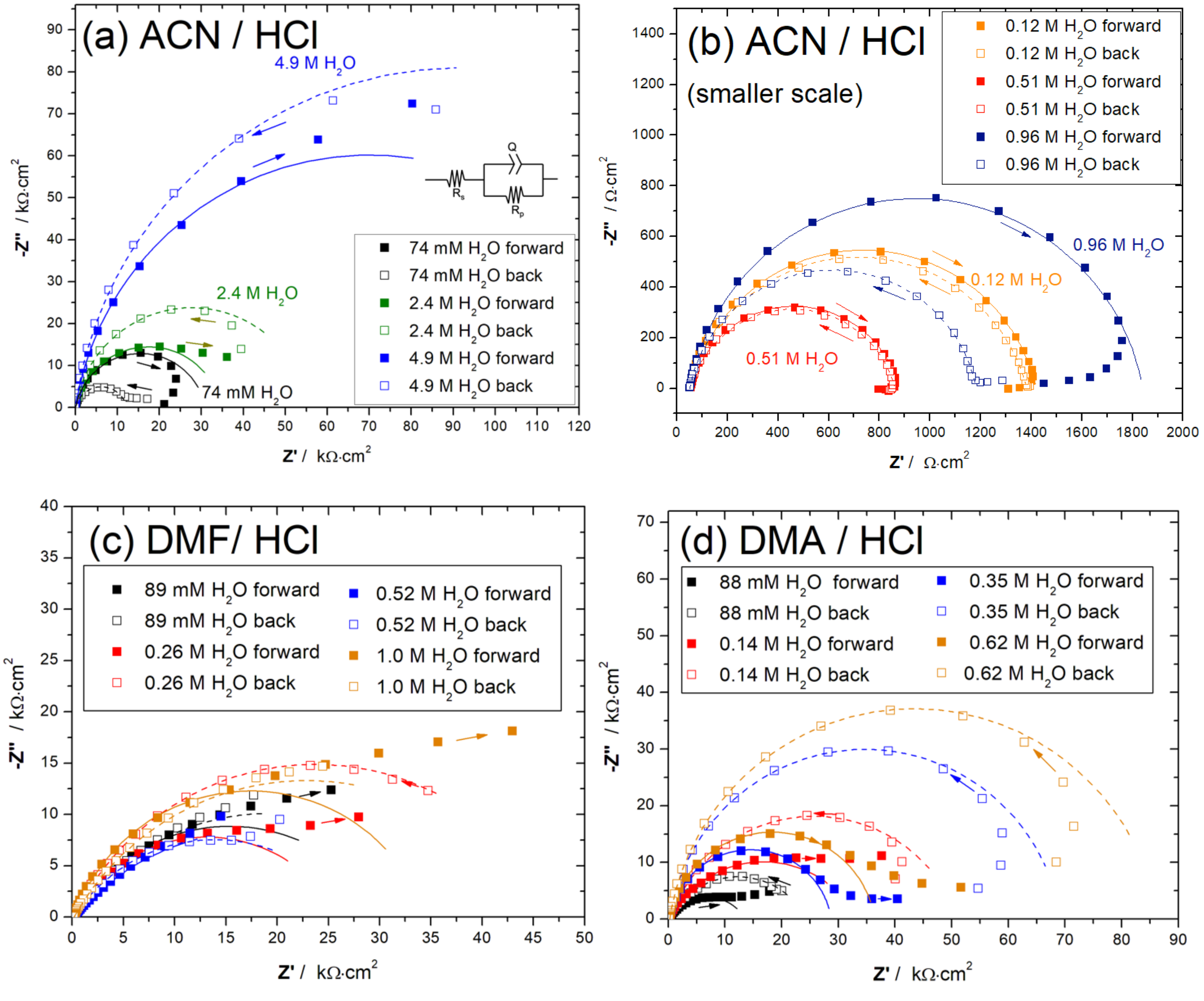

Figure 3.8: Electrochemical impedance spectra at open circuit potential for C-22 in ACN, DMF, or DMA with 0.11 M HCl and 0.1 M Bu_4NPF_6 as supporting electrolyte. Frequency was scanned in cycle, where "forward" denotes the sweep from high 100 kHz to 10 mHz, and "back" is the reverse sweep. Continuous lines are fits for the forward sweeps, dashed lines are fits for the back sweeps.

The results in ACN-HCL solutions (Figure 3.8-a,b) are divided in two plots due to the difference in magnitude between the spectra. Clearly, the concentration of water affects both the magnitude of impedance spectras and their change over time. For the very low (74 mM) and very high water concentrations (2.4 and 4.9 M) in Figure 3.8-a, the magnitude of impedance is considerably larger than in intermediate water concentrations in Figure 3.8-b. Only for 2.4 and 4.9 M H_2O does the semicircle diameter appear to be growing over time, with a reverse scan (increasing frequency) resulting in a larger semicircle than the forward scan (decreasing frequency); for lower water concentrations, the opposite behavior is observed. When DMF is used as a solvent (Figure 3.8-c), the magnitude of impedance spectra does not change much with the addition of water, and the transient behavior does not present any visually obvious trend. In the case of DMA, however, additions of water seem to increase the diameter of semicircles for all concentrations tested, and the modulus of impedance is generally growing over the time of acquisition.

Figure 3.9 shows the results of fitting of cyclic EIS data, along with E_{corr} measurements, for different water concentrations in different solvents. In ACN (Figure 3.9-a), increasing the concentration of water up to 0.5 M results in a decrease of R_P; above 0.5 M, further increase in water content causes an increase of R_P. The influence of water on E_{corr} is similar – up to a concentration of 1 M, water causes decrease of E_{corr}; above 1 M water causes an increase of E_{corr}, although the last data point deviates from that trend. When comparing initial and final values, a decrease in both E_{corr} and R_P over time is observed up to 1 M H_2O. For higher concentrations of water, R_P and E_{corr} both increase with time. According to mixed potential theory, because E_{corr} and i_{corr} (which is assumed inversely proportional to R_P) are moving in opposite directions, changes in i_{corr} are predominantly caused by changes in anodic kinetics. Thus, up to 0.5–1.0 M H_2O, water additions cause enhancement of anodic kinetics; for higher water concentrations, anodic dissolution is hindered. These results agree with the shift of the anodic branch in PDP observed in Figure 3.4-a. Using the same reasoning, it can be said that anodic processes become progressively more active with time for concentrations lower than 1.0 M, but decrease over time for higher concentrations.

When DMF or DMA are used as solvents, the effect of water on i_{corr} is much smaller. In DMA-HCl, both E_{corr} and R_P increase with water concentration and increase with time for all concentrations tested. As in the higher concentrations of water in ACN, the change in corrosion rate is driven primarily by the diminishing of anodic kinetics. In DMF-HCl, R_P (or i_{corr}) seems almost independent of water concentration, while E_{corr} increases to a maximum at circa 0.5 M and then decreases again. The increase in E_{corr} for a stable i_{corr} could be a result of an increase in cathodic kinetics while maintaining a passive condition. Generally speaking, the behavior of R_P in DMF and DMA is similar to that of high concentrations in ACN, with values in the order of 10^4 $\text{Ohm}\cdot\text{cm}^2$ and increasing with time of exposure.

The effective capacitance (C_{eff}) of the CPE used in fitting was estimated using the equation developed by Brug et al.[53]:

$$C_{eff} = Q^{\frac{1}{\alpha}} \left(\frac{R_e R_s}{R_e + R_s} \right)^{\frac{1-\alpha}{\alpha}} \quad (1)$$

For ACN-HCl (Figure 3.9-a), C_{eff} initially increases with water concentration, achieves a maximum at circa 1 M H_2O, and then decreases, showing a trend that is roughly the opposite of that of R_P. Assuming that the capacitive behavior is mostly determined by the properties of a surface film and assuming that C_{eff} is inversely proportional to the thickness of a surface film [54], the oxide film thickness can be assumed to be the smallest at 1 M H_2O, which lies near the highest i_{corr} measured. However, it should be noted that, because C-22 does not show a passive region near the corrosion potential for water concentrations below 1M, it is not clear what would be the nature of the surface film or if it exists in this case. Above 1 M H_2O , C_{eff} decreases with increasing water concentration and it is reasonable to state that a thicker passive film is present, which is in agreement with the predominantly passive behavior observed in PDP.

In DMF- and DMA-HCl solutions, C_{eff} is much lower than in ACN, which indicates a thicker oxide film at the E_{corr}. Also, in these cases C_{eff} does not vary as much with water concentration, in accordance with the more stable values for R_P. Nevertheless, it is observed that the interpretation of C_{eff} and R_P as indicators of film protectiveness is, in a few cases, in conflict with the analysis of R_P and E_{corr} using mixed potential theory. At concentrations above 1 M H_2O in ACN, for example, C-22 appears to be progressively more passive, as indicated by the increase in R_P associated with a rise in E_{corr}, suggesting a decrease in anodic kinetics. However, C_{eff} also increases with time, which suggests a thinning of the passive film or an increase in its dielectric constant. Thus, there could be other factors influencing the changes in capacitance as well as changes in dielectric properties of the film. Still, these differences are small and can easily fall in the error of the estimation of C_{eff} using equation (1), as pointed by Orazem et al. [54].

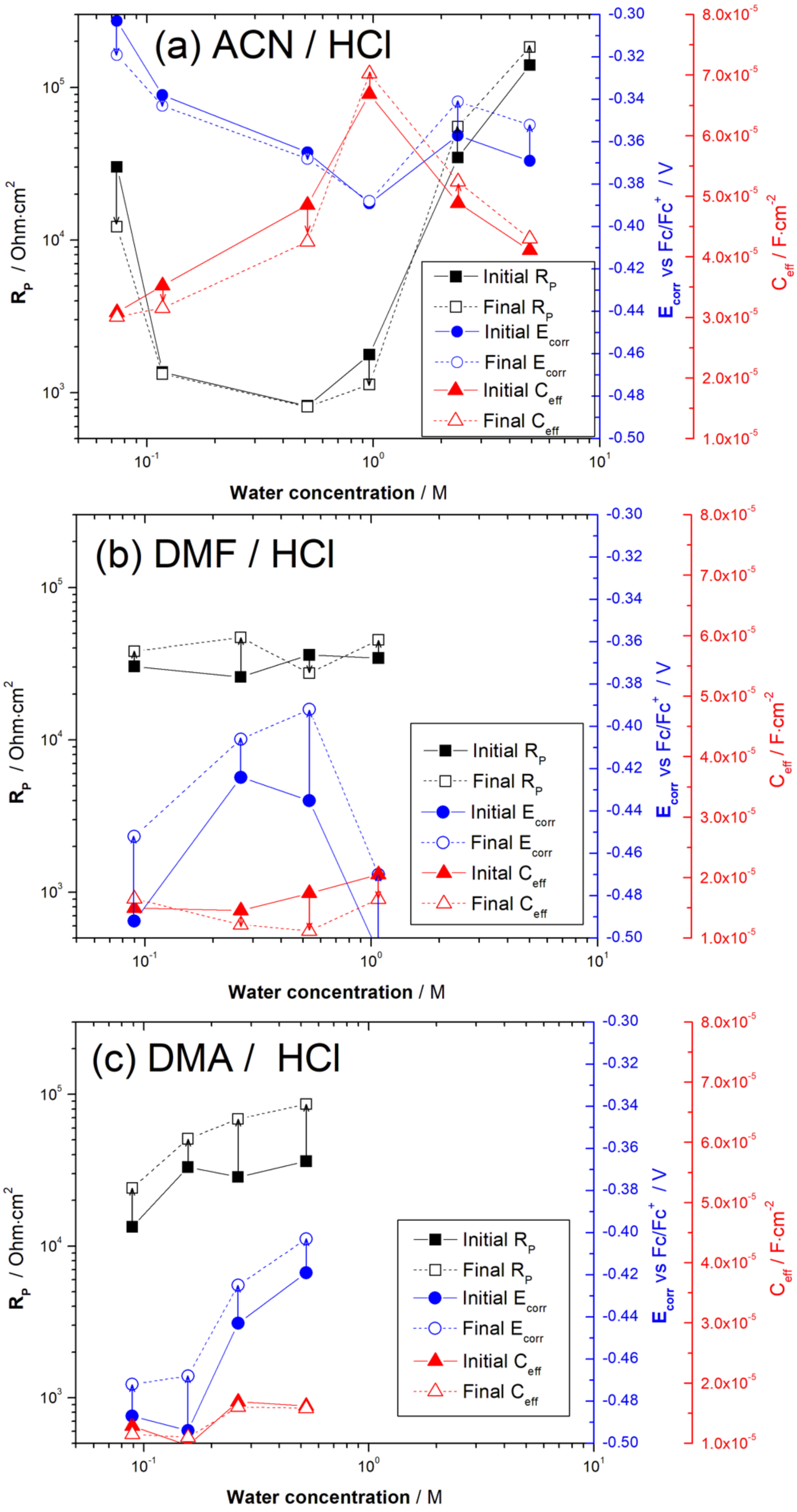

Figure 3.9: Parameters extracted from fitting of EIS spectra shown in Figure 3.8.

Discussion

Passivity in pure aprotic solvents

As shown in Figure 3.1 and Figure 3.2, in the absence of HCl, C-22 remains passive in all three solvents for a wide range of anodic polarization, and it can repassivate after local rupture of the oxide even at very low concentrations of water. Thus, in the absence of aggressive species, the passive oxide is stable in all three solvents despite their different chemical properties. Because water is more polar than the other solvents studied, even at small concentrations H_2O likely adsorbs readily on the surface of the metal when the oxide is removed, initiating the process of oxide formation. It can be observed that stirring of the solution also provokes temporary elevation of anodic current density. Some authors have attributed this mass transport effect to more unstable forms of passivation, afforded by adsorbed layers or interfacial salt films [19]. It should be noted that the working electrode was at the bottom of the electrochemical cell in all experiments, so corrosion products (which are typically dense) can accumulate in front of the electrode. Thus, we cannot exclude the possibility of an additional, less efficient form of passivation caused by the accumulation of some corrosion product on the face of the working electrode.

Chemical properties of solvents and their importance to corrosion

In order to understand how the properties of the solvent affect the corrosivity of HCl solutions, it is useful to examine the interactions between the solvent and species that play important roles in corrosion and passivation, such as Cl^-, H^+ and OH^-. The effect of solvent properties on the chemical and electrochemical behavior of such ionic species in solution has been described by authors using the scales of Acceptor Number (AN) and Donor Number (DN) developed by Gutmann [55]. The AN describes the acidity of the solvent, or its ability to solvate small anions such as Cl^- and OH^-. As discussed in a previous study, solutions of solvents with high AN could be very aggressive when containing chlorides due to the increased Gibbs free energy of solvation and, consequently, higher activity of Cl^- [52]. The DN describes the basicity of the solvent, which can be interpreted – amongst other descriptions – as the ability of the solvent to accept protons (and form cations SH^+, where S is a solvent molecule) or solvate small cations.

Because AN and DN can be interpreted as a measure of the stability of, respectively, solvated small anions and solvated protons in the solvent, these properties have a direct impact on the dissociation of HCl. Table 3.2 shows the values of AN and DN for ACN, DMF, and DMA along with pK_a of HCl. The pK_a can be interpreted as a measure of acidity (or acid strength) and is defined as follows for a neutral acid HA in equilibrium with its solvated protons SH^+ and its conjugate base A^- in a solvent S:

$$pK_a = -log\left(\frac{a(A^-)\cdot a(SH^+)}{a(HA)}\right) \qquad (2)$$

Values for pK_a of HCl in DMA could not be found in the literature, but a rough estimation can be made using the linear correlations proposed by Cox for acids in high-basicity aprotic solvents [50]. Thus, we assume $pK_a, HCl(DMA) = pK_a, HCl(DMSO) + 0.1$, for a $pK_a, HCl(DMSO) = 1.8$. As shown in Table 3.2, AN decreases in the order Water > ACN > DMF > DMA, and it can be inferred that the reactivity of chloride will increase in that order, being the least reactive in water and the most reactive in DMA. The much higher corrosivity of the aprotic organic solvents containing chlorides in comparison with aqueous solutions can, thus, be partially explained by the poor stability of chloride in solution. Once chloride is released from HCl, either by dissociation or as a biproduct of electrochemical HCl reduction, its reaction with the passive oxide that protects C-22 is expected to be more thermodynamically favorable in solvents of low AN than in water. Despite their low AN, the higher tendency of DMA and DMF to accept protons (as seen by a higher DN) results in a much lower pK_a in comparison with ACN. Thus, in DMF and DMA, HCl is much more dissociated than in ACN and Cl^- should be available at a concentration about 6 to 7 orders of magnitude higher.

Table 3.2: Acceptor number (AN), donor number (DN), $pK_a(HCl)$ and Gibbs free energies of solvation of Cl^- for different solvents.

Solvent	**DN**	**AN**	**pK_a(HCl)**	$\Delta G^{\circ}_{Cl^-,solvent} - \Delta G^{\circ}_{Cl^-,H_2O}$ *[kcal/mol]*
Water	33 [a]	54.8 [a]	-3.7 [a]	0 [c]
ACN	14.1 [a]	18.9 [a]	8.9 [a]– 10.4 [b]	12.0 [c]
DMF	26.6 [a]	16.0 [a]	3.3 [a]	12.3 [c]
DMA	27.8 [b]	13.6 [b]	1.9 [b, estimated]	14.1 [c]

a: K. Izutsu, *Electrochemistry in Nonaqueous Solutions*, Wiley-VCH Verlag GmbH & Co. KGaA, Weinheim, FRG, (2002).

b: B. Cox, *Acids and bases – Solvent effects on acid-base strength*, Oxford University Press (2013).

c: V. Gutmann, in *Nonaqueous Chemistry*,, p. 59–115, Springer-Verlag, Berlin/Heidelberg.

Influence of solvent properties on corrosion morphology

The pK_a of HCl in the different solvents appears to have great influence on the mode of corrosion observed. As indicated by the positive hysteresis loops in PDP and confirmed by SEM, when HCl is undissociated, such as in the case of ACN, C-22 undergoes uniform corrosion. In DMF and DMA, however, where HCl is far more dissociated, C-22 is initially passive but corrodes by pitting upon anodic polarization. Moreover, the higher pK_a value for HCl in ACN means it has the lowest acid strength amongst the solutions tested. Thus, dissolution of the passive oxide cannot be simply attributed to the molarity of H^+ in solution and these differences cannot be explained by the simple notion that acidity promotes passive film dissolution. Still, the different modes of corrosion may be a consequence of the effect of solvent chemical properties on chlorides and/or on water, which are both discussed below.

Although acidity alone cannot justify the dissolution of the passive oxide in ACN-HCl, the effect of solvent properties on HCl may still be a key aspect of the problem. Considering that the concentration of free chloride in ACN-HCl is negligible (about 14 orders of magnitude lower than in an aqueous HCl solution of same concentration), it is reasonable to assume that the oxide dissolves by reaction either with HCl or with its homoconjugated form $HClCl^-$. A particular feature of undissociated HCl is that it is polar and likely competes with H_2O for adsorption sites on the electrode surface. The results available in this study are not sufficient to explain the connection between undissociated HCl and uniform – instead of localized – attack, and similar comparisons were not found in the literature. A few similarities are observed in comparison with the results observed by Löchel and Strehblow for iron and nickel in aqueous HF, another halide acid which also has limited dissociation ($pK_a = 3.2$ in water) [56,57]. In their proposed mechanism, HF adsorbs on the surface of the oxide rapidly, forming stable metal fluoro complexes at the interface which catalyze the uniform dissolution of the metal by an oxide thinning mechanism, without observation of localized corrosion. Like HF in water, HCl in ACN is also expected to readily adsorb on the metal (or passive oxide), but we do not have sufficient information to claim that interfacial chloro complexes with the metal form. However, it should be noted that, due to the higher solvation energies of Cl^- in aprotic solvents, chloro complexes with metal cations are much more frequent than in water, as reported in the literature [58]. Kikuchi and Aramaki, for example, reported that Cl^- stimulated the anodic dissolution of Fe in ACN due to the formation of chloro complexes [13]. The description of such a mechanism still needs further investigation.

Although most often disregarded in the literature, another important element to consider is the effect of solvent chemical properties on water. It is known that the formation of a passive oxide film in aqueous solutions initiates by the reaction between the metal and either adsorbed H_2O or OH^-, and that the passive oxide is partially composed of hydroxides, at least at the interface with the solution [8]. The hydroxylation of the surface can be described by either of the following mechanisms involving a metal Me:

$$H_2O_{aq} \rightarrow H_2O_{ads} \qquad \text{Ia}$$

$$Me + H_2O_{ads} \rightarrow (MeOH)_{ads} + H^+{}_{aq} + e^- \qquad \text{Iab}$$

$$H_2O_{aq} \rightarrow H^+{}_{aq} + OH^-{}_{aq} \qquad \text{IIa}$$

$$OH^-{}_{aq} \rightarrow OH^-{}_{ads} \qquad \text{IIb}$$

$$Me + OH^-_{ads} \rightarrow (MeOH)_{ads} + e^- \qquad \text{IIc}$$

Although no information on the dissociation constant of water (pK_w) in each solvent was found in the literature, dissociation of water can be expected to obey a similar trend as that of HCl, since OH^- is an anion of high charge concentration, like Cl^-. As observed in reaction steps Ib or IIa, formation of surface hydroxides requires water splitting, either as a previous step (in the bulk of the solution) or on the surface of the metal during reaction with metal cations. In ACN both products of water splitting – H^+ and OH^-– are poorly solvated and depend on the solvation offered by other H_2O molecules, making both pathways of reaction with the metal energetically unfavorable. Also, under the same amount of residual water, less OH^- is expected to be available in ACN than in DMF and DMA. Additionally, free OH^- could be more reactive in DMA and DMF due to their lower AN. Thus, if the OH^- anion is more widely available and more efficient in reacting with the metal substrate in DMA and DMF, the formation of a hydroxide film at the interface may be easier in these solvents. The residual water in ACN, on the other hand, may be less effective in enabling oxide formation. Although a passive layer is initially maintained in DMA and in DMF, it can be broken down by anodic polarization, which agrees with the higher availability and higher activity of Cl^- in HCl solutions of these solvents.

Addition of small concentrations of water can facilitate uniform dissolution

The results in this study show that small additions of water to ACN (up to circa 1 M, or ≈ 2 wt%) decrease R_P in EIS and shift the anodic branch to less noble potentials in PDP (Figure 3.4 and Figure 3.9). According to the literature [51], small additions of water to acidified organic solvents should enhance passivity by stimulation of the formation of a passive oxide. The present study shows that, contrary to what has been reported in most solvents, water in small concentrations in acidic ACN promotes anodic dissolution. As mentioned earlier, water might be less effective in reacting with the metal to build a passive oxide in ACN. Under these circumstances, other chemical effects might be more influential at low water concentrations, such as the preferential solvation offered by water. Because water has a higher affinity for small anions and for most metallic cations than ACN, it is possible that small additions of water make metal cations more stable in solution and increase the solubility of corrosion products such as metal chlorides or hydroxides that may form at the interface of the metal with the solution. The increase in the dissolution of an interfacial film by addition of water agrees with the increase in C_{eff} observed up to 1 M H_2O. Only water additions above 1 M seem to increase R_P and decrease C_{eff}, indicating that water starts to improve passivity presumably by enabling the formation of an oxide film. Above 2.4 M, C-22 starts to show high R_P and a small active nose, indicating the possibility of spontaneous passivation.

On the other hand, in DMF and DMA, where C-22 maintains a passive oxide at the E_{corr}, water has a smaller influence on EIS data. Thus, at least in the range of concentrations tested, water does not have as much of an impact on the passive oxide at the E_{corr} in DMF and DMA.

Impact of water on localized corrosion

The PDP results (Figure 3.4) show that C-22 is highly susceptible to pitting in DMF- and DMA-based HCl solutions. In aqueous solutions containing chlorides, however, pitting of C-22 is rarely seen, even at elevated temperatures. The E_{pit} and E_{rep} extracted from curves in Figure 3.4 and E_{corr} measurements shown in Figure 3.9 are compiled in Figure 3.10. At low water concentrations E_{pit} and E_{rep} are generally close to E_{corr} and, in the case of DMF, E_{rep} can be lower than E_{corr} below circa 0.2 M H_2O. These results suggest that, given enough time or if mechanical rupture of the passive oxide takes place, C-22 is likely to corrode by pitting at the open circuit potential, especially in applications where oxidants are present [52]. Although water concentration has a smaller impact on the EIS results measured at the E_{corr} in DMF and DMA (Figure 3.9), it has a strong influence on the susceptibility to localized corrosion, as seen by the elevation of E_{pit} and E_{rep} with water addition. Thus, water improves both the resistance of the oxide film to the attack from chloride and the ability to repassivate ongoing localized corrosion. As observed for C-22 in ACN (above 1 M H_2O), addition of water improves passivity by stimulating the formation of a passive oxide due to higher concentrations of OH^- and H_2O. Furthermore, OH^- can migrate to local anodic zones in competition with Cl^-, improving the repassivation of pits and elevating the E_{rep}.

The comparison between results in the two solvents clearly shows that C-22 has a higher tendency to pitting in DMF than in DMA, for two reasons. First, at the same water concentration, E_{pit} and E_{rep} are always lower in DMF; secondly, the necessary water concentration to inhibit pitting is higher in DMF. As mentioned above, the high susceptibility to pitting observed in aprotic solvents might be a consequence of the poor chloride solvation in solution. However, this line of thought does not explain a higher susceptibility to pitting in DMF, since DMA has a slightly lower AN and, presumably, a lower pK_a for HCl. Also, it should be noted that the poor ability of aprotic solvents to solvate chloride in solution should also make metal halides less soluble, which can lead to the interpretation that corrosion products inside the pit would not be as soluble in solvents of low AN, mitigating localized corrosion. The tendency observed might also be caused by the effect of solvent properties on water. As explained earlier, H_2O is expected to dissociate more easily in DMA than in DMF, and OH^- may have a higher activity in solution due to the lower AN. Water additions in DMA may, thus, be more efficient in stimulating passivation by reaction II.

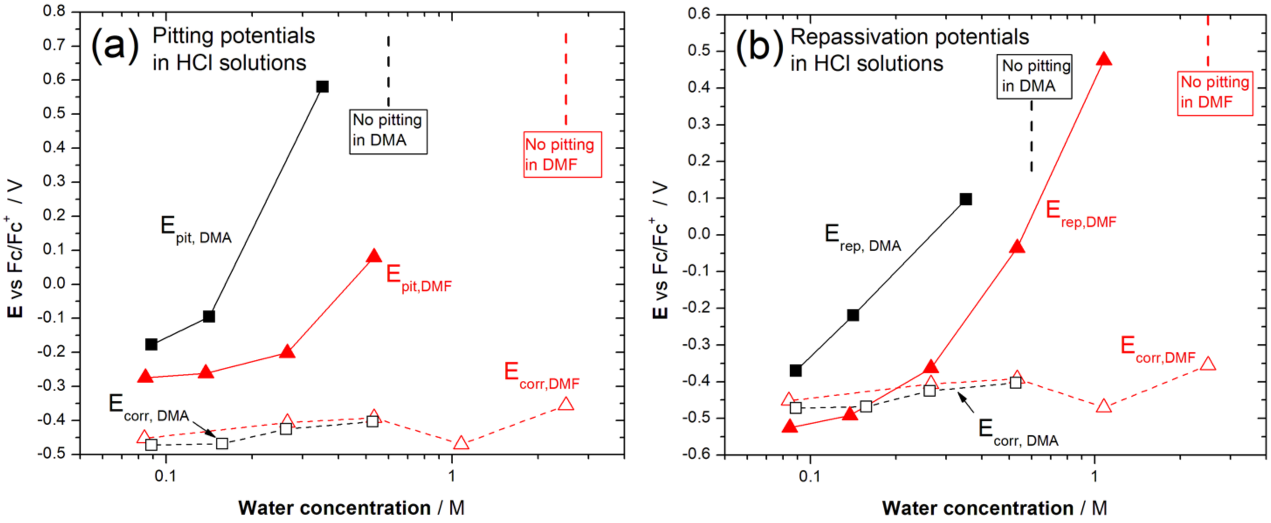

Figure 3.10: Pitting and repassivation potentials of C-22 in aprotic solvents containing 0.11 M HCl, along with E_{corr} measurements.

The scanning electron micrographs in Figure 3.6 and Figure 3.7 show that pit size increases with water concentration and the number of pits per area decreases with water concentration. This means that, in the range of concentrations where pitting was observed, water diminishes the pit nucleation rate and increases pit growth rate. We can infer that water diminishes the frequency of breakdown events by promoting stabilization of the oxide film. In the case of low water concentrations, pitting appears to propagate by continually nucleating new pits during anodic polarization, whereas in higher water concentrations fewer pits nucleate but continue to grow. At more passivating conditions, such as in DMA-HCl/0.35 M H_2O (Figure 3.7), pits appear to achieve stability by formation of subsurface channels and partially covered holes. These might allow the formation of an occluded chemistry of higher local acidity, which might be necessary conditions for pit growth in that case. A more detailed investigation focused on localized corrosion in aprotic solvents is presented in the next chapter.

Water facilitates transpassive dissolution

When HCl is added to ACN, DMF or DMA, a new oxidation reaction is observed in PDP above circa 0.4 V vs Fc/Fc$^+$. We can assume this is the oxidation of HCl, Cl$^-$, HClCl$^-$, or other complexes containing chloride, by some variation of the following reaction:

$$2\,HCl\ +\ 2e^-\ \rightarrow Cl_2 + 2H^+ \qquad \text{(III)}$$

This reaction takes place at the lowest potential in DMA, followed by DMF and ACN, which is the order of increasing pK$_a$ (HCl) in these solvents. Thus, oxidation of chloride will be easier in solvents where HCl dissociates more and more Cl$^-$ is available. Furthermore, the addition of water in high concentrations shifts the reaction to higher potentials, possibly because preferential solvation of Cl$^-$ by H_2O makes oxidation more difficult. Comparing the PDP on Pt and on C-22, it was seen that the transpassive region observed for C-22 takes place at relatively similar potentials and with similar Tafel slopes as the reaction observed on Pt. Thus, there is a chance that chloride oxidation is taking place on C-22 at high applied potentials. However, unlike on Pt, on C-22 this transpassive region shifts to lower potentials with addition of water. This is presumably not a consequence of water oxidation, or the same potential shift would also be seen on Pt.

It is known that alloys that passivate by formation of Cr-rich barrier oxides – as is the case of C-22 – undergo transpassive dissolution at elevated potentials, mainly due to the change in valence of Cr^{3+} to Cr^{6+}as follows:

$$Cr_2O_3 + 5H_2O \rightarrow 2CrO_4{}^{2-} + 10H^+ + 6e^- \qquad \text{(IV)}$$

This dissolution process is often reported to take place above circa 0.8 V vs SCE [37,59] (equivalent to 0.42 V vs Fc/Fc$^+$ [30]), which matches the transpassive potentials observed in this study. Because reaction 4 requires water, it is understandable that this process shifts to lower potentials with higher water concentrations. If HCl oxidation takes place simultaneously during transpassive dissolution, the formation of oxidizing Cl$_{ads}$ intermediates on the surface of the electrode could also be deleterious.

Conclusions

This study explored the different effects of residual water and solvent properties on the corrosion behavior of C-22 in aprotic solvents. The results obtained inform different aspects of the corrosion behavior of C-22 at room temperature, previously unreported in the literature. The investigation of corrosion phenomena of passive alloys in aprotic organic solvents not only is necessary for applications in the chemical and pharmaceutical industries, but also presents new opportunities for the study of fundamental aspects of uniform and localized corrosion mechanisms. The main findings of this study are summarized as follows:

- C-22 is passive in ACN, DMF or DMA even at very low (sub mM) water concentrations. When the oxide is broken by scratching the electrode with a scribe, C-22 repassivates readily.
- In solutions of aprotic solvents containing HCl with water concentrations below circa 1 M, C-22 is prone to different modes of corrosion which seem to depend on the dissociation constant of HCl in solution: in ACN, where HCl is less dissociated and has $pK_a \approx 9$, C-22 corrodes uniformly; in DMA and DMF, where HCl is more dissociated and has high $pK_a \approx 2–3$, C-22 corrodes by pitting.
- The effect of water is complex and depends on concentration and on the primary solvent. Addition of small concentrations of water (below 1 M) to ACN-HCl solutions is deleterious, promoting uniform dissolution. Above 1 M, water promotes passivation by formation of an oxide film.
- In DMF- and DMA-HCl solutions, addition of water was beneficial to passivity in all concentrations tested (between circa 80 mM and 2.5 M), as observed by the elevation of pitting and repassivation potentials, eventually mitigating localized corrosion. Additionally, increasing water concentration decreases the number of pits while increasing average pit size.
- Amongst the solvents studied, C-22 is most prone to pitting in DMF. In DMF-HCl, C-22 has the lowest pitting and repassivation potentials and requires the highest water concentration for mitigation of localized corrosion.

Chapter 4 : The localized corrosion of C-22 in neutral aprotic solvents containing chloride

Introduction

The passive oxide films formed on Ni-Cr-Mo are known to provide an excellent resistance to aqueous localized corrosion even at elevated temperatures and concentrated chloride solutions. However, the application of passive alloys in aprotic solvents can present unexpected corrosion behaviors. As shown in previous studies in this series, C-22 can corrode actively in ACN containing HCl[52]. Surprisingly, the results in the last chapter show that the mode of corrosion changes depending on the aprotic solvent used. For the protophilic aprotic solvents DMF and DMA, the mode of corrosion changes to pitting corrosion. Because in DMF and DMA HCl is more extensively dissociated, it was hypothesized that the transition to pitting corrosion was caused by the higher availability of Cl^-. However, the use of HCl to study pitting is challenging because both the equilibrium of HCl dissociation and the activity coefficient of Cl^- change between different aprotic solvents.

A few studies have reported pitting in organic solvents. In polycarbonate (PC), a few authors have observed pitting of 304 stainless steel and iron when perchlorate electrolyte oxidized on the surface of the metal, presumably due to the formation of reactive radicals [15,23,60]. In DMSO containing HCl, pitting of Fe and Ni has been observed for water concentrations above 2wt% by Schwabe and Berthold [11], but specifics of the phenomenon were not investigated. Other authors have reported pitting of Fe in DMF, unrelated to chloride[61]. Neither of these studies, however, were focused on the mechanism of non-aqueous pitting or its comparison with aqueous pitting.

In the present study, the mechanism of pitting of alloy C-22 in aprotic solvents was studied, by using a chloride-containing salt that dissociates well in aprotic solvents, Bu_4NCl. Differently from the previous chapter, in this study the concentration of Cl^- in solution can easily be controlled by additions of Bu_4NCl. Using a similar experimental approach, the hypothesis that pitting is dependent on the availability of Cl^- in solution was tested. Because the activity of chloride can differ depending on the aprotic solvent used, the influence of solvent properties was assessed by comparing different aprotic solvents. This way, the hypothesis that pitting will be facilitated in solvents where Cl^- has higher activity coefficient was tested. Furthermore, the effect of water and its relevance in the pitting process was assessed. Ultimately, the objective of this study is to understand the mechanism of pitting in aprotic solvents and whether it is comparable to the well-studied pitting processes in aqueous solutions.

Experimental

The experimental techniques used in this study were carried out as explained in previous chapters so most of the details are not listed here to avoid excessive repetition. The electrochemical techniques employed were potentiodynamic polarizations (PDP), as well as potentiostatic polarizations combined with in situ scratching of the working electrode (also referred to as "scratch tests"). After electrochemical tests, most samples were assessed by scanning electron microscopy, which was usually performed using secondary electron signal with an acceleration voltage of 15kV.

Differently from the last chapter, a few scratch tests experiments were done for a sequence of potentials with the same sample. Starting at the open circuit, potential was stepped to OCP+150 mV for 20 min. After 10 min in the potential hold, the sample was scratched, and let repassivate for the remaining 10 min. After the potential hold, the sample was allowed to rest at OCP for 5 min, then a new 20-minute potential hold started, 100 mV above the previous one. This cycle was repeated several times, until significant corrosion was observed.

Results

PDP on Pt in neutral polar aprotic solvents containing chloride

To understand the electrochemical reactions taking place in solutions of polar aprotic solvents containing Cl^-, PDP scans were carried out using Pt in 0.14 M Bu_4NCl with various water concentrations (Figure 4.1). As mentioned previously in Chapter 3, although Pt should have better catalytic properties than the oxide-covered C-22 surface, this approach allows the estimation of the contribution to the anodic current coming from electrochemical reactions that do not involve the oxidation of the metallic substrate. Clearly, in all three solvents the current density (i) starts rising at potentials around 0.150 and 0.250 V vs Fc/Fc^+. Arbitrarily choosing the i value of 30 $\mu A \cdot cm^{-2}$ at the lowest water concentration for comparison between solvents, we see this oxidation process takes place at the lowest potential in DMA (0.184 V vs Fc/Fc^+), followed by DMF (0.278 V vs Fc/Fc^+), and ACN (0.286 V). Furthermore, the Tafel slopes obtained in this same region (69 mV/dec in ACN, 72 mV/dec in DMF, 73 mV/dec in DMA) indicate that this is probably the same (or a similar) process in all solvents. These PDP curves can be compared with the results in the same solvents containing Bu_4NPF_6 instead of Bu_4NCl in the first part of this study (*in Chapter 2*). Because the only difference in these solutions is the presence of the anion Cl^- instead PF_6^-, we can infer that the electrochemical reaction observed is the result of chloride oxidation from Cl^- or some Cl^--containing complex. Also, similarly to what was observed for the oxidation waves observed in HCl-containing solutions in chapter 3, Tafel slopes are around 70 mV/dec and the potential necessary for oxidation decreases with increasing acceptor number (AN) of the solvents used (Table 3.2). In this case, however, oxidation takes place at lower potentials. In all solvents the addition of water shifts the oxidation of Cl^- to higher potentials, although this effect seems more pronounced in DMA.

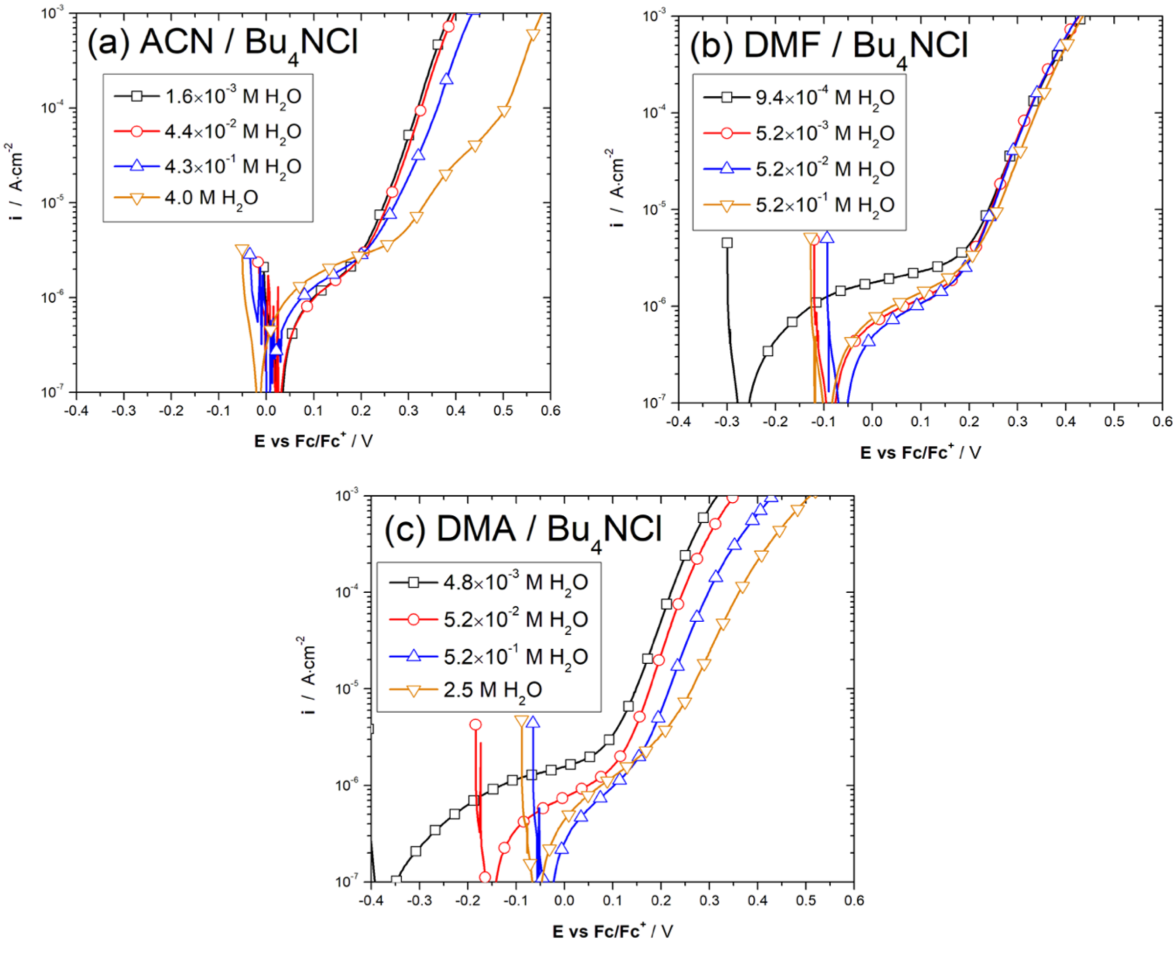

Figure 4.1: Potentiodynamic polarization scans (1 mV/s) of Pt in aprotic solvents (ACN, DMF and DMA) with 0.14 M Bu_4NCl.

Cyclic PDP on C-22 in neutral polar aprotic solvents: varying water concentrations

Figure 4.2 shows cyclic PDP scans measured on C-22 in ACN (a), DMF (b) and DMA (c) solutions containing 0.14 M Bu_4NCl and various concentrations of water. For lower water concentrations (typically below 100 mM) in all three solvents, C-22 presents a passive region limited by a breakdown or pitting potential (E_{pit}), where current density elevates rapidly. After reversal of the scanning direction, C-22 repassivates at a lower potential (E_{rep}) forming a positive hysteresis loop, typically associated with localized corrosion. In DMF and in DMA, increase in water concentration results in elevation of E_{pit} and E_{rep}. In ACN, however, the effect of water is not very clear, as the lowest water concentration (2.6 mM) presents one of the highest E_{pit} and E_{rep}. For higher concentrations, the trend is similar to that observed in DMF and DMA. A general trend across solvents is the elevation of the peak anodic current in the reverse sweep when water concentration is increased.

In ACN and DMF, E_{pit} of C-22 is always lower than the potential range for the oxidation of Cl^- observed on Pt. In DMA, C-22 presents an elevation in current density before breakdown at E_{pit}, and E_{pit} is situated at potentials that overlap with oxidation of Cl^- on Pt. However, because the Tafel slope in this region is different (≈120 mV/dec) and the catalytic properties of oxide-covered C-22 are presumably worse than those of Pt, it is not clear if Cl^- oxidation or transpassive dissolution begin before pitting. As observed in DMA and DMF/HCl solutions (Figure 3.4), features associated with localized corrosion disappear above a certain concentration of water, and the behavior becomes passive, followed by an elevation of current density and negative hysteresis at high potentials. It should be pointed that, in ACN/Bu_4NCl with H_2O concentrations between 44 and 430 mM, an anodic peak is observed near -0.1 in forward sweeps, and a cathodic peak is observed near -0.5 V in the reverse sweeps, after repassivation. Possibly, redox species generated by oxidation in the forward sweep later get reduced in the reverse sweep, potentially participating in the repassivation mechanism.

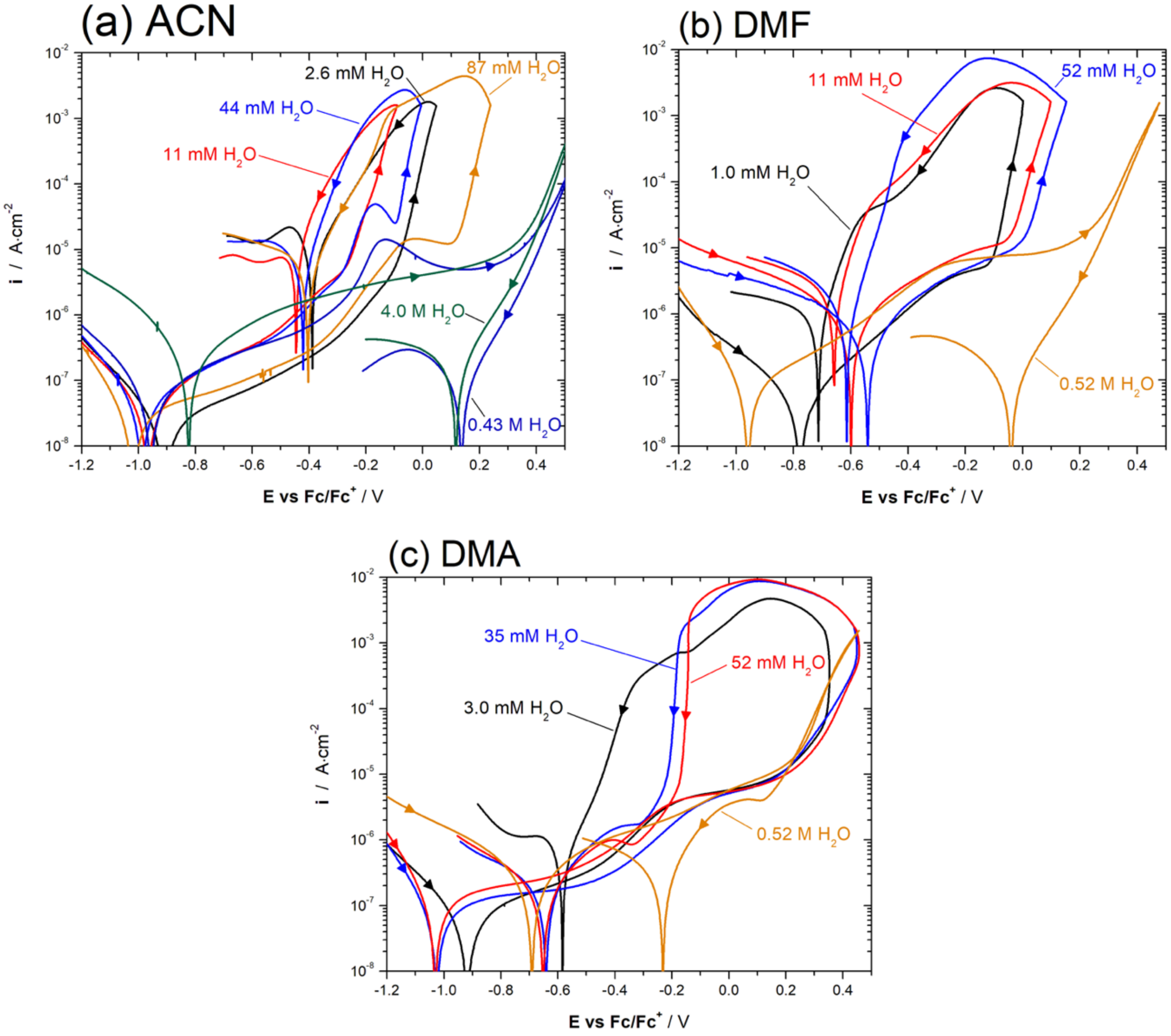

Figure 4.2: Potentiodynamic polarization scans (1 mV/s) of C-22 in aprotic solvents (ACN, DMF and DMA) with 0.14 M Bu_4NCl.

E_{pit} and E_{rep} values extracted from PDP scans in various water concentrations are shown in Figure 4.3, as well as the E_{corr} before beginning each scan. It should be noted that in most cases the transition between passive and active behavior is smooth, so E_{pit} was determined as the intersection between a straight line fitted to the passive portion and another straight line fitted to the active portion of the curve. E_{rep} was determined as the point where the anodic current density in the reverse scan intercepts the passive current density in the

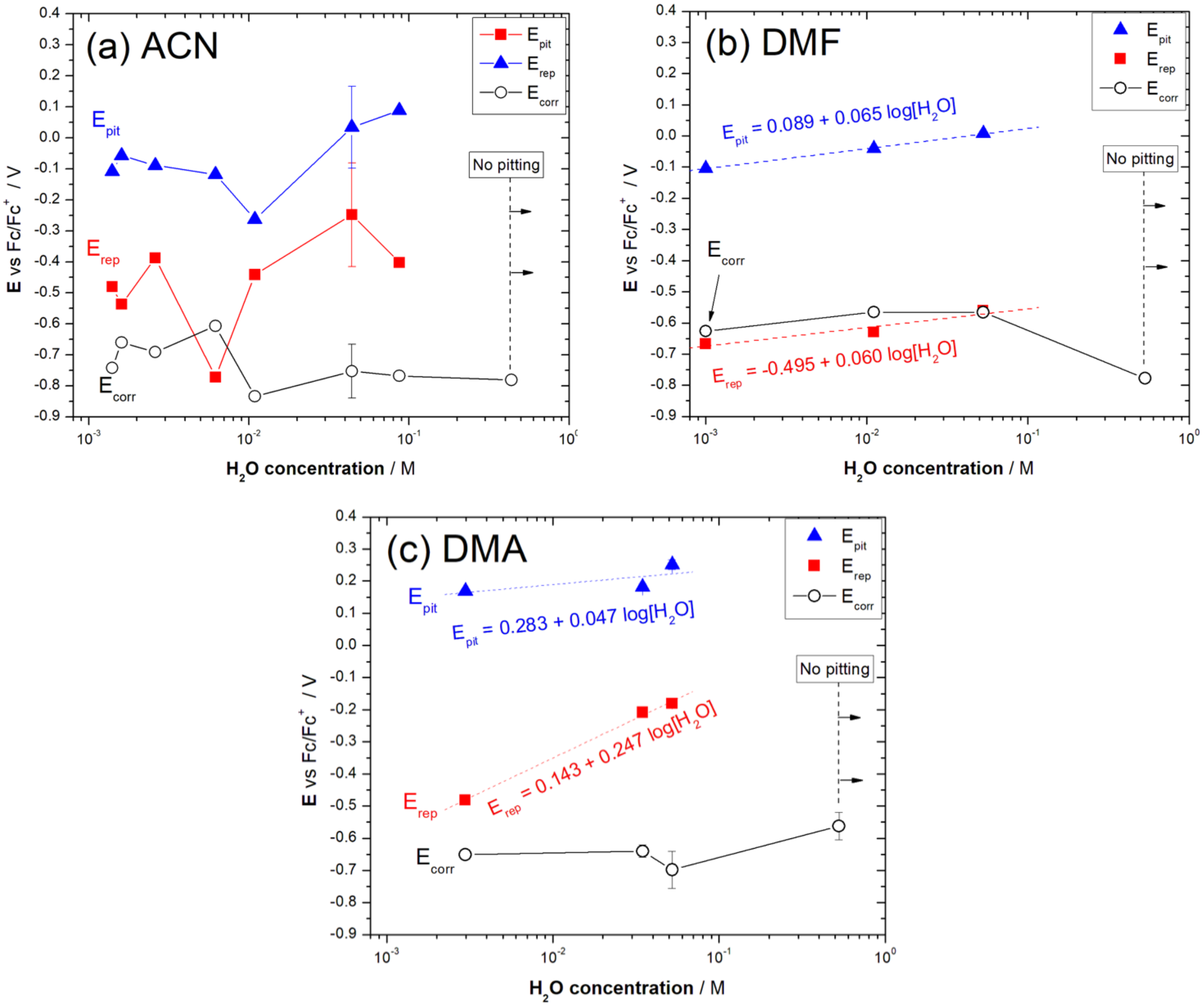

Figure 4.3: Pitting (E_{pit}) and repassivation potentials (E_{rep}) from PDP scans and E_{corr} measured after 1 hour of exposure, before starting PDP scans, in 0.14 M Bu_4NCl solutions.

forward scan or its linear fit. In Cl^--containing DMF and DMA solutions, both E_{pit} and E_{rep} increase with the logarithm of water molarity, evidencing the beneficial effect of water on the mitigation of localized corrosion. In DMA, the effect of water on E_{rep} is more intense than in DMF, as indicated by the higher slope of the fitted line. The dependence of E_{pit} and E_{rep} on water does not seem simple in ACN, for which the datapoints do not show a constant log-linear behavior. E_{pit} decreases with water concentration up to circa 10 mM H_2O, then starts to rise; E_{rep} follows a somewhat similar trend. Particularly in DMF, E_{rep} is often lower than or very near the E_{corr}, indicating the possibility of pitting at open circuit.

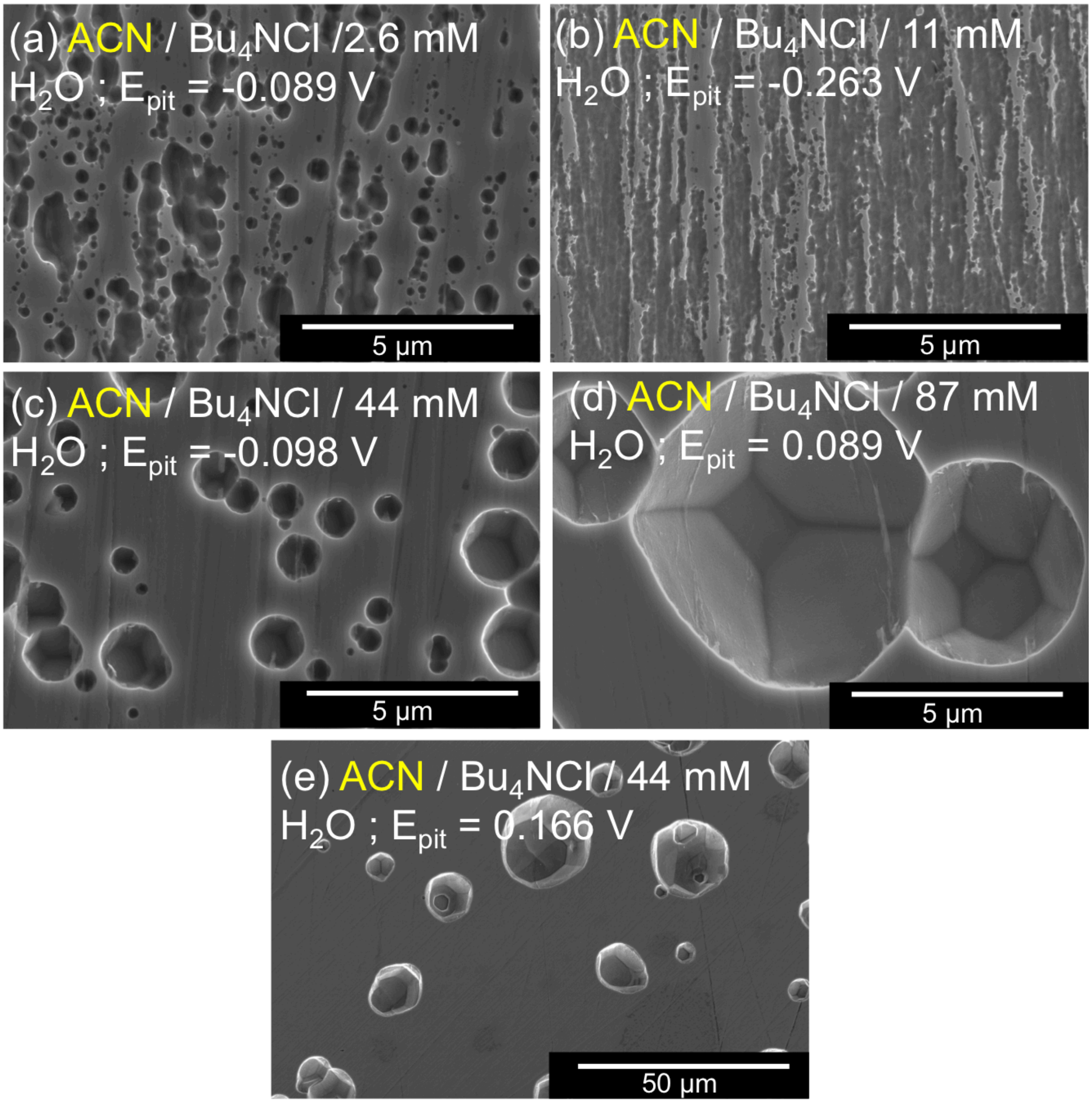

Figure 4.4: Scanning electron micrographs of C-22 samples after PDP in ACN / 0.14 M Bu_4NCl with various concentrations of residual water.

Figure 4.4 and Figure 4.5 show scanning electron micrographs of the C-22 surface after PDP experiments. Although there are clear differences, the mode of corrosion in all solvents is localized, showing pits surrounded by preserved portions of the original surface, which still show scratches from sample preparation. In all three solvents, C-22 generally presents bigger and more crystallographic pits when water concentration increases. In ACN (Figure 4.4), pit size and density of pits (area^{-1}) change markedly with water concentration. However, when comparing E_{pit} and water concentration of each analyzed specimen, we can see that size and density of pits correlate better with E_{pit}. The higher the E_{pit} is, the larger is the final pit diameter and the lower is the density of pits. This trend is evidenced when comparing specimens that were exposed to the same solution (Figure 4.4d and e) but showed different E_{pit} – the one with higher E_{pit} has larger and fewer pits.

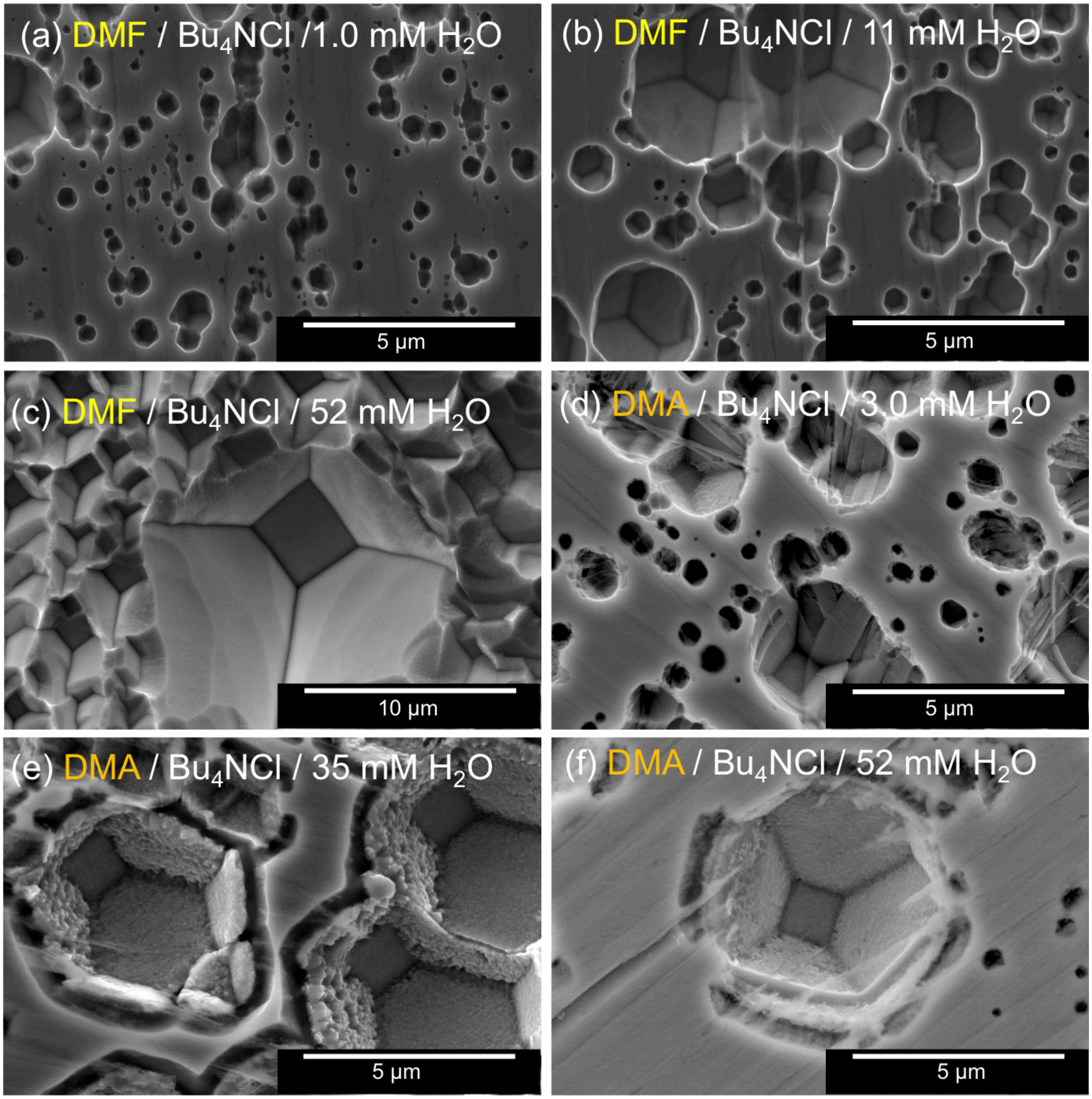

Figure 4.5: Scanning electron micrographs of C-22 after PDP in DMF (a-c) or DMA (d-f) with 0.14 M Bu_4NCl and various concentrations of residual water.

In DMF- and DMA-Bu_4NCl solutions (Figure 4.5), the influence of water on corrosion morphology is not as clear as in ACN, but pit size still seems to increase with water concentration. As indicated by the elevation of peak anodic current with water concentration in PDP, the degree of corrosion also changes with water concentration. Therefore, a few specimens corroded in higher water concentrations presented an almost completely attacked surface, with very small portions of the original surface remaining (Figure 4.5c). Particularly in DMA with higher water concentrations, pits are often surrounded by attacked areas, which can grow to form a ring around the pit. No corrosion was observed in DMF- and DMA-Bu_4NCl solutions with 0.52 M water concentration.

Cyclic PDP on C-22 in neutral polar aprotic solvents: varying chloride concentration

The effect of chloride concentration on the corrosion of C-22 in polar aprotic solvents was assessed by PDP in solutions with Bu_4NCl concentrations between 2 and 140 mM (Figure 4.6). All solutions contained 0.1 M Bu_4NPF_6 to ensure a baseline of solution conductivity and to avoid excessive distortion of the PDP curves at low chloride concentrations. For all chloride concentrations in all three solvents (with the exception of DMA / 2 mM Bu_4NCl), C-22 presents a positive hysteresis loop, indicating localized corrosion even at very low concentrations of chloride. E_{pit} and E_{rep} appear to increase with decreasing chloride concentration in all solvents. Furthermore, the peak anodic current density on the reverse scan increases with chloride concentration, indicating a higher stability of pits. For low chloride concentrations (typically at 2 and 7 mM), when passivity is broken the anodic current density starts rising but soon reaches a plateau that can be surpassed only at higher potentials. This plateau indicates the transition from a charge transfer control to a mass transport control, which results in a constant current density across a range of potentials. After the current density rises again and the sweep direction is reversed, a positive hysteresis is still seen before repassivation. Like in the PDP of C-22 in ACN/0.14 M Bu_4NCl in Figure 4.2, a cathodic current peak is observed in the reverse sweep after repassivation in all three solvents (around -0.4 V in ACN; -0.5 V in DMF, and between -0.8 and -0.4 V in DMA). The effect of chloride concentration on this peak's position is not clear.

The E_{pit} and E_{rep} gathered from PDP results along with E_{corr} measurements (after 1h exposure) prior to the beginning of the scans are shown in Figure 4.7. In all solvents, chloride has an opposite effect to that of water: increasing $[Cl^-]$ lowers E_{pit} and E_{rep}, as observed by the negative slopes obtained in the linear fitting. As an alternative to the E_{pit} estimation method described for Figure 4.3 (intersection between fitted lines in the passive and active region), E_{pit} data are also shown as the potential required to achieve a current density $i = 0.5\ mA \cdot cm^{-2}$ in the forward scan (blue circles). The validity of this approach depends on whether the current density measured at E_{pit}*(i = 0.5 mA·cm^{-2})* is solely due to pitting or not. Using the intersection method, E_{pit} and E_{rep} typically have a negative linear dependence on log[Bu_4NCl]. However, because the transition between the passive and the active region can be gradual, the intersection method seems imprecise for solvents such as DMA, where the E_{pit} data acquired by this method correlate poorly with [Bu_4NCl]. In this case, E_{pit}(*i = 0.5 mA·cm^{-2})* seems a more adequate measure, and the data follows a negative linear dependence on log[Bu_4NCl]. Both in ACN and in DMA, the values of E_{pit} and E_{pit}*(i = 0.5 mA·cm^{-2})* become closer as log[Bu_4NCl] increases, indicating that increasing chloride concentration results in a steeper elevation of current density after pitting corrosion starts – in other words, a lower value for the Tafel slope.

For situations where the corrosion process becomes controlled by mass transport and the anodic current density plateaus, E_{pit}*(i = 0.5 mA·cm^{-2})* can present outliers, as observed in DMF / 2 mM Bu_4NCl. The same would happen with DMA if a higher current density (such as *i = 1.0 mA·cm^{-2}*) were chosen to determine E_{pit}. Considering that the rise in current density before the mass transport region (represented by E_{pit}) correlates well with log[Bu_4NCl] and the subsequent rise in current at higher potentials presents a breach from this correlation, we can infer that there are two distinct phenomena. By comparison with higher chloride concentrations, it is most probable that the rise in current at lower potentials is due to pitting, which progression becomes limited at low chloride concentrations, and the active behavior transitions into mass transport control. Finally, comparing the three solvents, C-22 presents the lowest E_{pit} and E_{rep} in DMF solutions. Nevertheless, the smaller slopes of the fitted lines indicate that E_{pit} and E_{rep} in DMF are not as affected by chloride concentration as in the other solvents. In DMA, on the other hand, E_{pit} and E_{rep} are the most affected by chloride concentration.

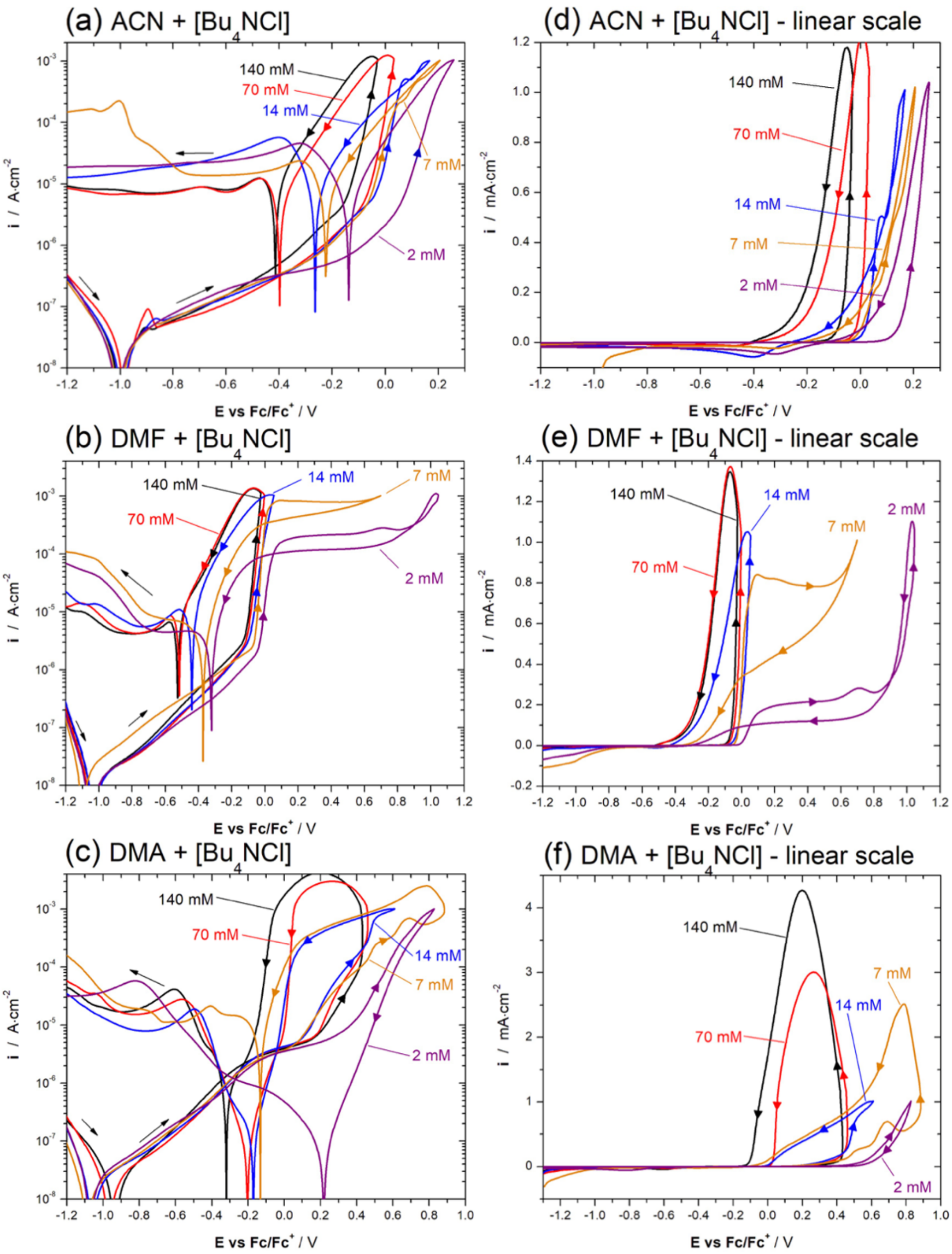

Figure 4.6: PDP on C-22 at scan rate 1 mV/s in polar aprotic solvents containing 0.1 M Bu4NPF$_6$ and varying concentrations of Bu$_4$NCl. ACN-Bu$_4$NCl solutions contained 4.2±0.5 mM H_2O; DMF-Bu$_4$NCl solutions contained 5.1±0.2 mM H_2O; DMA-Bu$_4$NCl solutions contained 8.9±0.1 mM H_2O.

The surface of C-22 after PDP in ACN with varying chloride concentrations is shown in Figure 4.8. For all concentrations tested, C-22 presents pits that are aligned with the direction of scratches from surface polishing. The effect of chloride concentration on pit size is not very clear, and, despite the different pitting potentials in PDP, pit size does not change much. In DMF (Figure 4.9), the effect of chloride is more pronounced. Between 140 and 14 mM, reduction of chloride concentration results in reduction of the density of pits, and fewer pits larger than 1 μm are found. When concentration is lowered to 7 and 2 mM, pits cease being crystallographic, and the surface becomes more uniformly attacked, especially at 2 mM, where the surface is smoother. The highest impact of chloride concentration on corrosion morphology is observed in DMA solutions (Figure 4.10), where pit size clearly decreases when chloride concentration is lowered. Similarly to DMF, in DMA with higher chloride concentrations pits have a crystallographic morphology, but are hemispherical with round bottoms at lower chloride concentrations (14 and 7 mM Bu_4NCl). In DMA / 7 mM Bu_4NCl, the surface is a combination of pits and uniform attack, as was seen for 2 mM Bu_4NCl in DMF. In DMA / 2 mM Bu_4NCl, for which no positive hysteresis is observed in PDP, the attack is shallow and laterally spread, being comparable to a uniform corrosion process.

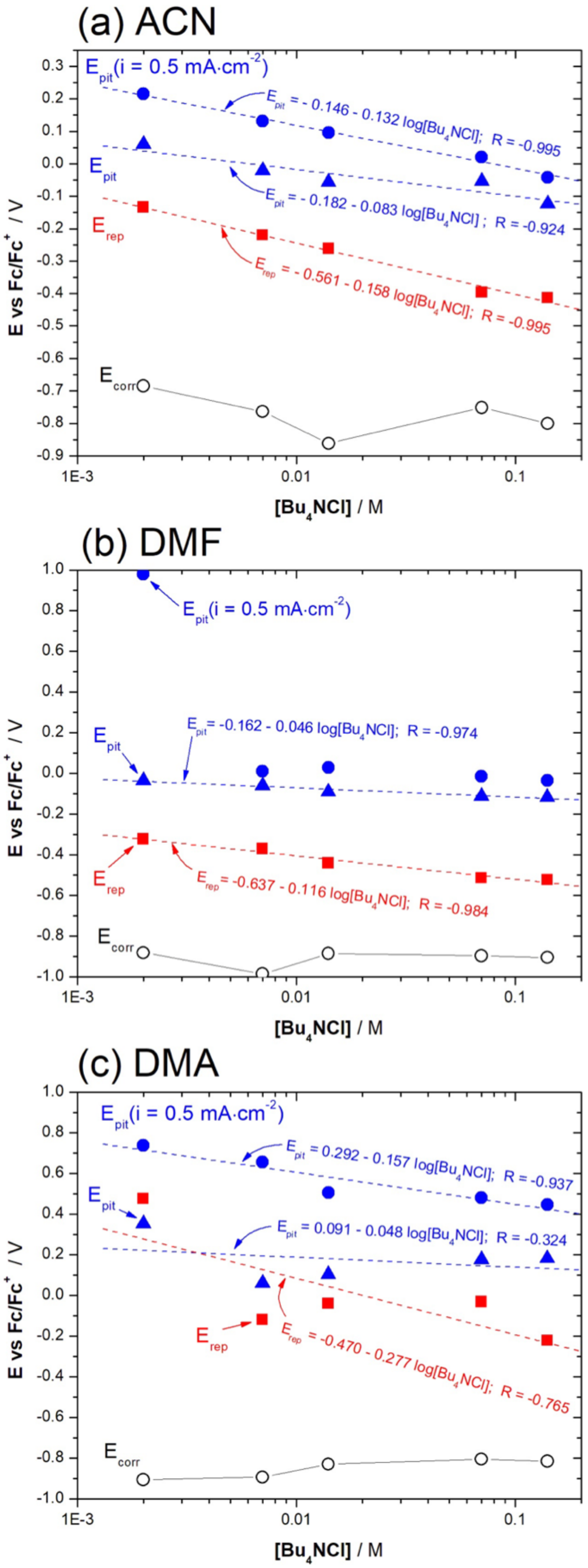

Figure 4.7: Pitting (E_{pit}) and repassivation potentials (E_{rep}) from PDP scans and E_{corr} measured after 1 hour of exposure, before starting PDP scans, in solutions with varying choride concentration.

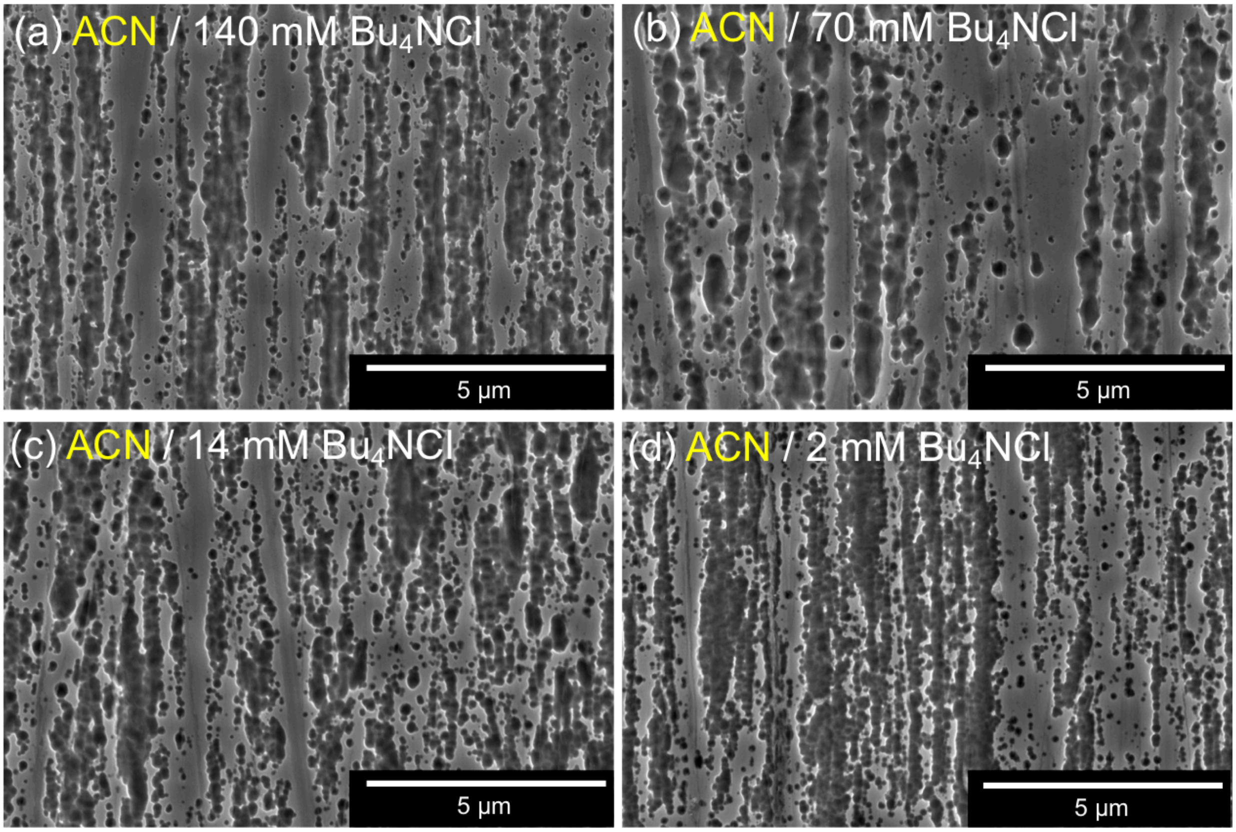

Figure 4.8: Scanning electron micrographs of C-22 after PDP in ACN with varying Bu_4NCl concentrations. All solutions contained 0.1 M Bu_4NPF_6 and 4.2±0.5 mM H_2O.

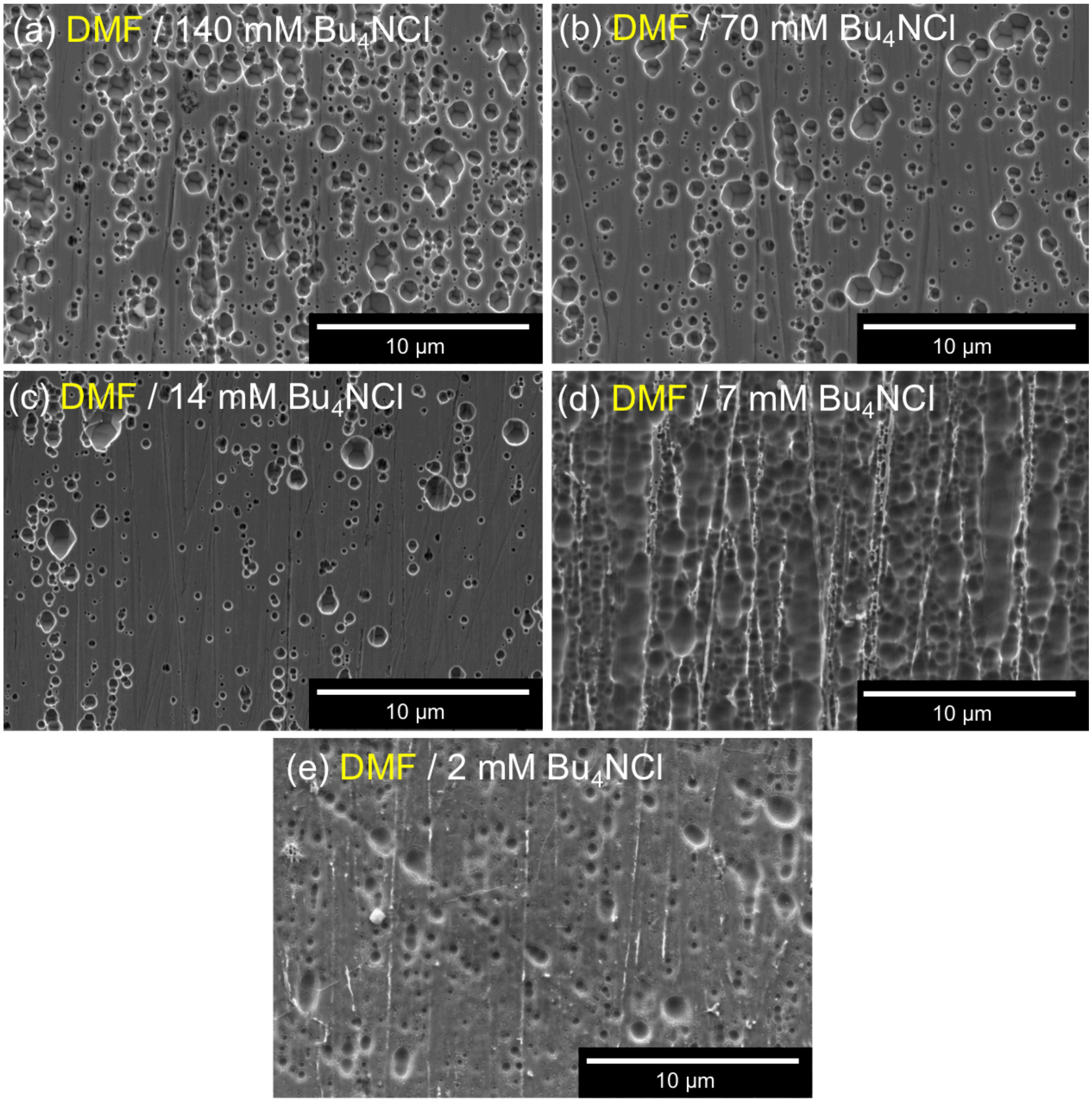

Figure 4.9: Scanning electron micrographs of C-22 after PDP in DMF with varying Bu_4NCl concentrations. All solutions contained 0.1 M Bu_4NPF_6 and 5.1±0.2 mM H_2O.

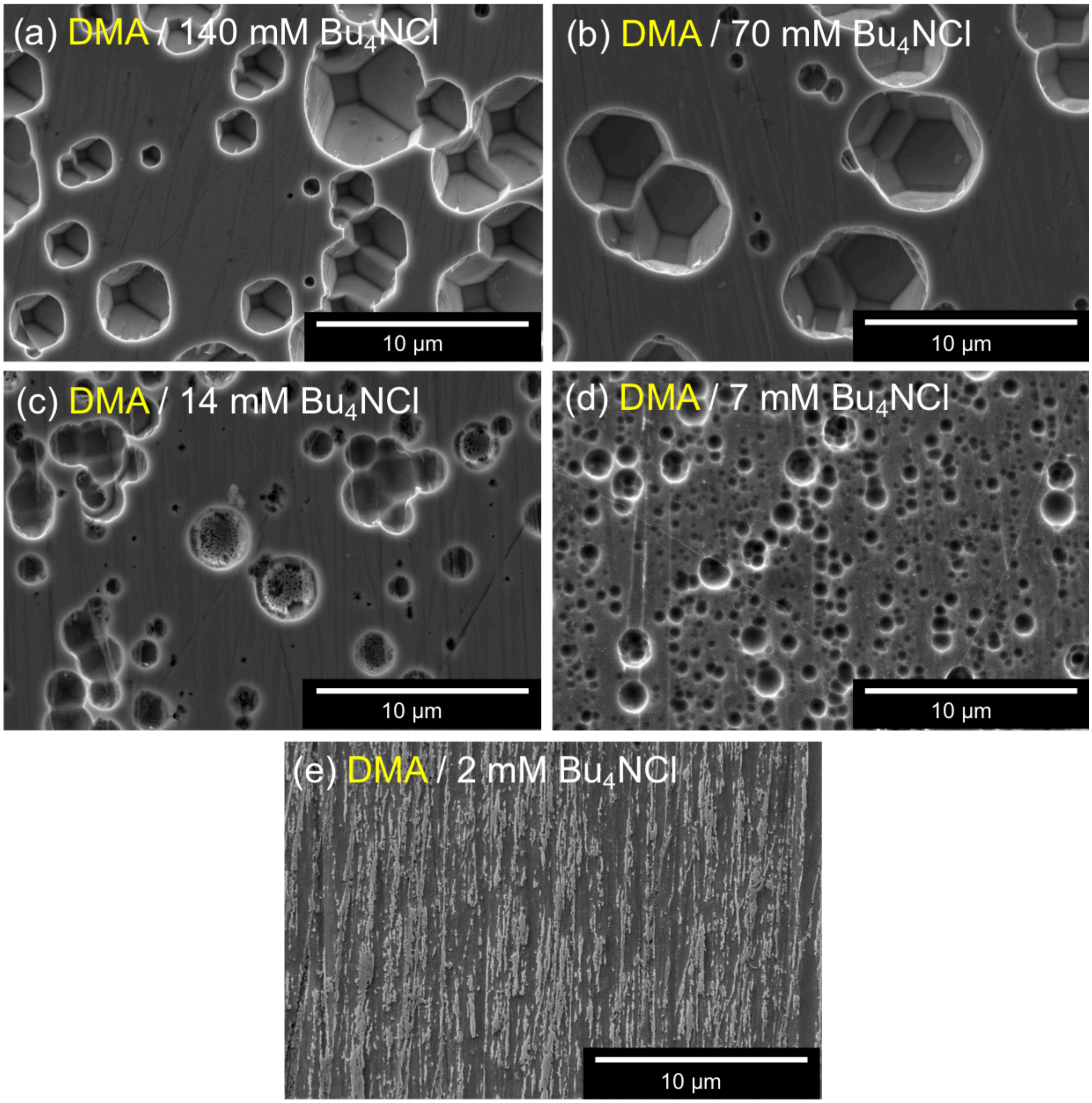

Figure 4.10: Scanning electron micrographs of C-22 after PDP in DMA with varying Bu_4NCl concentrations. All solutions contained 0.1 M Bu_4NPF_6 and 8.9±0.1 mM H_2O.

Potentiostatic polarization with the scratched electrode technique

To obtain additional information about the localized corrosion process observed in polar aprotic solvents, potentiostatic chronoamperometry was used in association with the scratched electrode technique. Using this approach, the passivity of C-22 at a given potential is studied by mechanically breaking the passive oxide and observing the anodic kinetics thereafter. This way the accuracy and relevance of pitting and repassivation potentials extracted from PDP scans can be investigated. Figure 4.11 shows current transients of C-22 obtained at different potentials (vs Fc/Fc^+) in ACN / 0.14 M Bu_4NCl with two different initial water concentrations. It should be noted that, for the lower water concentration, Karl-Fisher titration measurements before and after the test showed that the residual water in the solution had increased from 1.4 to 6.1 mM during the test. The increase in water concentration can be attributed to moisture uptake from the air, which penetrates the electrochemical cell when the scriber is inserted. In both plots, $t=0$ is the moment that the C-22 electrode is scratched, which was done always after 10 min at the potential of interest.

In 1.4 mM H_2O, the lowest potential shown is -320 mV vs Fc/Fc^+. At this potential, current decreases during the initial 10 minutes of polarization and, after the surface is scratched, C-22 rapidly repassivates and the current reaches a similar value as those before the scratch. Because the surface repassivates and localized corrosion is not stable at this potential, we can infer that -320 mV < E_{rep}. When C-22 is polarized at -220 mV, the current transient is distinct: current starts rising after circa 200 s of polarization and, after scratching, current continues to rise. Because the current starts rising without the necessity of a scratch, we can infer we pitting happens spontaneously at this potential and, thus, -320 mV< $E_{rep} < E_{pit} <$ -220 mV. For applied potentials higher than -220 mV C-22 is active, and scratching of the electrode does not affect the electrode kinetics significantly. In comparison with the E_{pit} and E_{rep} obtained from PDP in ACN / 0.14 mM Bu_4NCl in Figure 4.3, the values obtained by this method show a smaller hysteresis (<100 mV) that falls inside the hysteresis values obtained in PDP, where $E_{pit} \approx$ -100 mV and $E_{rep} \approx$ -450 mV vs Fc/Fc^+ for similar water concentrations. The decrease in $E_{pit} - E_{rep}$ (here referred to as hysteresis) is expected when PDP is performed at lower scan rates, mainly because E_{pit} approaches E_{rep} at steadier conditions. However, it should be noted that E_{rep} also shifts to higher potentials in comparison with the values determined in PDP, which is commented in the *Discussion* section.

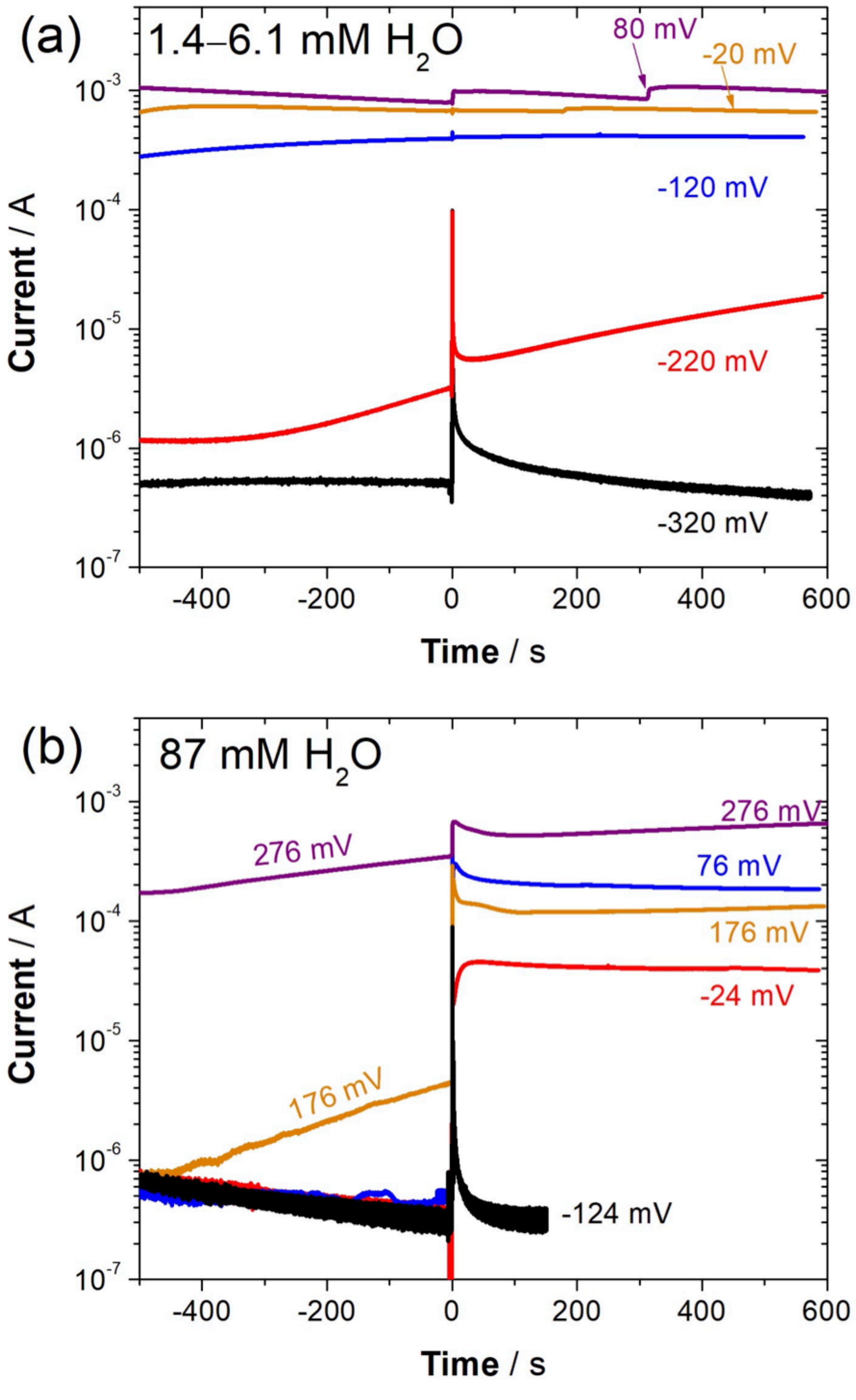

Figure 4.11: Potentiostatic chronoamperometry with the scratched electrode technique of C-22 at various potentials, in ACN / 0.14 M Bu_4NCl with (a) 1.4 mM and (b) 87 mM H_2O. After finishing tests in (a), KF titration of the solution results in 6.1 mM H_2O. Exposed area = 0.785 cm^2.

When the same procedure is used in an ACN / 0.14 M Bu_4NCl solution with more water (87 mM H_2O = 0.2 wt%), activation takes place at higher potentials. At -124 mV, C-22 is passive before and after the scratch, indicating that -124 mV < E_{rep}. At -24 mV, C-22 is initially passive but, after scratching, the current rises to a new plateau. Although the current obtained is in the order of 40 µA, it should be noted that the active area of the scratch is small, so the local current density should be compatible with an active behavior. This means that the sample was protected by a passive film until the moment it was scratched, after which the metal activates, and the passive film is not able to form again. Thus, it can be inferred that -124 mV < E_{rep} < -24 mV. The current transient at 76 mV is similar to the one at -24 mV, although a higher anodic current is observed after scratching. When the potential applied is 176 mV, the current starts rising before scratching the surface, indicating that pitting happens spontaneously. Still, scratching the electrode results in an elevation of the current by more than one order of magnitude, accelerating the corrosion process. Due to the spontaneous degradation of the oxide at 176 mV, it can be concluded that 76 mV < E_{pit} < 176 mV. Potentials above 176 mV result in higher currents which are not significantly affected by scratching the electrode. We can infer that the hysteresis is greater in 87 mM H_2O (between 300 and 200 mV) than in 1.6 mM H_2O, where hysteresis was not observed, and is determined to be less than 100 mV. The E_{pit} observed in potentiostatic scratch tests is compatible with the value near 100 mV observed in PDP in the same solution. E_{rep}, on the other hand, is higher than the value observed in PDP (near -400 mV). Comparing the two water concentrations used in scratch tests, it becomes clear that increasing water concentration from nearly 1.6 mM to 87 mM results in the elevation of E_{pit} and E_{rep}, as well as the formation of a potential range where passivity is metastable, akin to the potential range of the hysteresis loop formed in PDP.

The assumptions regarding the relationship between the current transients from scratch tests and the corrosion phenomena taking place on the surface of C-22 can be better understood using SEM. Figure 4.12 shows a series of micrographs after potentiostatic polarization of C-22 in ACN / 0.14 M Bu_4NCl with two different water concentrations. The specimens were scratched in solution after 10 min at -200 mV vs Fc/Fc^+. Comparing with results from PDP in Figure 4.3-a, it would be expected that for both 2.3 and 44 mM H_2O, -200 mV vs Fc/Fc^+ would fall between E_{pit} and E_{rep} of C-22. However, at 2.3 mM H_2O the current rises before scratching, which indicates that pitting takes place spontaneously. In this condition, scratching the electrode does not affect the anodic current. As verified in subsequent micrographs, the corrosion damage is widespread and occurs on the entire surface of the sample. The damage inside the scratch seems less intense and pits are smaller, probably due to shorter time of exposure and the modifications caused by the intense local deformation.

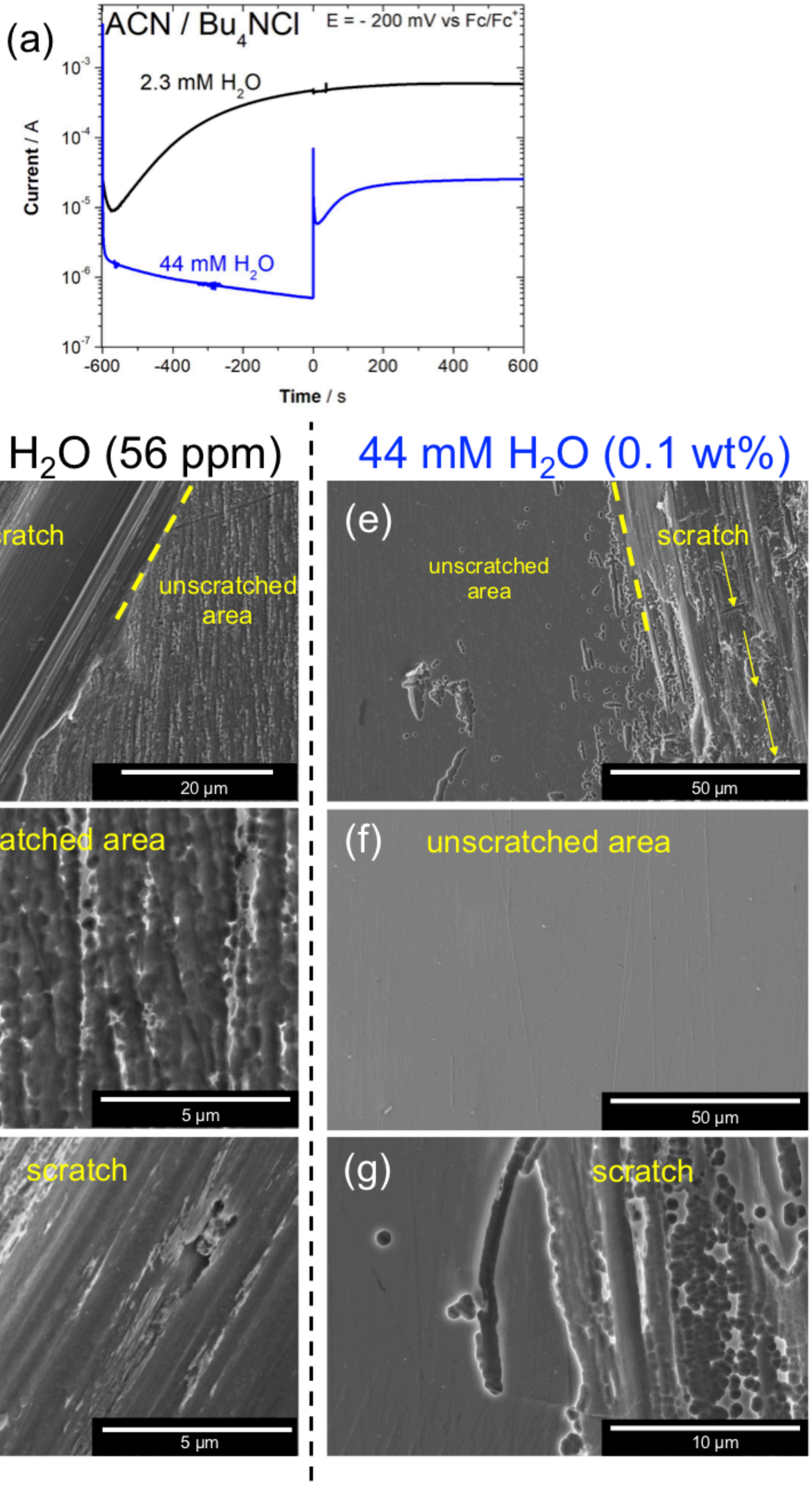

Figure 4.12: Potentiostatic chronoamperometry with the scratched electrode technique of C-22 at -200 mV vs Fc/Fc$_+$, in ACN / 0.14 M Bu$_4$NCl, varying water concentration. Exposed area = 0.785 cm^2.

At 44 mM H_2O, the current transient indicates a situation of metastable passivity: before the scratch, the surface was protected by a passive oxide film but, once this film is removed by scratching, the current rises and stays high. This behavior is compatible with the data from PDP and with the notion that, because we are above the repassivation potential, stable pitting can occur. Upon inspection of the micrographs after the test, it can be seen that the nucleation of new pits is limited to the scratched area and its surroundings. Regions far from the scratch did not corrode during the entire 20 min of polarization. It can be seen that pits spread out of the scratch forming channels, and some new pits nucleate near the scratch. This might be a consequence of two reasons: intense plastic deformation imposed at the surroundings of the scratch – which can be expected to cause cracking of the oxide film and favorable sites for pit nucleation; and changes in local chemistry due to anodic dissolution which results in local acidification.

Discussion

In polar aprotic solvents, the transition between passivity and pitting is smooth

The process of pitting corrosion in aprotic organic solvents presents a few general characteristics which are different from the pitting phenomena observed in water. The main features observed are discussed below, in comparison with recent developments on the theory of aqueous pitting.

The first remarkable difference is that the transition between passivity and pitting usually presents a smooth and gradual elevation of current density, presenting a difficulty to the determination of the exact moment where pitting starts in PDP. Other works with Ni-Cr-Mo alloys in aqueous HCl solutions [62] have observed that, at temperatures in which the passive film is very stable, pitting occurs by a sudden elevation of current density by several orders of magnitude (a non-polarizable electrode behavior), indicating a mechanism controlled by passive layer breakdown. These characteristics are usually associated with conditions where passive layer breakdown is the limiting step [63]. By contrast, it can be inferred that passive film breakdown in aprotic solvents of low water concentration takes place easily and it is not the limiting step, a situation commonly associated with more aggressive environments. The post-test morphology replete with small pits can thus be explained by a high rate of passive film breakdown and a high pit nucleation rate consequently. However, in most situations where the passive film breakdown happens easily, numerous metastable pits are found to nucleate and quickly repassivate below the potential for stable pit growth [62]. This phenomenon was not observed in this study, which suggests that the nucleated pits can easily achieve the critical local chemistry necessary for stable pit growth. In the existing pit models (developed for aqueous environments), the survival of pits is attributed to the development of high local concentrations of metal cations (and consequent changes in pH and migration of Cl^-). In polar aprotic solvents the requirements for pit stability might be completely distinct because activity of Cl^-, activity of metal cations and availability of H_2O differ by orders of magnitude from the values found in water.

Pits can grow to substantial sizes while maintaining a crystallographic morphology

Another surprising difference is that the pits formed in polar aprotic solvents can grow to substantial sizes while holding a crystallographic morphology. Crystallographic pits are generally associated with growth under activation control, in the absence of a salt film separating the pit surface and the electrolyte. It has been proposed by Li et al.[64] that a pit can grow under activation control when the concentration of metal cations at the pit/electrolyte interface(C_{surf}) is lower than the concentration required for precipitation of a salt film (C_{sat}), while still being higher than a critical concentration below which the pit would repassivate

(C_{crit}). In aqueous solutions, these conditions are met at the early stages of pit growth or under very low applied potentials (low driving force). In the present study, crystallographic pitting is the main form of corrosion, and in most cases pits repassivate without ever entering a mass transport control. The fact that metal halides are generally less soluble in ACN than in water[9] could lead to the expectation that C_{sat} would be lower, thereby making pits transition into mass transport control more easily, which is not the case. The following combination of hypotheses are proposed as an explanation to this peculiarity:

1. Because of the low availability of water, pits have a much lower tendency to repassivate. Thus, the pit local chemistry does not need to be as harsh as in aqueous solutions for the pit to survive – a lower concentration of metal cations is needed (C_{crit} is low), and pits can survive at low current densities.
2. The combination of the widespread passive oxide breakdown and the ability to survive at low current density results in a large number of stable pits growing simultaneously. Thus, in a cyclic PDP experiment the anodic current density recorded is shared by a large number of pits, each of them with a very small local current density. Pits will therefore grow slowly, and C_{surf} will fail to surpass C_{sat} because diffusion of metal cations out of the pit is faster than anodic dissolution.
3. The solutions used in this study are generally of higher resistivity than most aqueous chloride solutions. The increase in ohmic drop (ϕ_{sol}) during pit growth is therefore not negligible, and the effective potential at the pit/electrolyte interface (E_{max}) will be lower than the applied potential (E_{app}), as pointed by Li et al.: $E_{max} = E_{app} - \phi_{sol}$. Because ϕ_{sol} will increase as pits grow, E_{app} will not change so rapidly, and the dissolution current density will remain low, under charge transfer control. Thus, the local ohmic drop should help ensure $C_{surf} < C_{sat}$.

Clearly, the careful testing of these hypotheses would require a simplified experimental setup such as “lead-in-pencil” single pit experiments, where ϕ_{sol} can be more accurately estimated and the actual pit dissolution current can be measured.

Addition of water increases pitting and repassivation potentials

With a fixed chloride concentration, the increase in water concentration in aprotic solvents generally beneficial and results in elevation of E_{pit} and E_{rep}. Above a critical concentration of water usually around 0.5 M, pitting ceases. As mentioned previously, the models describing the pitting mechanism have been developed for aqueous solutions, where molarity of water can be assumed a constant. However, water should impact both passivity breakdown and pit stability. Before breakdown, it is reasonable to assume that

H_2O (as well as OH^-) adsorbs on the surface of the passive oxide in competition with Cl^- anions, hindering chloride attack of the passive oxide.

After local breakdown, OH^- is expected to migrate to local anodic sites in competition with Cl^-. However, if the mechanism were dependent on the activity of OH^-, one should expect extreme differences in E_{pit}, E_{rep} and critical water concentration between the solvents used, because both water dissociation and activity coefficient of OH^- can be expected to decrease drastically from ACN to DMF and to DMA. This does not seem the case, as pitting ceases at similar water concentration in all three solvents. It can also be hypothesized that increasing water concentration enhances a pit's ability to repassivate, requiring a higher C_{crit} to maintain a pit active. Thus, a pit needs a higher dissolution current density to survive and a higher applied potential consequently. This could also explain why pits become larger as water concentration increases. However, the dependence of pitting variables on water concentration does not seem so straightforward, as evidenced by experiments in ACN, where E_{pit} and E_{rep} seem to initially decrease with small additions of water. Although the present results cannot confirm, this phenomenon could be of the same nature as the increase in the kinetics of active dissolution observed when small concentrations of water are added to ACN-HCl solutions (previous chapter). The reason why this is only seen for ACN might be that water in ACN is expected to remain mostly H_2O, whereas in DMF and DMA a higher dissociation is expected.

Comparing scratch tests at a potential between E_{rep} and E_{pit} (Figure 4.12), it seems that passive film breakdown becomes more important at higher water concentrations. At low water concentration, anodic current density increases over time even below E_{pit}. At higher water concentration at the same potential (44 mM), the current density only rises when the sample is scratched. Two interpretations are possible: (i) at higher H_2O concentrations, passive film is more stable and its breakdown becomes the slow limiting step, or (ii) when the scratch bares the metal surface metal dissolution occurs, which creates a local solution chemistry that allows pitting to progress. If the second line of interpretation is used, the small size of pits nucleated on the scratch is justified because they do not grow under strong driving force. However, even if explanation (ii) is valid for this potential (-0.2 V vs Fc/Fc^+) and H_2O concentration (44 mM), passive film breakdown will eventually become the limiting step if $[H_2O]$ continues to increase, as the corrosion behavior should eventually approach that of C-22 in aqueous chloride solutions. Clearly, the addition of water increases the potential interval where pitting can be stable but is still not spontaneous ($E_{rep} < E < E_{pit}$), indicating a higher stability of the passive film.

Decrease of bulk chloride concentration elevates E_{pit} and E_{rep}, and changes kinetics of pit growth

The results in this study show that C-22 can corrode by pitting at room temperature in aprotic solvents with small concentrations of chloride (140 to 2 mM). The tests with different chloride concentrations reveal a dependence of E_{pit} and E_{rep} on chloride concentration of the kind $E = a - b \log[Cl^-]$. Such a dependence has been explained by different models on the initiation and progression of pitting with basis on passive film breakdown[65] or pit stability [64,66]. The present results do not contradict the models developed, but some considerations are necessary regarding the application of existing models.

A particular characteristic of aprotic solvents is their poor acceptor strength, characterized by a low acceptor number (AN) (Table 3.2). As a consequence, the solvation energies for small anions such as Cl^- and OH^- are much higher than in water, thereby elevating their activity coefficients [9]. The concept of transfer activity coefficient $\gamma_t(Cl^-, R \rightarrow S)$ can be used to estimate the difference between activity coefficients of chloride in a reference solvent (R) and in the solvent of interest (S), using the Gibbs free energy of solvation ($\Delta G^\circ_{Cl^-,solvent}$):

$$\log \gamma_t(Cl^-, R \rightarrow S) = \frac{\Delta \boldsymbol{G}^\circ_{\boldsymbol{Cl^-,S}} - \Delta \boldsymbol{G}^\circ_{\boldsymbol{Cl^-,R}}}{2.303\, R\, T} \qquad (1)$$

Using the data in Table 3.2 and water as a reference solvent, it can be calculated that $\log \gamma_t(Cl^-, H_2O \rightarrow ACN) = 8.8$, $\log \gamma_t(Cl^-, H_2O \rightarrow DMF) = 9.0$, and $\log \gamma_t(Cl^-, H_2O \rightarrow DMA) = 10.3$ (assumptions used in this approach can be found in reference [9]). Thus, it can be inferred that Cl^- in all three solvents will be roughly 10^9 times more reactive than in water. This may cause large changes on the chemical effects of chloride on passive film breakdown – such as adsorption and initial reaction with passive oxide – and on pit stability, where a change of reactivity of Cl^- might impact the tendency to repassivation of an existing pit.

The higher activity of chloride might explain why pitting of C-22 is much easier in aprotic solvents than in water. However, the participation of Cl^- in heterogeneous reactions will also depend on its competition with OH^- for adsorption sites, considering that the latter should also have a high activity coefficient in aprotic solvents ($\Delta G^\circ_{OH^-,solvent}$ values necessary for a similar calculation were not found). This complicates the comparison between solvents because H_2O will have different dissociation constants – in ACN, Cl^- is more likely to compete with H_2O instead of OH^-. At a fixed water concentration, one could expect that the change in chloride concentration would result in a steeper change in pit parameters in the solvents where $\gamma_t(Cl^-)$ is higher. However, the slopes of E_{pit} and E_{rep} vs log $[Cl^-]$ did not follow such a trend, which indicates that the differences in chloride activity coefficient between the aprotic solvents was not the determining factor for pit stability or initiation. Still, the general observation that a decrease in $[Cl^-]$ results in a higher necessary potential for pit growth suggests that a higher local dissolution rate and higher anodic potential are necessary for pit stability and maintenance of a C_{crit}.

When [Cl^-] decreases to a few mM, pits start to transition into mass transport control, and cease being crystallographic, which is associated with the precipitation of salt film in the pit. Using the model developed by Li et al.[64], this could be explained by a narrower range between C_{crit} and C_{sat} or a more rapid transition between the two limits. Possibly because pitting starts at a high potential, the dissolution current increases more rapidly in the activation control phase, causing C_{surf} to surpass C_{sat} and thereby precipitating a salt film. It is also possible that corrosion products from the dissolution process inside the pit require complexation with chloride for their solubility and become less soluble when chloride concentration is lower. C_{sat} would therefore decrease in lower chloride concentrations, resulting in precipitation of a salt film at a lower current density. For some of the PDP in low Cl^- concentrations which exhibited mass transport control, a rise in current was observed at high potentials. Because the samples showed a uniform attack of the surface in subsequent SEM, this region can be associated with transpassive corrosion.

Comparison between acidified and neutral chloride solutions

The comparison between the results found in this study and the results obtained in HCl solutions of the same solvents allows one to reflect on the influence of different chloride species on passivity and localized corrosion. As previously mentioned, because of the different degree of acid dissociation in ACN, DMF and DMA, the availability of free Cl^- anions will differ by orders of magnitude for HCl solutions of different solvents. In this study, however, because the source of chloride is an electrolyte salt that dissolves in the three solvents, we can assume that the concentration of Cl^- is roughly the same. One of the main observations in the study in HCl solutions was the dependence of the mode of corrosion on the dissociation of HCl: in DMA and DMF, where HCl is more dissociated ($pK_a = 1.9$ and 3.3, respectively), pitting occurs; in ACN, where HCl dissociates the least ($pK_a \approx 10$), corrosion is uniform. This study shows that, when Bu_4NCl is used instead of HCl, C-22 undergoes pitting in all three solvents, which corroborates with previous observations.

For solutions of DMA and DMF, where C-22 pits both in HCl and in Bu_4NCl, E_{pit} and E_{rep} values can be compared. In DMF / 0.14 M Bu_4NCl solutions, despite the higher concentration of Cl^- used, pitting potentials are higher than in 0.11 M HCl solutions of similar water concentration: in DMF-HCl with 84 mM H_2O, E_{pit} is circa -0.275 V vs Fc/Fc^+; in DMF-Bu_4NCl extrapolated to the same water concentration, E_{pit} is 0.020 V vs Fc/Fc^+, a difference of almost 300 mV. Repassivation, on the other hand, seems to occur at similar potentials for the same range of water concentration: in DMF-HCl with 84 mM H_2O, E_{rep} is circa

-0.525 V vs Fc/Fc$^+$; in DMF-Bu_4NCl extrapolated to 84 mM H_2O, E_{rep} is circa -0.560 V vs Fc/Fc$^+$. A similar trend is observed when comparing DMA solutions: in DMA-HCl near 90 mM H_2O, $E_{rep} \approx -0.375$ V and $E_{pit} \approx -0.175$ V; in DMA-Bu_4NCl extrapolated to the same water concentration, $E_{rep} = -0.115$, $E_{pit} = 0.234$ V. Thus, neglecting any effects of methanol from the HCl reagent, it can be inferred that pitting occurs at lower potentials in HCl than in neutral chloride solutions of DMF and DMA. Because the Bu_4NCl solutions had a higher Cl^- concentration, this observation appears to be in contradiction with the notion that a higher availability of Cl^- anions will lower E_{pit} and E_{rep}. However, because HCl is more dissociated in DMF and in DMA than in ACN, the effect of solvated protons in these solvents might play a role in destabilizing (or thinning) the passive oxide or in impeding pits from repassivating. It should be noted that the pit morphology in HCl and Bu_4NCl solutions with near values of water concentration also differs: in HCl, pit size is smaller and density of pits is higher than in Bu_4NCl. Thus, bulk solution acidity might facilitate passive oxide breakdown, increasing the frequency of pit nucleation events.

Conclusions

Although Ni-Cr-Mo alloys are well-known for their resistance to pitting at room temperature, their application in aprotic organic solvents remains challenging, due to the limited knowledge of non-aqueous wet corrosion. In this study, the pitting corrosion of C-22 in neutral aprotic solvents containing chloride was studied using electrochemical techniques and microscopy. The effect of solvent, water concentration and chloride concentration was studied, and the compatibility with existing models of pitting corrosion was discussed. The main findings can be summarized as follows:

- The transition between passivity and pitting in aprotic solvents happens by a gradual elevation of currents, producing numerous pits of similar size. This behavior indicates a process happening under small driving force, as consequence of the unstable nature of the passive oxide at low water concentrations. When water concentration increases, the stability of the passive oxide apparently increases.
- Pits can maintain a crystallographic morphology while growing to unusually large sizes. This fact can be explained by the unusual combination of high pit stability (due low tendency to repassivation) and slow increase in local current density (as consequence of local ohmic drop and large number of pits). Therefore, pits can survive long periods under activation control without precipitating a salt film.

- Addition of water is generally beneficial to the inhibition of pitting corrosion. E_{pit} and E_{rep} increase with water concentration in most conditions and above a critical concentration (circa 0.5 M H_2O in 0.14 M Cl^- solutions) pitting is completely mitigated in all solvents studied. The dependence of pitting corrosion on [H_2O] seems more complicated in ACN, perhaps due to multiple effects of water on the anodic kinetics of pits growing under activation control.

- Pitting occurs even at very small chloride concentrations, which might be a consequence of the high activity of Cl^- in aprotic solvents. When chloride concentration is varied, E_{pit} and E_{rep} vary following a dependence of the type $E_{pit;rep} = a - b\log[Cl^-]$, where a and b depend on the solvent used. At low chloride concentrations, pits tend to transition into mass transport control.

- The results obtained in this study support previous observations that a high availability of Cl^- anions in aprotic solvents leads to pitting corrosion, whereas undissociated HCl promotes uniform dissolution.

Chapter 5 : The influence of alloy composition on the passivity of Ni-Cr-Mo alloys in aprotic solvent containing HCl

Introduction

According to the literature on corrosion resistant alloys, alloys with a higher %Mo and higher %W (and, consequently, lower %Cr) present the highest corrosion resistance in reducing aqueous solutions. Conversely, alloys with high % Cr have the highest corrosion resistance in oxidizing aqueous solutions[67]. The suitability of an alloy for an oxidizing or reducing environment is empirically assessed with the atomic percent factor (APF) [2]:

$$APF = \frac{4Cr}{2Mo + W} \tag{1}$$

where the symbols represent the weight percentage of the element in the alloy. Generally, an alloy with a high APF will have higher corrosion resistance in an oxidizing environment, whereas an alloy with a low APF will have a higher corrosion resistance in a reducing environment. Because these guidelines are based on research carried in aqueous solutions, it is not known if the same is valid in aprotic organic solvents. Therefore, alloys with different APR were chosen for the comparison with C-22 in ACN solutions. Table 5.1 shows the chemical composition and APF of alloys G-35 and Hybrid BC-1 (BC-1 for simplicity) in comparison to that of C-22. Due to its high Cr and low Mo content, G-35 has the highest APF and the opposite can be said of BC-1.

Table 5.1: Nominal chemical compositions of Ni-Cr-Mo alloys used in this study.

Alloy (UNS number)	Cr (wt%)	Mo (wt%)	W (wt%)	Fe (wt%)	Ni	APF
Alloy 22 (N06022)	22	13	3	3	Bal.	3.03
G-35 (N06035)	33	8	-	-	Bal.	8.25
Hybrid BC-1 (N10362)	15	22	-	-	Bal.	1.36

In this study, the corrosion behaviors of Ni-Cr-Mo alloys of different compositions were characterized in ACN-HCl solutions, aiming to answer the following questions: (i) What is the effect of alloy composition on the active-passive characteristics observed for C-22? (ii) Is the effect of water on passivity dependent on alloy composition? (iii) Are high-Cr alloys suited for application in oxidizing solutions of aprotic solvents?

(The experimental approach of this chapter has been suppressed because all techniques have been explained in previous chapters)

Results

Electrochemical tests in reducing solutions: ACN-HCl

The anodic kinetics of Ni-Cr-Mo alloys in ACN-HCl solutions of various water concentrations [H_2O] was studied by anodic PDP starting below OCP, and results are shown in Figure 5.1. The three alloys show a similar behavior, characterized by active dissolution at small positive polarizations. Near the open circuit potential, increasing the concentration of water results in a shift of the anodic branch to lower potentials, which is associated to a less noble (more active) behavior. This shift is observed for all three alloys but it

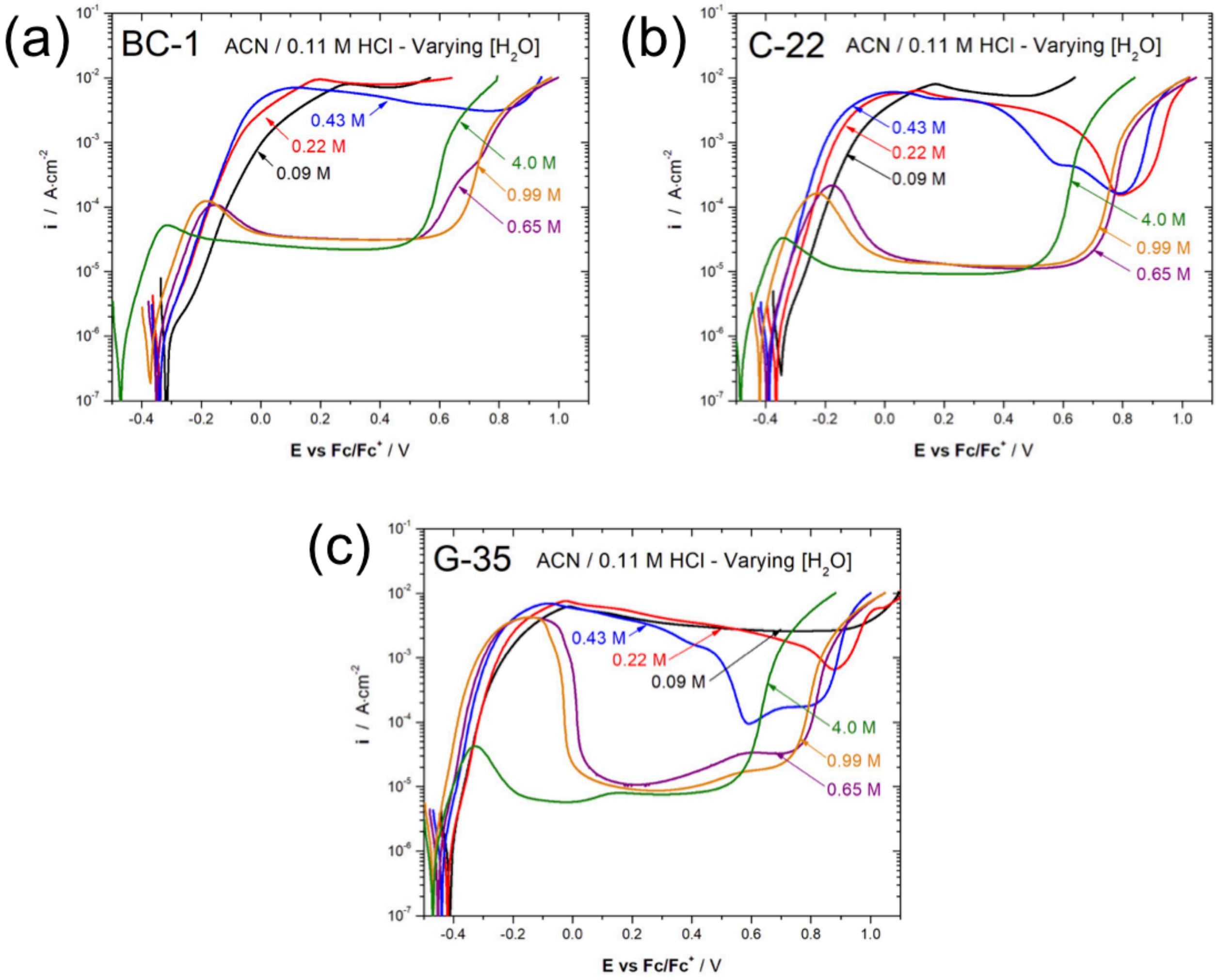

Figure 5.1: PDP of alloys G-35, C-22, and BC-1 in ACN / 0.1 M HCl with different concentrations of residual water.

is more intense for BC-1 (high Mo, low Cr), whereas in the case of G-35 (low Mo, high Cr) the shift is smaller. At lower [H_2O], the active behavior is maintained up to anodic current densities of almost 10 $mA\cdot cm^{-2}$, where current stabilizes and then presents slow decay with potential. In this region the dependence of current density on small changes in [H_2O] is not clear. However, if [H_2O] increases sufficiently, all alloys present an active-passive transition, characterized by the formation of a 'nose' followed by a negative *i vs E* dependence until a small stable anodic current density is achieved (i_{pass}). For BC-1, this transition is observed at between 0.43 and 0.65 M H_2O. For C-22 and G-35, which have higher concentrations of Cr, a high potential active-passive transition is observed at (typically > 0.6 V) for water concentrations as low as 0.22 M H_2O. For [H_2O] ≥ 0.65 M, C-22 and G-35 undergo an active passive transition like that of BC-1, with current densities in the order of 10 $\mu A\cdot cm^{-2}$. In contrast, the high-potential passive state at 0.22 M ≤ [H_2O] ≤ 0.43 M has higher current densities of hundreds of $\mu A\cdot cm^{-2}$. In all cases, the passive behavior ends when the current density rises at high potentials associated with transpassive dissolution. The potential where transpassive dissolution begins is strongly affected by [H_2O], decreasing with the elevation of [H_2O]. This potential shift is more intense for C-22 and G-35, which have more Cr.

Figure 5.2a shows the maximum current density at the active nose (i_{max}), extracted from PDP experiments in ACN-HCl solutions. Although at low [H_2O] an active-passive transition is not observed at low potentials, a peak still forms due to the decrease in current density with increase in potential. In such conditions, all alloys present high i_{max}, and BC-1 presents the highest values. When [H_2O] increases above 0.43 M an active-passive transition is seen for all alloys and i_{max} drops for C-22 and BC-1 but remains high for G-35, indicating a higher rate of oxidation required for the formation of a passive film. As [H_2O] keeps increasing,

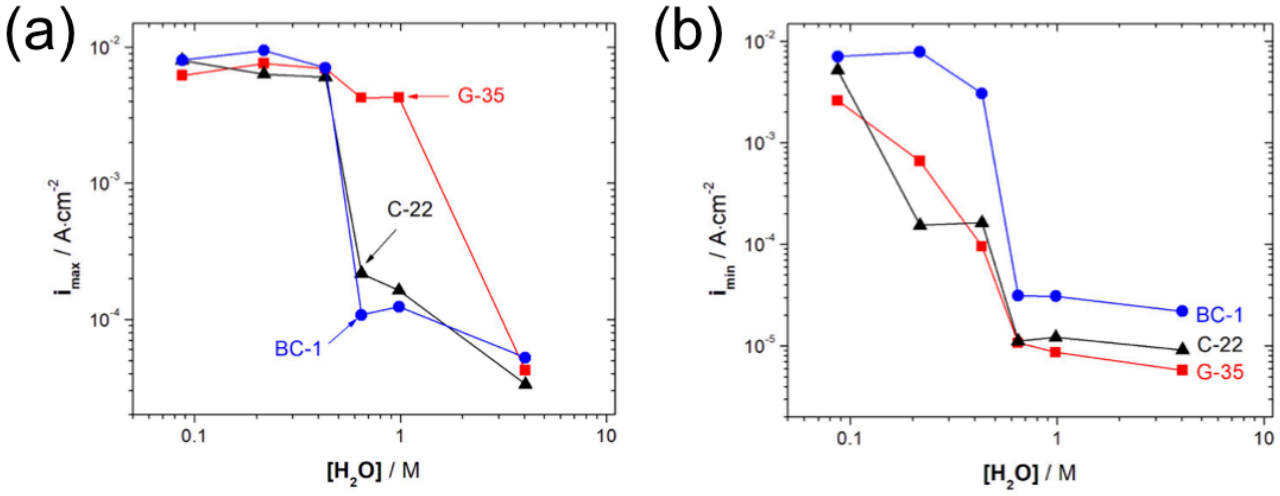

Figure 5.2: Maximum current density at the active nose (i_{max}) and minimum current density after the active nose (i_{min}) extracted from PDP experiments.

i_{max} continues to drop and, at 4.0 M H_2O, G-35 presents a similar i_{max} as other alloys. Figure 5.2b shows the minimum values of current density after the active nose (i_{min}), measured at different potentials. At low [H_2O], BC-1 presents the highest values. The i_{min} of G-35 and of C-22 present a more gradual decrease with [H_2O] because the values measured at 0.22 and 0.43 M H_2O correspond to the high-potential passive zone. Above 0.43M, i_{min} drops for all alloys indicating a passive state, so i_{min} corresponds to the lowest passive current density (i_{pass}). i_{min} keeps decreasing for higher [H_2O], indicating an improvement in passivity with higher water concentrations.

The potential that marks the lowest limit of the passive region in a PDP scan is known as the Flade potential (E_{flade}). In this study E_{flade} was measured by fitting the current density in the pre-passive region (where *i* decreases with *E*) of a *log(i) vs E* plot with a straight line, then finding the intersection of this line with the passive current density. The results obtained for the active passive transition at lower potentials are shown in Figure 5.3. The transition observed at high potentials for C-22 and G-35 was not included in the plot, since it could be a phenomenon of different electrochemical nature. All alloys present a reduction of E_{flade} with increase in [H_2O], with a dependence of the type $E_{flade} = a + b\log[H_2O]$. The E_{flade} of G-35 appears

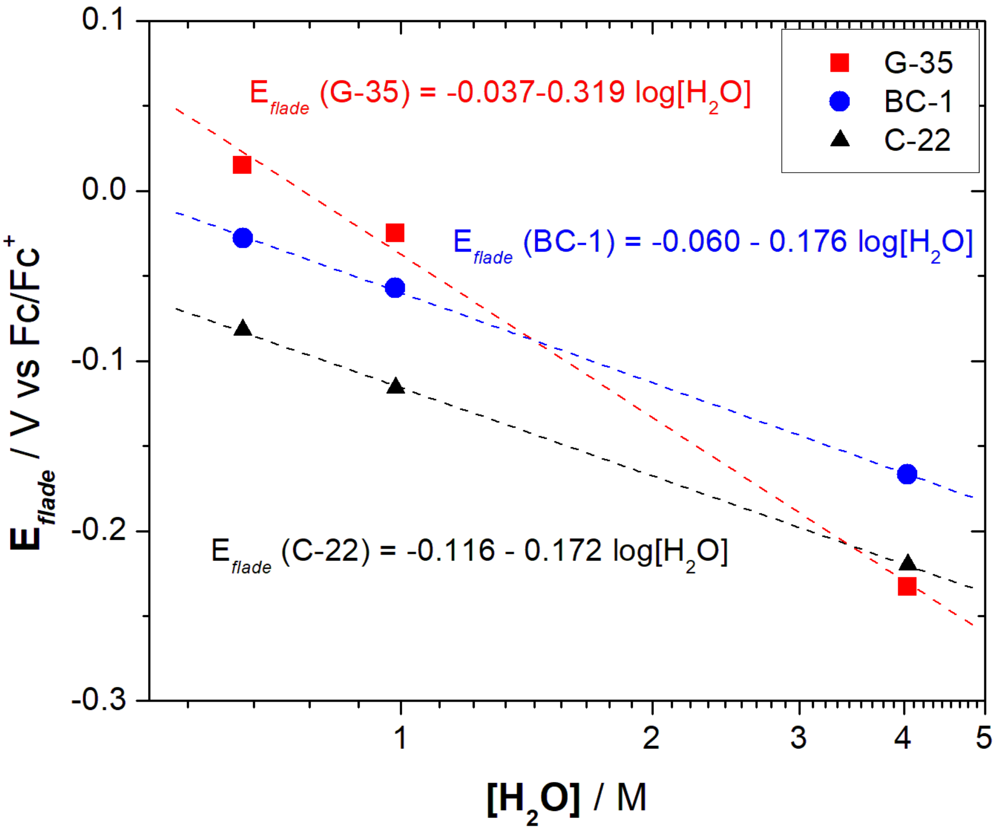

Figure 5.3: Flade potential (E_{flade}) obtained from PDP in ACN / 0.1 M HCl with different

more sensitive to [H_2O], showing a more negative slope (*b*) than the other two alloys. At low water concentration, C-22 presents the lowest E_{flade}, followed by BC-1 and G-35. At high water concentration (4.0 M), G-35 has the lowest E_{flade}, followed by C-22 and BC-1.

The tendency to passivation can also be assessed by measuring the potential where i_{max} is reached (E_{max}), shown in Figure 5.4. When [H_2O] > 0.43 M, E_{max} shows a similar trend as E_{flade}, with a $b \approx -200$ mV for all materials. For G-35 this relation seems to hold even at low water concentrations. For C-22 and BC-1, in contrast, the E_{max} data below 0.65 M H_2O shows a different behavior.

The potential where the passive oxide breaks down and the transpassive dissolution starts (E_{trans}) was estimated by measuring potentials at $1 mV \cdot cm^{-2}$ in the transpassive region, instead of using the interpolation method (Figure 5.5). Also in this case a dependence of the type $E = a + b \log([H_2O])$ is found, with a *b* between -201 and -186 mV, which similar values found for the functions of E_{flade} and E_{max}. The value of *b* appears independent of alloy composition. The parameter *a* however, increases with Cr concentration (or decreases with Mo concentration) in the alloy, causing a shift of the line.

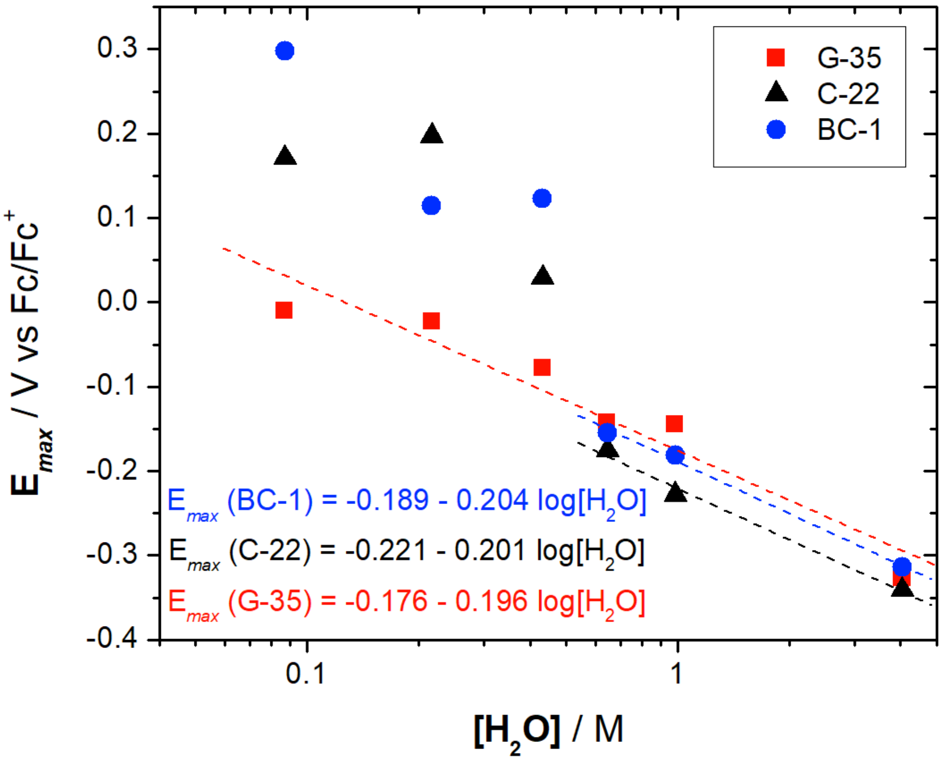

Figure 5.4: Potential of maximum current density (E_{max}) in the active nose. Solution: ACN/ 0.1 M HCl with various water concentrations.

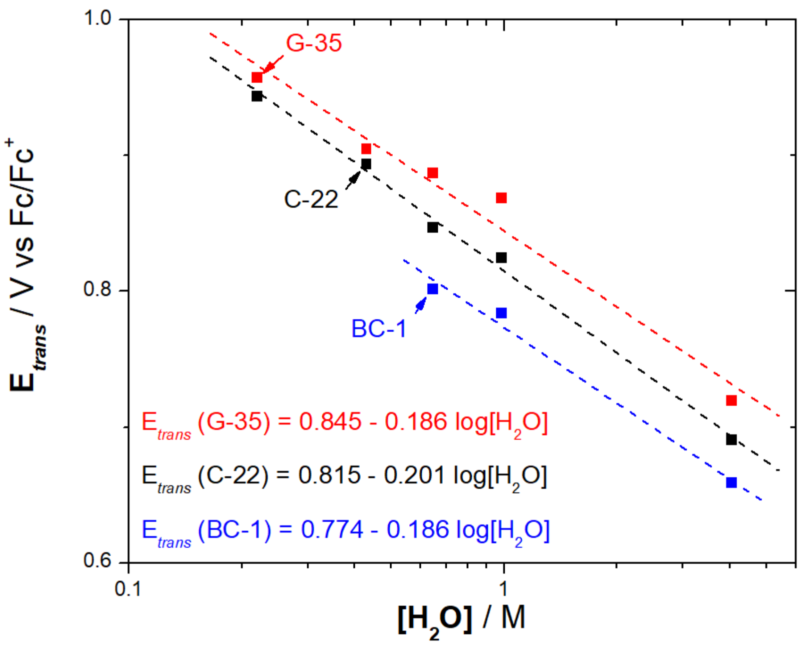

Figure 5.5: Potential marking the beginning of the transpassive region (E_{trans}). Solution: ACN/ 0.1 M HCl with various water concentrations.

Electrochemical tests in oxidizing solutions: ACN–HCl–DDQ

The choice of Cr content in Ni-Cr-Mo alloys often depends on how oxidizing the environment is, PDP was also performed in solutions containing DDQ (Figure 5.6). The strong oxidizing power of DDQ was characterized in the first study of this series. DDQ dry reagent was added to solutions ACN / 0.1 M HCL solutions containing 90 mM H_2O. The amount of residual water on the solution was not determined after addition of DDQ because of its interference with the KF-titration process. Thus, the DDQ-containing solutions shown may have slightly higher water concentrations. Clearly, the final water concentration is not high enough to provide an active-passive transition.

The cathodic PDP scans in Figure 5.6a contain information about the change in cathodic kinetics caused by the addition of DDQ. In ACN/HCl, all alloys are at corrosion potentials between -0.5 and -0.3 V vs Fc/Fc$^+$. The predominant cathodic reaction in this solution is presumably hydrogen evolution from HCl reduction, which is under charge transfer control down to circa -1.0 V vs Fc/Fc$^+$, where the current density gets limited by diffusion. In the charge transfer control phase, hydrogen evolution is more intense on BC-1 than on the other two alloys. When DDQ is added to the solution, the OCP of all alloys is elevated by circa 300 mV, due to the increase in cathodic current density, which appears diffusion-limited near the E_{corr}. The cathodic kinetics of DDQ reduction appear similar on the three alloys, with slightly higher current density values on G-35 at lower potentials.

The anodic PDP scans on Figure 5.6b show that the positive shift in OCP is also a consequence of inhibition in anodic kinetics, as indicated by the lower anodic current observed up to circa 0.25 V vs Fc/Fc$^+$. This phenomenon has been discussed in a previous study in solutions containing DDQ[52]. It should be noted that this effect ceases shortly above the equilibrium potential for the DDQ reduction reaction ($E[DDQ^{-/0}] \approx 0.2$ V vs Fc/Fc$^+$)[43]. This suggests that the reduced states of DDQ could have an anodic inhibition effect, as observed for quinones of lower potential [25]. Up to 0.3 V, G-35 is still the alloy with the highest anodic current density. For polarizations above circa 0.25 V, G-35 becomes the alloy with lowest anodic current density. At this point, however, all alloys present high anodic current density, and the advantages of using a high-Cr alloys appear to be small.

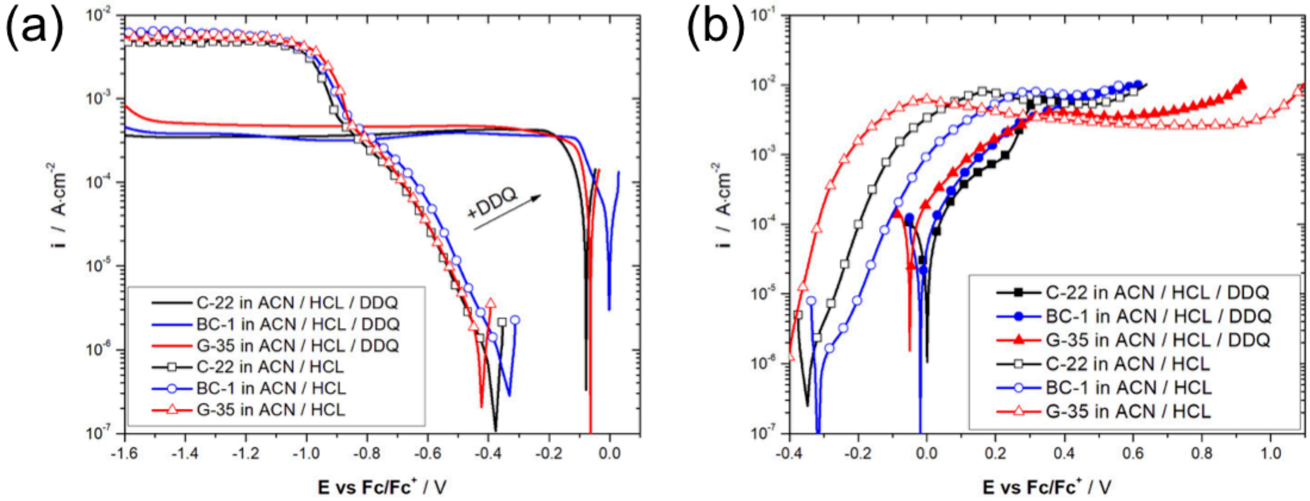

Figure 5.6: Cathodic (a) and anodic PDP (b) in ACN / 0.1 M HCl with and without 0.1 M DDQ addition.

To estimate the corrosion behavior at the corrosion potential, electrochemical impedance spectroscopy was carried out in ACN-HCl solutions with and without DDQ (Figure 5.7). The addition of DDQ has a profound impact on the impedance spectra. When DDQ is added, the magnitude of impedance (|Z|) at low frequencies decreases by more than one order of magnitude. In ACN-HCl solutions, the negative phase angles show that impedance has a capacitive behavior. When DDQ is added, the phase angle achieves positive values in the low frequency range, indicating a pseudo-inductive behavior. This behavior is often associated with electrochemical reactions (either in the cathodic or anodic half-cell) that depend on the surface coverage of an intermediate [68], which could be associated with the anodic inhibition effect of DDQ. Furthermore, the phase angle in ACN-HCl-DDQ solution presents only small absolute values, which means that Z has a resistive character, probably because the electrolyte resistance and polarization resistance have similar magnitudes.

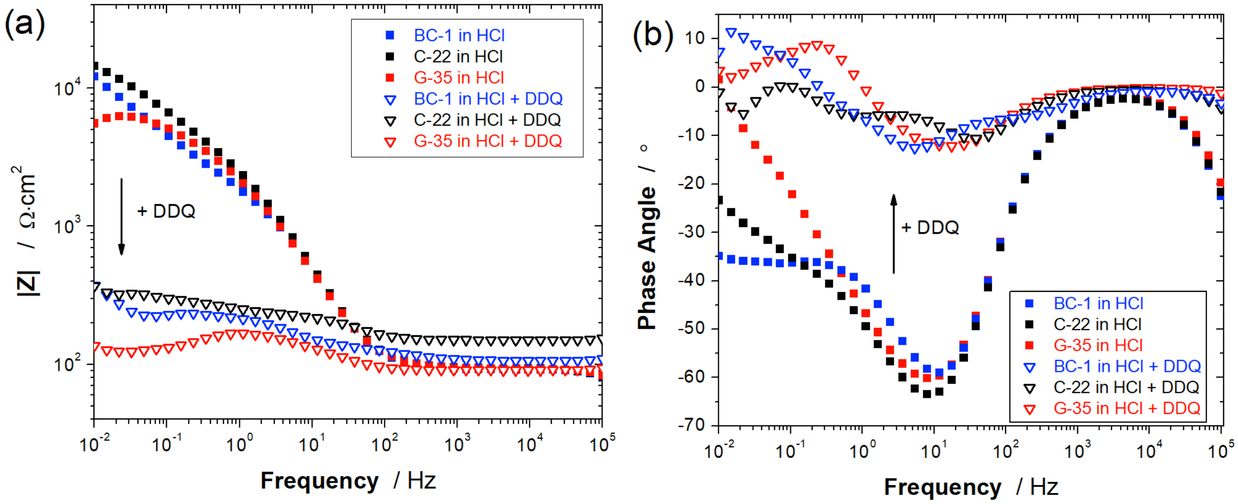

Figure 5.7: Bode plots of electrochemical impedance spectra of BC-1, C-22 and G-35 at the corrosion potential. Solutions: ACN / 0.1 M HCl, and ACN / 0.1 M HCl / 0.1 M DDQ.

For the spectra obtained in ACN-HCl solutions, the impedance behavior could be fitted with typical circuits used in the literature of Ni-Cr-Mo alloys of varying complexity [32,69]. The spectra obtained in ACN-HCl-DDQ solutions would require a different approach, utilizing inductive elements. The comparison between fitting parameters obtained by largely different and complex equivalent circuits can be questionable, especially when solution resistance (R_S) is high. Because the purpose of this analysis is providing a comparison between corrosion rates at open circuit, a more straightforward approach was adopted, comparing Z at 0.01 Hz with subtraction of solution resistance (R_S). R_S was determined as the |Z| when $\theta \rightarrow 0$ in the low frequency region (Figure 5.8). With the assumption that the polarization resistance (R_P) is inversely proportional to the corrosion current density, and that R_P can be approximated as $R_P \approx |Z|_{0.01\text{Hz}} - R_S$, it can be inferred that i_{corr} is highest for G-35 both in ACN/HCl and in ACN/HCl/DDQ. In the presence of DDQ, C-22 has a slightly lower $|Z|_{0.01\text{Hz}} - R_S$ than BC-1, indicating that BC-1 corrodes at a lower rate. If the cathodic reaction were diffusion-limited at the corrosion potential, the three alloys would have very similar corrosion current densities, which is not the case. The increase in i_{corr} associated with an increases in in E_{corr} is an evidence that the net effect of DDQ is the elevation of corrosion rate by intensification of cathodic kinetics, for all alloys.

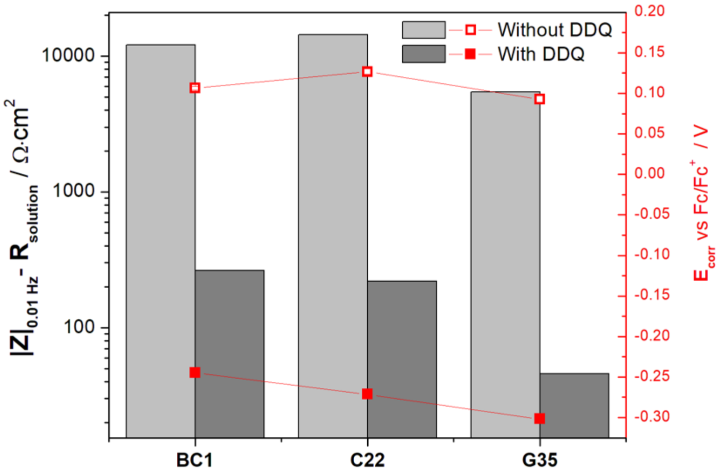

Figure 5.8: Low frequency impedance ($|Z|_{0.01Hz}$) after subtraction of solution resistance (R_s), from EIS spectra in ACN / 0.1 M HCl, with and without 0.1 M DDQ, and E_{corr} measure in the same solutions.

Mass loss tests

24-h mass loss tests were carried out to obtain a direct measure of the rate of corrosion of Ni-Cr-Mo alloys in ACN/HCl solutions of various DDQ molarities (Figure 5.9). The corrosion rate (CR) calculated for all alloys increases with DDQ concentrations. In the case of C-22, for which more data is available, a clear first order dependence on *log([DDQ])* is observed. With the assumption that the other alloys also have the same kind of dependence on [DDQ], the data were fitted and the slope of the logarithm function can be compared. The CR of BC-1, which has the lowest Cr content, presents the most positive growth with [DDQ], indicating that this alloy corrodes the fastest at very oxidizing conditions. Accordingly, G-35, which has the highest Cr content, will corrode the slowest at the more oxidizing conditions, but will probably corrode the fastest at less oxidizing conditions.

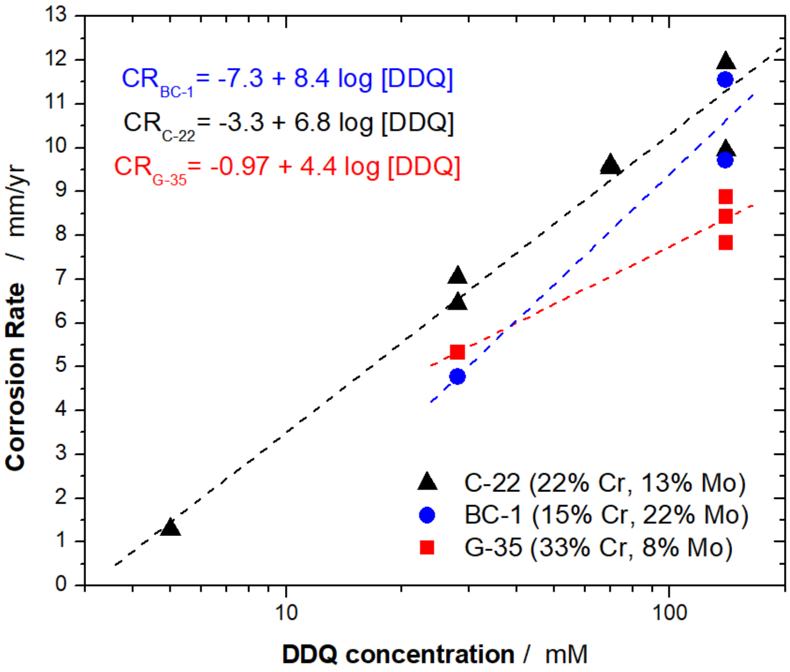

Figure 5.9: Corrosion rates calculated mass loss tests in the first 24 h of exposure to ACN / 0.1 M HCl with different DDQ concentrations, and approximately 90 mM (0.2 wt%) H_2O.

Discussion

Water concentration determines the limits of passivity

The results obtained from PDP experiment show that the passivity of Ni-Cr-Mo alloys is strongly affected by water concentration. At low water concentrations, all the three alloys present a strong active behavior. These results are similar to those obtained in aqueous solutions of concentrated acids [36]. If potential is elevated, the dissolution process ceases being controlled by charge transfer – anodic current density gets limited. The behavior in this potential region will be more carefully analyzed in the next chapter. The discussion in this chapter is focused on the potential range where active-passive transition may occur. When $[H_2O]$ reaches a critical value between 0.43M and 0.65 M, all alloys present an active-passive transition – this water concentration will thus be called $[H_2O]_{crit}$. Because $[H_2O]_{crit}$ falls in the same interval for all alloys used, these results do not suggest any relation between $[H_2O]_{crit}$ and alloy composition.

For any given potential in the active region of all alloys, an increase in water concentration results in an elevation of current density, often by over one order of magnitude. Clearly, in this range of potentials, addition of water will stimulate anodic dissolution even in concentrations above $[H_2O]_{crit}$. The explanation to this phenomenon has been discussed in Chapter 3. At potentials above the E_{max} (the potential of the nose tip) and below the transpassive region (E_{trans}), the effect of water will be beneficial, lowering the current density in the pre-passive and passive regions. Thus, the effect of water (positive or negative) is not only dependent on concentration, but also on applied potential and solution red-ox potential.

As seen in Figure 5.3 and Figure 5.4, an increase in [H_2O] provokes a decrease in E_{max} and E_{flade}, shifting the beginning of passivity to lower potentials. In aqueous solutions, the linear dependence of E_{flade} and E_{max} on pH has been extensively discussed [70]. This logarithmic dependence of E_{flade} on the activity of H^+ (a_{H^+}) stems from the fact that the net reaction involving oxide formation on a metal in aqueous solution will generate H^+ as a byproduct – when a metal oxide or hydroxide is formed, H_2O is consumed and H^+ is produced. In non-aqueous solutions the same principle applies. In a study on the passivation of pure Cr in anhydrous methanol [71], Banas found the equation $E_{flade} = E^0_{flade} - 58\ mV \log[H_2O]$, which was used to justify passivation by a reaction of the type:

$$Cr + 3H_2O \rightarrow Cr(OH)_3 + 3H^+ + 3e^- \qquad \text{(I)}$$

for which the Nernst potential can be calculated as

$$E = E^0 - \frac{RT}{nF}\ln\frac{a^3_{H_2O}}{a^3_{H^+}} = E^0 - 59mV\log\frac{a_{H_2O}}{a_{H^+}} \qquad (2)$$

for a $n = 3$, room temperature, and unity activities of Cr and $Cr(OH)_3$. Assuming that a_{H^+} does not change with water addition and that the activity coefficient of water ≈1, the dependence found by Banas is valid. The same reaction could control E_{flade} in ACN-HCl, but the slope (*b*) found in this study in the *E_{max} vs log(i)* plot is around -200 mV. If the reaction I controls E_{flade}, the deviation could be caused by interference of water on the equilibrium or the activity coefficient of H^+, which should be a more intense effect in aprotic solvents like ACN, as opposed to protic solvents like methanol. Indeed, Banas could not find the same potential relation for the passivation of Cr in DMF (also aprotic), where the dependence of E_{flade} on [H_2O] was much more complicated. Nevertheless, the fact that the three alloys present similar *b* in the *E_{max} vs log(i)* plot suggests that the active-passive transition is controlled by the same reaction irrespective of alloy composition.

Interestingly, water affects the passive-transpassive transition in a similar manner as it affects the active-passive transition. E_{trans} also obeys a function of the type $E = a + b\log([H_2O])$, with $b \approx -200$ mV. This means that water does not expand the passive region, only shifts it to lower potentials. As mentioned in Chapter 3, this can be explained by the participation of water in reactions that lead to the oxidation of Cr^{3+} to Cr^{6+}. Due to same *b* value, it can be said that the reaction that results in the degradation of the passive oxide has the same relation between n and the coefficients of a_{H^+} and a_{H_2O}. For both pure Cr and pure Mo in DMF-H_2SO_4 solutions, Banas found a b = -110 mV [72]. Further investigations need to be conducted to determine the exact nature of each reaction, considering the influence of solvent properties on activity coefficients of H_2O and H^+ in different solvents.

High-Cr alloys are not suitable when water concentration is below critical value

The choice of alloy for application in non-aqueous solutions is clearly not a simple task, due to the number of variables involved. For $[H_2O] < [H_2O]_{crit}$, the application of a high-Cr alloy such as G-35 is not a good choice, and alloys with a slower kinetics of active dissolution (such BC-1) are better suited. For potentials in the active region, the active dissolution of G-35 is faster (Figure 5.6); for potentials above E_{max}, G-35 has a lower current density than alloys with lower Cr, but the dissolution rate is still too high for practical use. When an ACN-HCl solution with $[H_2O] < [H_2O]_{crit}$ contained DDQ as an oxidant, the performance of G-35 was still inferior, since the redox potential of the solution was not high enough. However, mass loss tests showed that for longer exposure time G-35 can have a better performance in solution with higher concentrations of DDQ. Generally speaking, the application of high-Cr alloys in ACN with $[H_2O] < [H_2O]_{crit}$ is probably not advisable even in the case of oxidizing solutions, because these materials cannot form a Cr-rich passive oxide later.

When water concentration is just above $[H_2O]_{crit}$, Ni-Cr-Mo alloys can remain passive for a wide range of potentials. If potential is above $E_{flade(G\text{-}35)}$, G-35 becomes a good alternative due to its lower passive current density and higher E_{trans} in comparison with alloys of lower Cr content. If water concentration is further increased, the advantages associated with the application of high-Cr Ni-Cr-Mo alloys in oxidizing solutions seem to improve.

Conclusions

The anodic behaviors of Ni-Cr-Mo alloys BC-1, C-22, and G-35 in ACN-HCl reducing and oxidizing solutions were studied using electrochemical techniques with careful control of water concentration. The main findings can be summarized as follows:

- When water concentration is lower than the critical value necessary for an active-passive transition $[H_2O]_{crit}$, all alloys present an extended active region. For corrosion processes taking place in the active region, addition of water is detrimental to corrosion because it increases the kinetics of anodic dissolution. At elevated potentials, all alloys present a limited anodic current density above 1 $mA \cdot cm^{-2}$.

- When water concentration is above $[H_2O]_{crit}$, all alloys present an active-passive transition. $[H_2O]_{crit}$ is probably similar for all alloys tested, falling between 0.43 and 0.65 M. In this condition, an alloy with higher Cr concentration (such as G-35) generally will have lower passive current density and a higher potential for the onset of transpassive dissolution. Especially for G-35, however, the current density at the active nose can remain high even above $[H_2O]_{crit}$, so the potential needs to be above E_{flade} for corrosion protection.
- The active-passive transition (E_{max}, E_{flade}) and the passive-transpassive transition (E_{trans}) are similar dependent on water concentration, obeying a function $E = E^0 + b\ log([H_2O])$ with b ≈ -200 mV. Thus, increasing water concentration above $[H_2O]_{crit}$ does not widen the passive region, only shifts is to lowe potentials. The value of b is higher than the values reported in the literature for other organic solvents, which has been hypothesized to be a consequence of the effects of aprotic solvents on the activity of H_2O and H^+.
- The classical notion that Ni-Cr-Mo alloys of elevated Cr concentration have a better performance in oxidizing environments is generally not valid for low water concentrations (below $[H_2O]_{crit}$) where the formation of a passive oxide film is hindered.

Chapter 6 : Characterization of passive films formed in acetonitrile

Introduction

The corrosion resistance of Ni-Cr-Mo is dependent on the formation of a passive film that protects the bulk of the material. The composition of the passive film depends on the chemical composition of the alloy. Cr is known to promote the formation of a surface oxide film with good barrier properties and it has been shown that Cr is the main species in the passive films of Ni-Cr-Mo alloys[73]. The effect of Mo is usually associated with the stabilization of the oxide film and protection against localized corrosion, but the exact mechanism of its action is still subject research[7]. Some authors have proposed the formation of an ion-selective layer formed by Mo species which protects the underlying portions of the oxide[74]. Other reports have shown that the addition of Mo results in a higher content of Cr species in the passive oxide [75]. The determination of Cr and Mo species in the oxide layer is therefore essential for the understanding of corrosion behavior in passive conditions.

The results in the previous chapters have shown that, in ACN-HCl solutions with low water concentrations, a protective surface film does not form on Ni-Cr-Mo alloys. Still, anodic dissolution becomes limited under higher anodic polarizations, indicating a breach from charge transfer control, which could be caused by the formation of a film of poor protective properties. Above the critical water concentration which allows passivity to become possible, passive films form on the surface of the material. The results in the last chapter have shown that these films have a lower passive current density, and thus, slower anodic dissolution when water concentration is increased. The objective of this study is to characterize the composition and performance of the passive oxide films formed in low water concentrations to answer whether the passive films formed in ACN solutions are fundamentally different than those produce in aqueous solutions.

Experimental

(To avoid excessive repetition, only the experimental procedures which are different from those described in previous chapter are shown here).

Surface analysis by X-ray Photoelectron Spectroscopy (XPS)

Prior to surface analysis, samples were electrochemically prepared using a closed cell under N_2 atmosphere. The entire electrochemical preparation process was carried out inside an inflatable glovebox purged and filled with N_2 gas. The samples were submitted to a sequence of galvanostatic activation and anodic potentiostatic polarization (AP) steps, which are described in the results section. For the situations where the water concentration needed to be increased between the activation and AP steps, water was added with a micropipette through a port on the top of the cell, and the solution was quickly stirred. After the AP step, samples were quickly removed from the cell, rinsed with pure ACN and attached to the XPS sample holder inside the glovebox. Then, the glovebox was opened, and the sample was inserted in the XPS, and the vacuum pumps were immediately initiated. It is estimated that all samples were exposed to the lab air for no more than 30 s during the transfer process. XPS spectra were collected in a Scientra Omicron R3000 using monochromatic Al Kα with an excitation of 1486.7 eV and pass energy of 20 eV for the high-resolution spectra.

Results

Potentiostatic scratch tests at various water concentrations

The passivity of Ni-Cr-Mo alloys in ACN-HCl solutions and the kinetics of film formation in solution can be analyzed by scratching the working electrode while holding the electrode potential at a specific value, as done in previous chapters. In this study, the potential 0.3 V vs Fc/Fc$^+$ was chosen for potentiostatic tests. In ACN-HCl solutions where BC-1, C-22 and G-35 are able to passivate, this potential is about halfway between the active-passive transition and the transpassive region in PDP (Chapter 5), being a good choice for characterization of the passive behavior. Additionally, 0.3 V vs Fc/Fc$^+$ is far above the open circuit

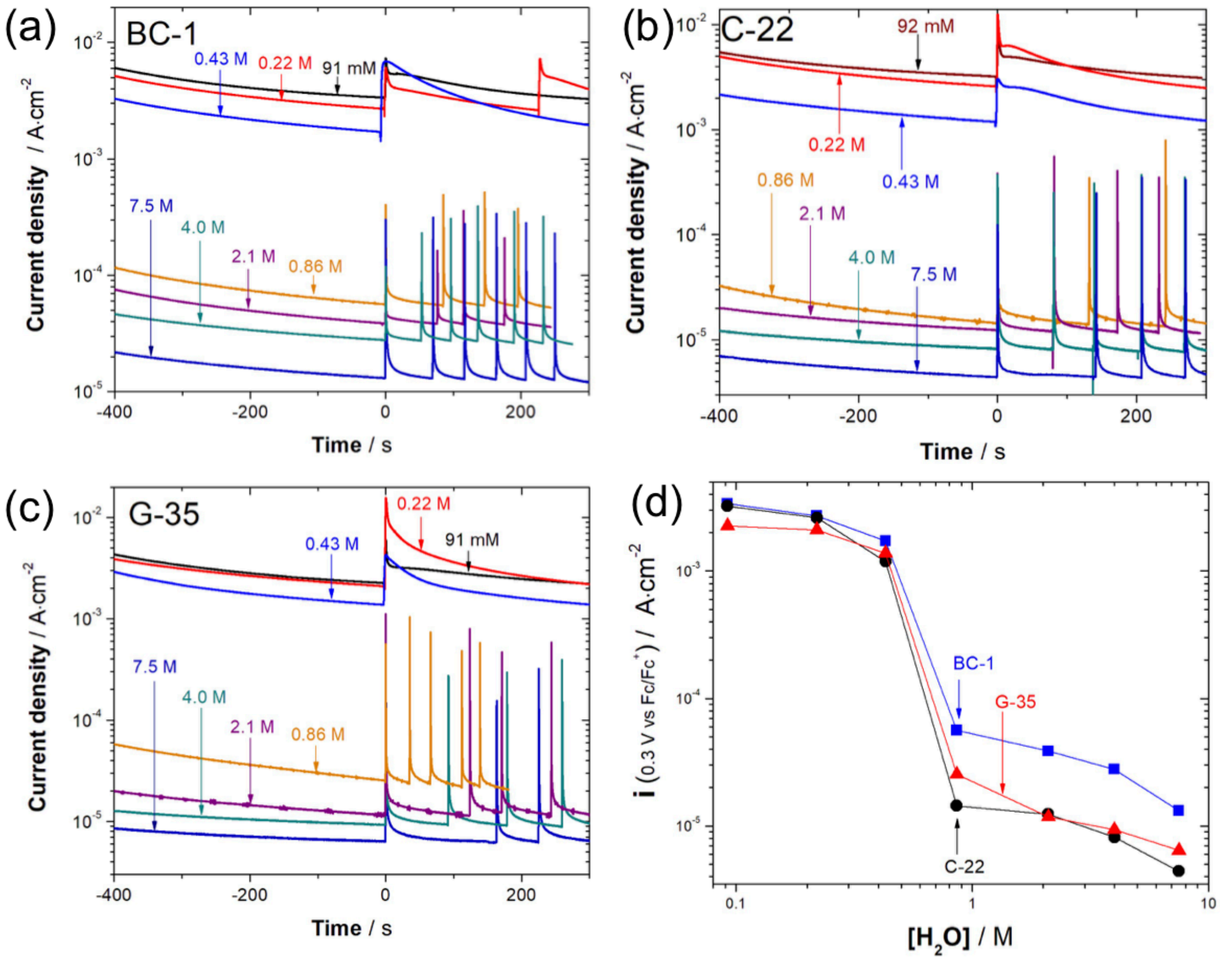

Figure 6.1: Potentiostatic scratch tests at 0.3 V vs Fc/Fc$^+$ for (a) BC-1, (b) C-22, and (c) G-35 in ACN / 0.1 M HCl, and various concentrations of residual water (indicated in figure). Plot (d) shows current density after 10 min of polarization, before scratching.

potential, which minimizes the effects of negative currents (due to changes in cathodic kinetics) while analyzing anodic potential holds.

Figure 6.1 shows the current transients obtained during potentiostatic polarizations in ACN-HCl with different water concentrations, for samples of 0.785 cm^2. The moment marked $t = 0$ is when the electrode was scratched, always 10 min after the potential hold had started. For all three alloys, the decrease in anodic current with increase in water concentration is clear. The current acquired after 10 min at 0.3V (before scratching) is shown in plot (d). The change in current density is evidently not smooth or gradual – there is a critical value between 0.43 and 0.86 M where the current drops to values around 10^{-5} $A \cdot cm^{-2}$ for all alloys. The current densities after the transition are compatible with a passive behavior. This limit can therefore be called the critical water concentration for passivation, $[H_2O]_{crit}$. A similar behavior was seen in PDP experiments using the same three alloys, where a $[H_2O]_{crit}$ was determined between 0.43 and 0.65 M H_2O. Both below and above $[H_2O]_{crit}$, BC-1 presents the highest current density. At very low $[H_2O]$, G-35 has the lowest current density but at water $[H_2O] > [H_2O]_{crit}$ G-35 and C-22 have similar values. Clearly, the passive current density continues to decrease above $[H_2O]_{crit}$.

After scratching, the current transients of all alloys can be separated in two groups: when $[H_2O] < [H_2O]_{crit}$, current decays slowly, taking a few hundreds of seconds to reach the initial values; when $[H_2O] > [H_2O]_{crit}$, scratches are repassivated rapidly. Additionally, the shape of the current transients after scratching is different depending on water concentration. For water concentration below $[H_2O]_{crit}$ (Figure 6.2a), the current starts decaying faster for the first circa 10 s (stage 1), then reaches a plateau and decays slowly (stage 2). For water concentration above $[H_2O]_{crit}$ (Figure 6.2b), the current decay is faster and appears to obey a power law.

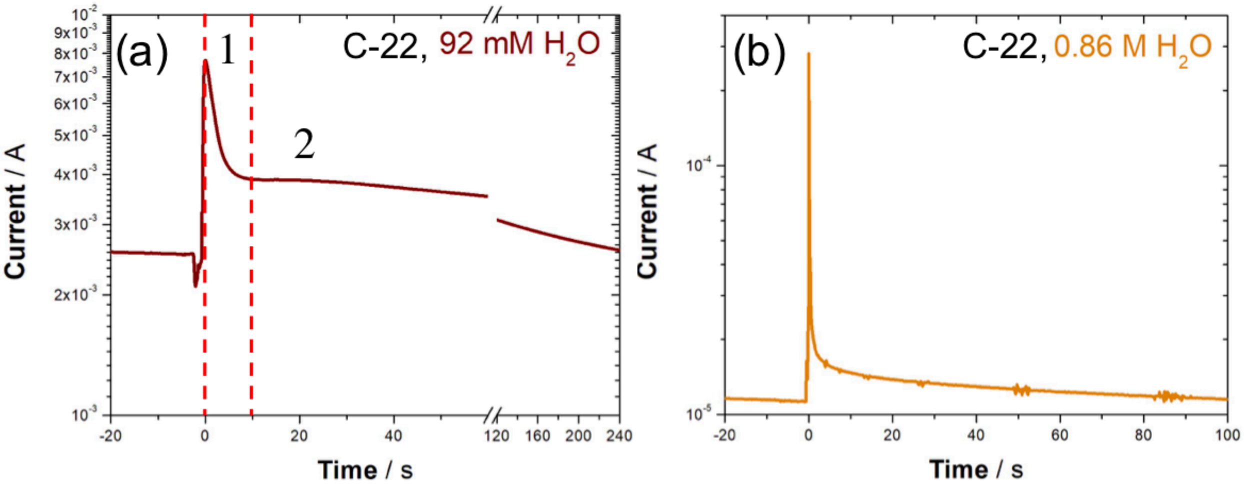

Figure 6.2: Scratch current transients with C-22 in ACN / 0.1 M HCl solutions of two different water concentrations, showing different shapes of current decay.

Different metrics have been used in the literature to characterize passive film growth. A simple and effective approach is measuring the time it takes for the current to decay to a percentage of the peak value, after baseline subtraction[76]. Thus, the time for the scratch current to decay to 10% of the difference between its peak value (I_{peak}) and the current baseline before scratching (I_{base}), is the time when the current measured is:

$$I_{10} = 0.1\left(I_{peak} - I_{base}\right) \tag{1}$$

The time to achieve I_{10} (t_{10}) for different water concentrations are shown in Figure 6.3. The highest t_{10} is found at 0.43 M H_2O for all alloys. However, when water concentration surpasses $[H_2O]_{crit}$, t_{10} drops by almost 3 orders of magnitude. For water concentrations above $[H_2O]_{crit}$, t_{10} does not seem much affected by water concentration. BC-1 presents the highest t_{10} values, taking the longest time to repassivate. For $[H_2O] > 3$ M, C-22 presents the lowest t_{10}, and G-35 and BC-1 have show similar values. It should be pointed that measurements of repassivation time may overlook changes of small time scale. Additionally, in situations such as that shown in Figure 6.2a where the decay is not uniform, the use of t_{10} offers no distinction between the two stages of decay.

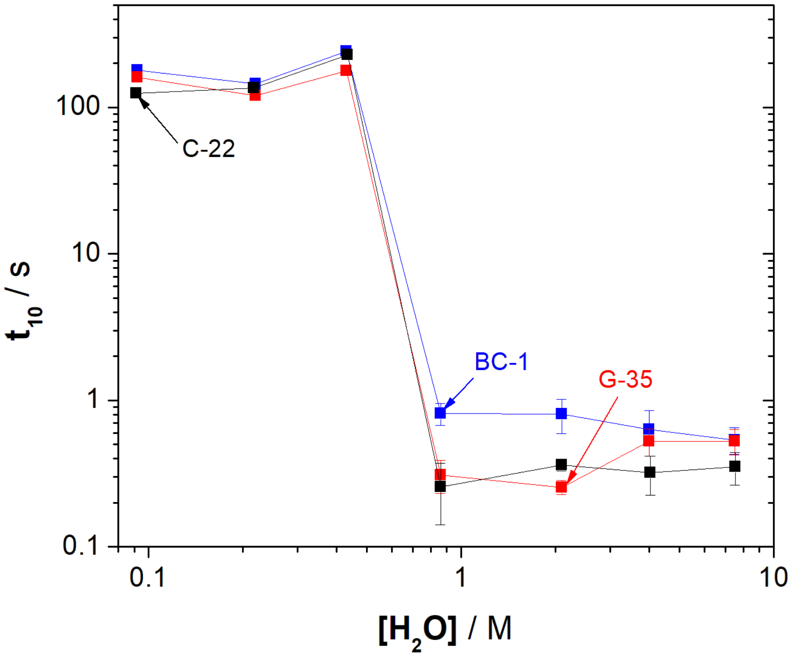

Figure 6.3: Time required for current to decay to 10% of peak value after scratching (t_{10}) in ACN/ 0.1 M HCl with various water concentrations.

The model developed by Kirchheim[77] has successfully characterized the potentiostatic growth of passive films on bared electrodes [78–80]. Kirchheim has shown that, under potentiostatic control, the thickening of the passive film on the bared metal surface is associated with a decrease in current density (*i*) with time, following a power law:

$$i(t) \propto t^{m} \tag{2}$$

where m is a negative constant which reflects the repassivation rate. The current decay in a *log(i) vs log(t)* plot can be fitted with a straight line, and the parameter m can be correlated with the efficiency of the passivation process. The *log(i) vs log(t)* plots of current density transients of BC-1, C-22 and G-35 is shown in Figure 6.4. It should be noted that time was analyzed with reference to the moment of peak current ($t = 0$ at I_{peak}), the current was normalized to account for differences in scratch size and current baseline as follows:

$$I_{norm} = \frac{I_{measured} - I_{base}}{I_{peak} - I_{base}} \tag{3}$$

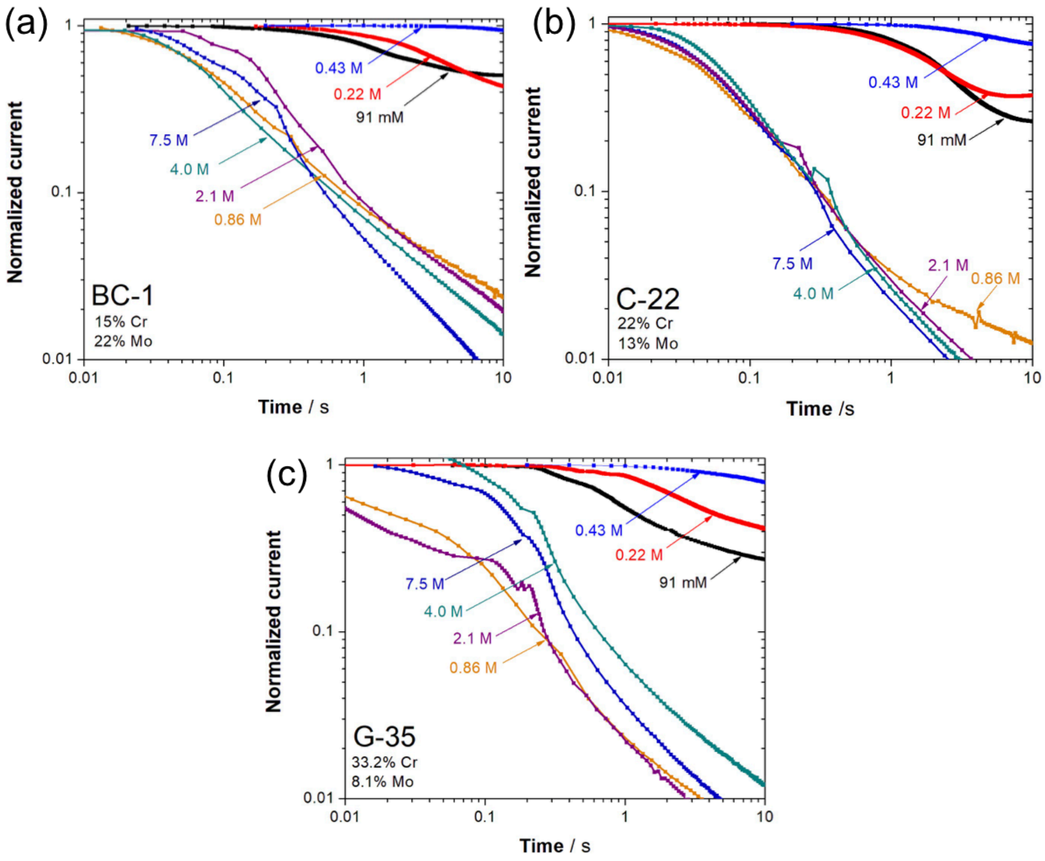

Figure 6.4: *log(I) vs log(t)* plots of current decays after scratching at 0.3 V vs Fc/Fc$^+$. Solutions: ACN / 0.1 M HCl with varying water concentrations (indicated in Figure).

As shown in Figure 6.4, water has an intense influence on the current decay, and the curves can be roughly separated in two different groups: for [H_2O] ≤ 0.43M, the current decay is slow; for [H_2O] ≥ 0.86 M, current decays rapidly. The effect of water on these two ranges also seems different. The increase in [H2O] from 91 mM to 0.43 M slows down the current decay. When [H_2O] ≥ 0.86 M, the effect of water varies depending on the alloy, but it generally accelerates the current decay. To characterize the differences in passivation rate at different water concentrations, the current transients can be fitted with a function of the type $\log I_{norm} = a + m \log t$, where the parameter *m* corresponds to the signature of the power law in equation 2.

The fact that the slope in a *log(I) vs log(t)* plot changes over time suggests that passivation rate changes as the passive layer grows. This behavior is observed most easily with G-35 when $[H_2O] \geq 2.1$ M. Two different time scales were therefore analyzed separately: between 0.1 and 1 s; and between 1 and 10 s. Figure 6.5 shows the slope *m* found in these two regions. Between 0.1 and 1 s (a), the impact of water on *m* is the most abrupt, causing a sudden change in *m* around $[H_2O]_{crit}$. Between 1 and 10 s (b), on the other hand, the effect of water is more gradual. Below $[H_2O]_{crit}$, the modulus of *m* is small (<0.6), indicating a slow decay in current. In this range, *m* becomes smaller in modulus – and, thus, the decay is slower – if water concentration is increased. When $[H_2O]$ surpasses $[H_2O]_{crit}$ *m* decreases suddenly and, if $[H_2O]$ is further increased, *m* becomes more negative (higher modulus). Thus, above $[H_2O]_{crit}$, the current decay is faster, and it becomes faster if more water is added, approaching values around -1. It should be pointed that values of $m \approx -0.7$ and less have been linked to the formation of a film superimposed with dissolution, such as in the case of Fe in 1N H_2SO_4. For a film that effectively passivates the underlying metal without dissolving, *m* is reported to be close to -1.0 [77–79].

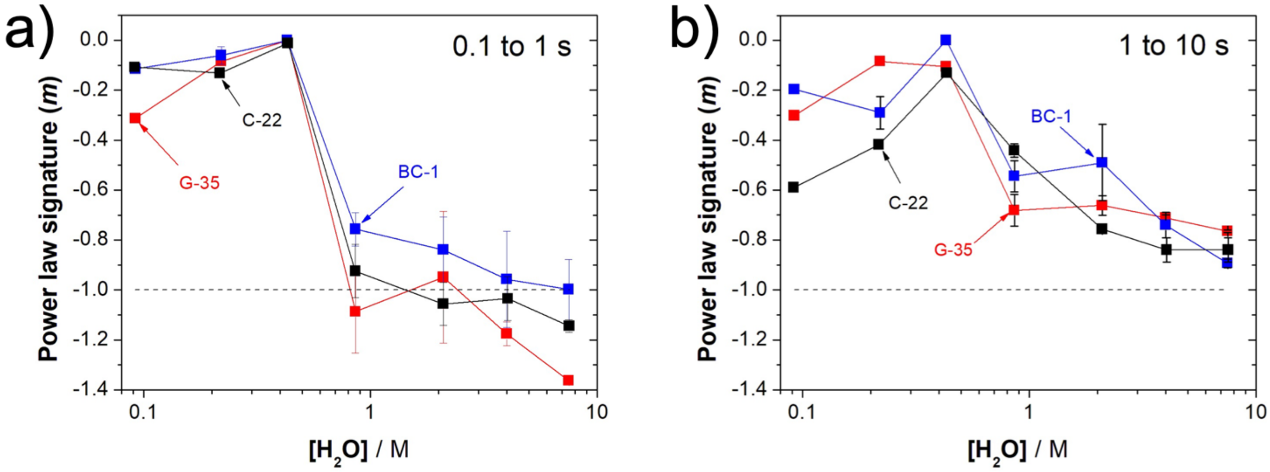

Figure 6.5: Power law signature (*m*) obtained by fitting of current decay curves, analyzed in two different time scales: a) between 0.1 and 1s and b) between 1 and 10 s after scratching. Solution: ACN / 0.1 M HCl

Electrochemically assisted film growth

The chemical composition of films formed on the surface of Ni-Cr-Mo alloys in solution was analyzed by XPS in a few critical conditions. The films were formed by applying a sequence of galvanostatic-potentiostatic polarization steps (Figure 6.6), shortly before inserting sample in the XPS chamber. In the galvanostatic activation step, a constant positive current was applied with the objectives of removing the air-formed oxide layer and removing the top layer of material which is intensely deformed during sample preparation. Henderson et al. [81] have used a negative current to activate the surface of Ni-Cr-Mo alloys, but in this situation a positive current is a more adequate choice for the following reasons: (i) As seen in our previous studies, all three alloys are under activation control in ACN / 0.1M HCl / with low water concentration, so uniform congruent dissolution can be assumed without formation of a passive film in this step; (ii) applying a strong negative potential in ACN-HCl would result in the reduction of undissociated HCl, yielding highly active Cl^- anions on the surface of the electrode. The total charge per area (C_{act}) required in the anodic activation step was determined for C-22 using the following form of Faraday's law:

$$C_{act} = \frac{\rho F d}{EW} \tag{4}$$

where EW is the equivalent weight of C-22 (mass oxidized by one mol of e^- = 26.04 g) [29], and ρ is the density of C-22 (8.69 g), F is the Faraday constant, and d is the desired depth of dissolution. For an arbitrary depth d = 10 nm, the necessary charge calculated was $3.22 \cdot 10^{-2}$ C/cm^{-2}. To avoid the possibility of the formation of films or potential swings under galvanostatic control, all activation steps were carried in 87 mM H_2O, where C-22 has a wide active region, with a current density of 30 μA·cm^{-2}. This required an activation time of circa 18 minutes. Although the difference in chemical compositions between the alloys should result in a slightly different depth of attack, the same activation time was used for C-22, G-35 and BC-1.

After the activation step, alloys were polarized at 0.3V vs Fc/Fc$^+$ for 2 minutes, to allow the formation of a film, either in 87 mM or 1.0 M H_2O. For 1.0 M H_2O, the potential hold was initiated immediately after addition of water. The current density at the end of each polarization was compatible with the values observed in PDP at 0.3 V. As observed by PDP, in ACN-HCl with low water concentration (87 mM), C-22 is active at open circuit. Still, if potential is elevated, the behavior changes from charge transfer control to mass transport control. Although the current density observed is high (circa 3 mA·cm^{-2}), this suggests that a film might form on the surface of the electrode even at low water concentration. A similar behavior was observed for BC-1 and G-35 in the last chapter, with differences in current density. At 1.0 M H_2O, we know that all three alloys undergo an active passive transition, but the nature of the passive film is unknown. Therefore, C-22 was oxidized in 87 mM and 1.0 M H_2O to assess the effect of water. G-35 and BC-1 were oxidized only in solutions containing 1 M H_2O, for the comparison of passive films.

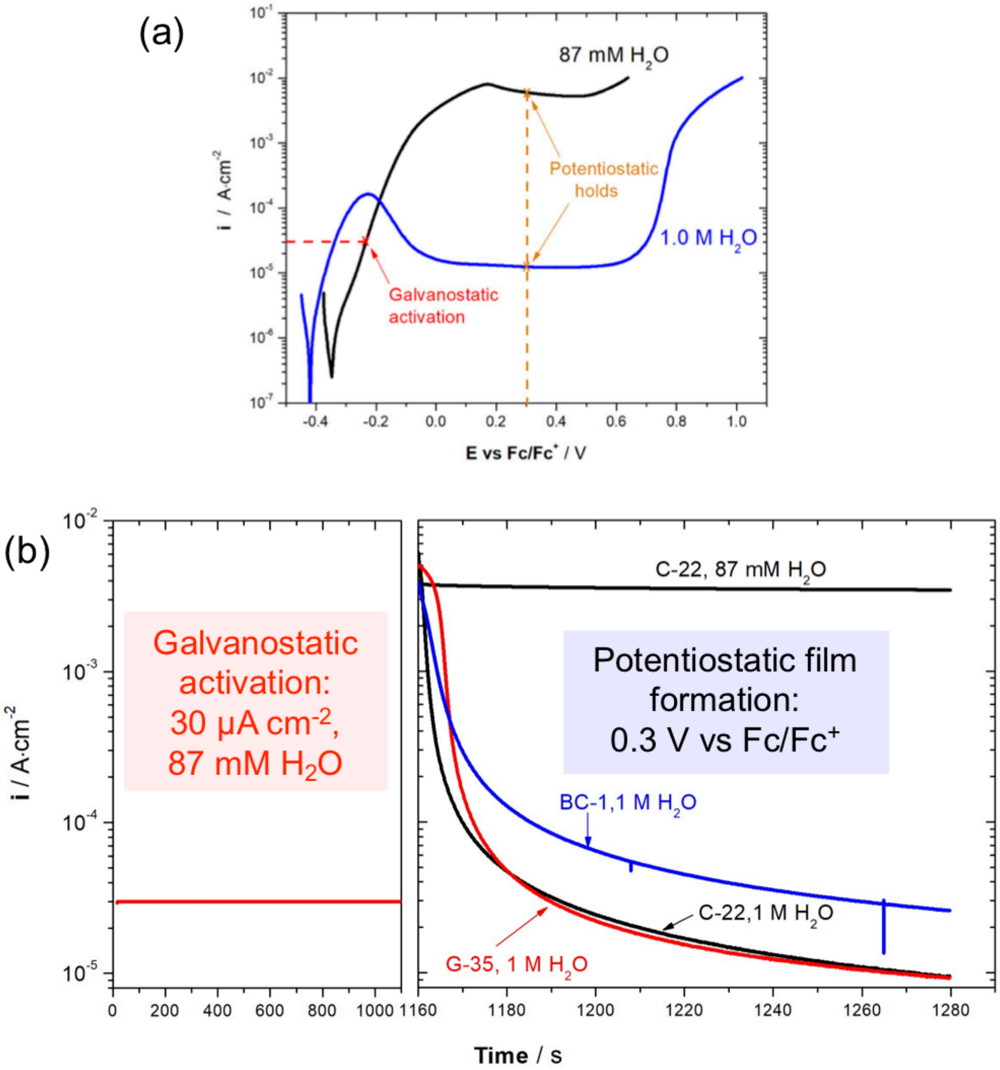

Figure 6.6: Electrochemically assisted film growth process used. (a) PDP of C-22 showing current density and potential used. (b) chronoamperometry showing galvanostatic and potentiostatic steps used.

Surface analysis of C-22 oxidized in different water concentrations

The high resolution XPS scans of C-22 after activation or after anodic polarization (AP) at 0.3 V vs Fc/Fc$^+$ in ACN-HCl with 87 mM or 1.0 M H_2O are shown in Figure 6.7. The elements of interest were Ni, Cr and Mo, since these are the most important oxidized species present in the passive oxide formed on the alloys used in this study. Considering that the XPS has a depth of analysis of 5–10 nm, which is typically thicker than the oxide film, the signal is expected to originate from both oxidized and metallic states. The information on oxide chemical composition was extracted by deconvolution of the chemical states in the high-resolution spectra.

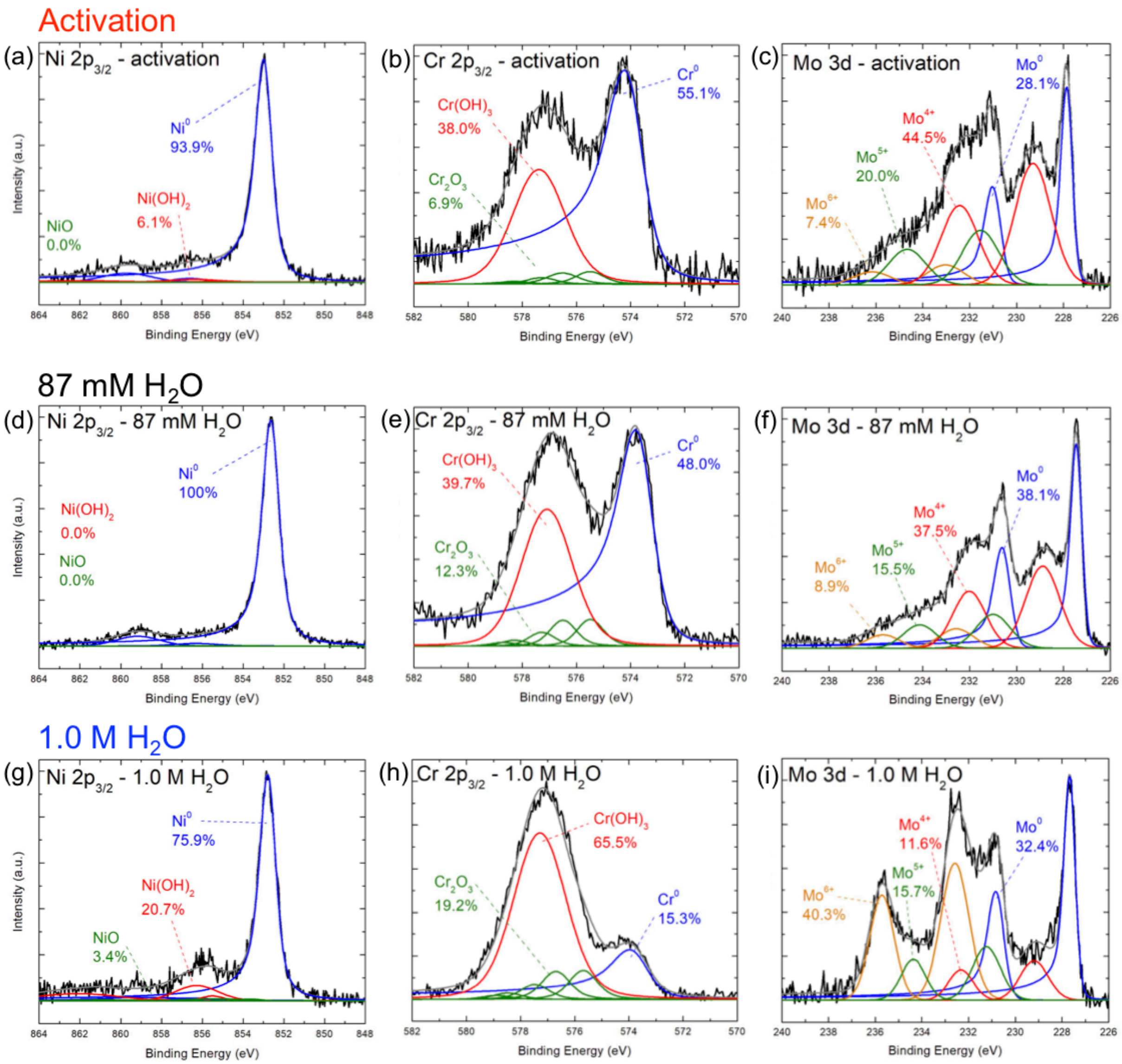

Figure 6.7: XPS high resolution spectra of C-22 after activation (a-c), potentiostatic polarization in 87 mM H_2O (d-f), or potentiostatic polarization in 1.0 M H_2O (g-i). The black line is the original data; the gray line is the fitting obtained.

Analyzing the Ni $2p_{3/2}$ region, both after activation or AP in 87 mM H_2O, the signal is dominated by metallic Ni. After AP in 1.0 M H_2O, however, $Ni(OH)_2$ becomes a substantial contribution (20.7%). In the Cr $2p_{3/2}$ region, the signal for the activated sample comes mostly from metallic Cr, with some contribution from $Cr(OH)_3$ (38%) and little Cr_2O_3 (6.9%). After AP in 87 mM H_2O, the amount of metallic Cr is smaller

(48%), but $Cr(OH)_3$ is in similar concentration (39.7%), while contribution from Cr_2O_3 increases to 12.3%. After AP in 1.0 M H_2O, the relative amounts of $Cr(OH)_3$ and Cr_2O_3 increase substantially (65.5% and 19.2%, respectively), while metallic Cr is seen in smaller proportion (15.3%). The ratio of $Cr_2O_3/Cr(OH)_3$ after AP is similar for the two water concentrations, around 0.3. In the Mo 3d region, after activation most of the signal comes from oxidized Mo and the most prominent oxidized species is Mo^{4+} (37.5%). After AP in 87 mM H_2O, the relative amount of metallic Mo is the highest (38.1%). The biggest difference is seen after AP in 1.0 M H_2O, where the ratio of Mo^{4+}/Mo^{6+} is 0.3 whereas after AP in 87 mM H_2O and after activation the ratios are 4.2 and 6.0, respectively. In summary, the oxidation states after AP in 87 mM H_2O have similarities with the activated condition – Ni is mostly metallic – and similarities with AP in 1.0 M H_2O – same $Cr_2O_3/Cr(OH)_3$ ratio. Compared to the activated condition, the Mo^{4+}/Mo^{6+} is circa 30% smaller, but remains far from the values seen for AP in 1.0 M H_2O.

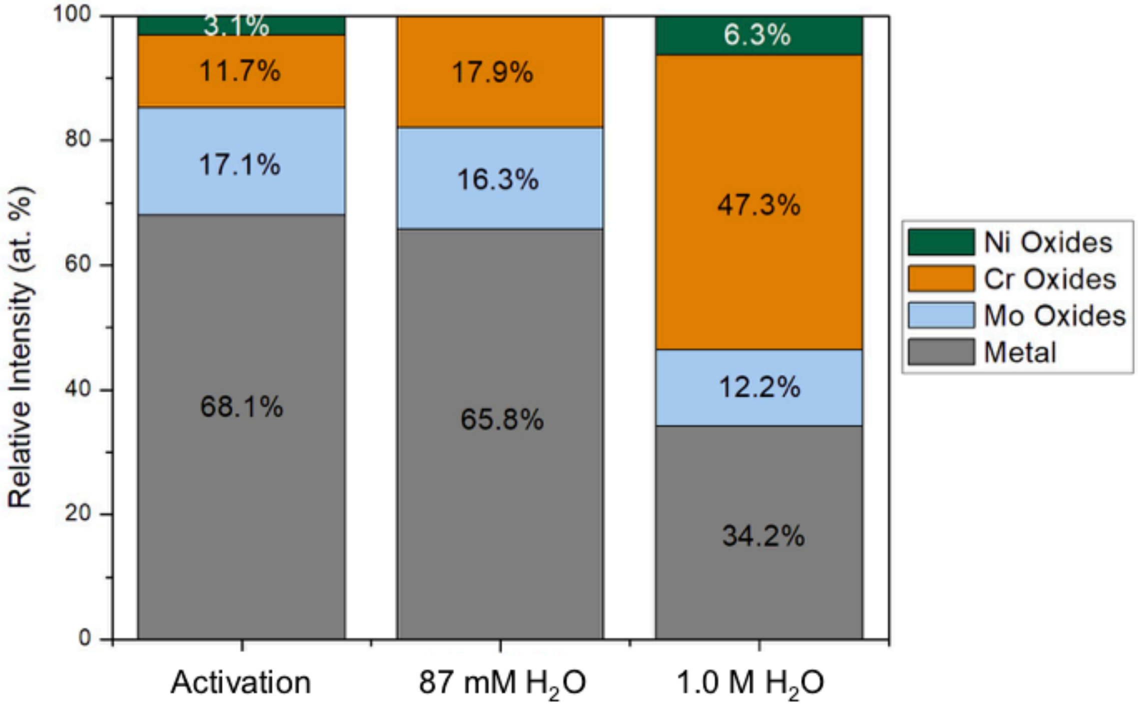

Figure 6.8: Estimation of surface composition by XPS after polarization of C-22 in ACN / 0.1M HCl solutions: galvanostatic activation with 87 mM H_2O ("Activation"), potentiostatic anodic polarization with 87 mM H_2O, and potentiostatic anodic polarization with 1.0 M H_2O.

To provide a semi-quantitative comparison of surface composition between the different conditions, the proportion between Ni, Cr, and Mo oxidized species and metallic species was obtained by accounting the absolute intensities for Ni $2p_{3/2}$, Cr $2p_{3/2}$, and Mo 3d regions from survey spectra, and using ratios obtained in high-resolution spectra. In the results shown in Figure 6.8, the metallic contributions were combined as "Metal", and the oxidized contributions from NiO, $Ni(OH)_2$, Cr_2O_3, $Cr(OH)_3$, Mo^{4+}, Mo^{5+}, and Mo^{6+} were combined as their respective metallic oxides. The amount of metallic signal is similar after the activation process and after applying a positive potential in low water concentration, but the latter shows higher proportions of Cr oxides (vs Mo oxides). After anodic polarization in 1.0 M H_2O the relative amount of oxidized species is much greater, and the oxide composition is composed primarily of Cr oxides, with a much lower proportion of Mo oxides, and small concentration of Ni oxides. A comparison between these values and the results obtained in aqueous solutions in the literature can be found in the Discussion.

The films formed in water concentrations ≤ 0.43 M are poorly protective – although they limit the current density and provoke a departure of activation control, the current density is still too high. These films therefore cannot be called passive films, and it is possible that they have a different nature than the oxide films formed in the passive condition. Figure 6.9 shows the high-resolution spectra obtained in the Cl 2p region for the three conditions. Both samples which were anodically polarized (AP) present more Cl than the activated sample. However, because the difference between the two AP samples is small, it cannot be said that these films are fundamentally different. Both films should have similar small concentrations of metal chlorides, which is reasonable for films grown under anodic polarization in chloride-containing solutions.

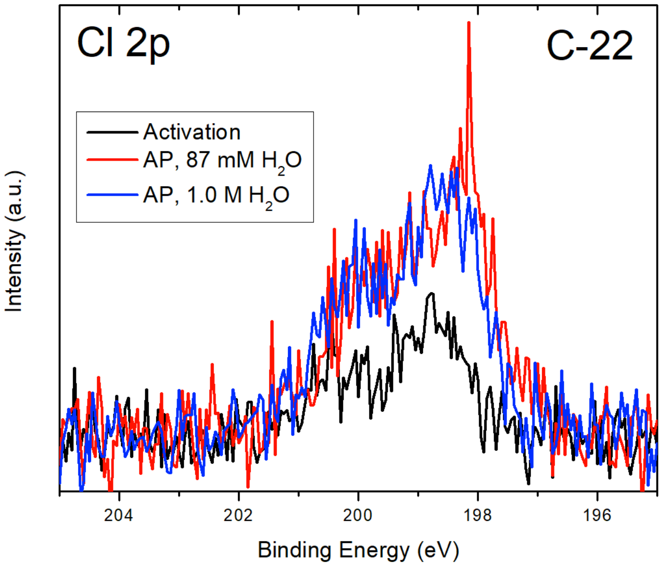

Figure 6.9: High-resolution spectra of Cl 2p region for C-22 in ACN-HCl solutions, after activation (black line), anodic polarization with 87 mM H_2O (red line) or anodic polarization with 1.0 M H_2O (blue line). Intensity is not normalized.

Surface analysis of passive films formed on different alloys

The high-resolution XPS analysis obtained on G-35 (33.2% Cr, 8.1% Mo) and on BC-1 (15% Cr, 22% Mo) after passivation in ACN / 0.1 M HCl / 1.0 M H_2O are shown in Figure 6.10. The results show similar trends as those obtained on C-22 (22% Cr, 13% Mo), with quantitative differences. In Ni $2p_{3/2}$ region, the predominant oxidized Ni species is $Ni(OH)_2$, and this region does not show any changes that correlate with Cr or Mo contents. Analyzing the Cr $2p_{3/2}$ region, the percentage of metallic Cr signal does not change significantly between the three alloys. The ratio of $Cr_2O_3/Cr(OH)_3$ however increases markedly with bulk Cr concentration: 0.22 for BC-1 < 0.29 for C-22 < 0.66 for G-35. The oxidized species in the Mo 3d energy range also change according to alloy bulk Cr concentration. A higher Cr (or lower Mo) in the alloy apparently increases the ratio of Mo^{4+}/Mo^{6+}: 0.26 for BC-1, 0.29 for C-22, and 0.43 for G-35.

Figure 6.11 shows estimations of oxide chemical composition using the signal from Ni $2p_{3/2}$, Cr $2p_{3/2}$, and Mo 3d energy regions and the proportions between the intensity in each of these regions. With the assumption that the intensity of signal from the oxide is proportional to its thickness, it can be inferred that the oxide layer on C-22 and G-35 is slightly thicker than on BC-1. Clearly, as bulk Cr increases and bulk Mo decreases, the percentage of Cr oxides in the passive layer increases, while the percentage of Mo oxides decreases. As shown in Figure 6.11b, the change in oxidized Cr is mostly attributed to variations in Cr_2O_3, as all passive layers have similarly high amounts of $Cr(OH)_3$, between 44.5 and 55.6%. Adding the concentrations of $Ni(OH)_2$ and $Cr(OH)_3$, above 50% of the passive layer signal comes from hydroxides for all three alloys.

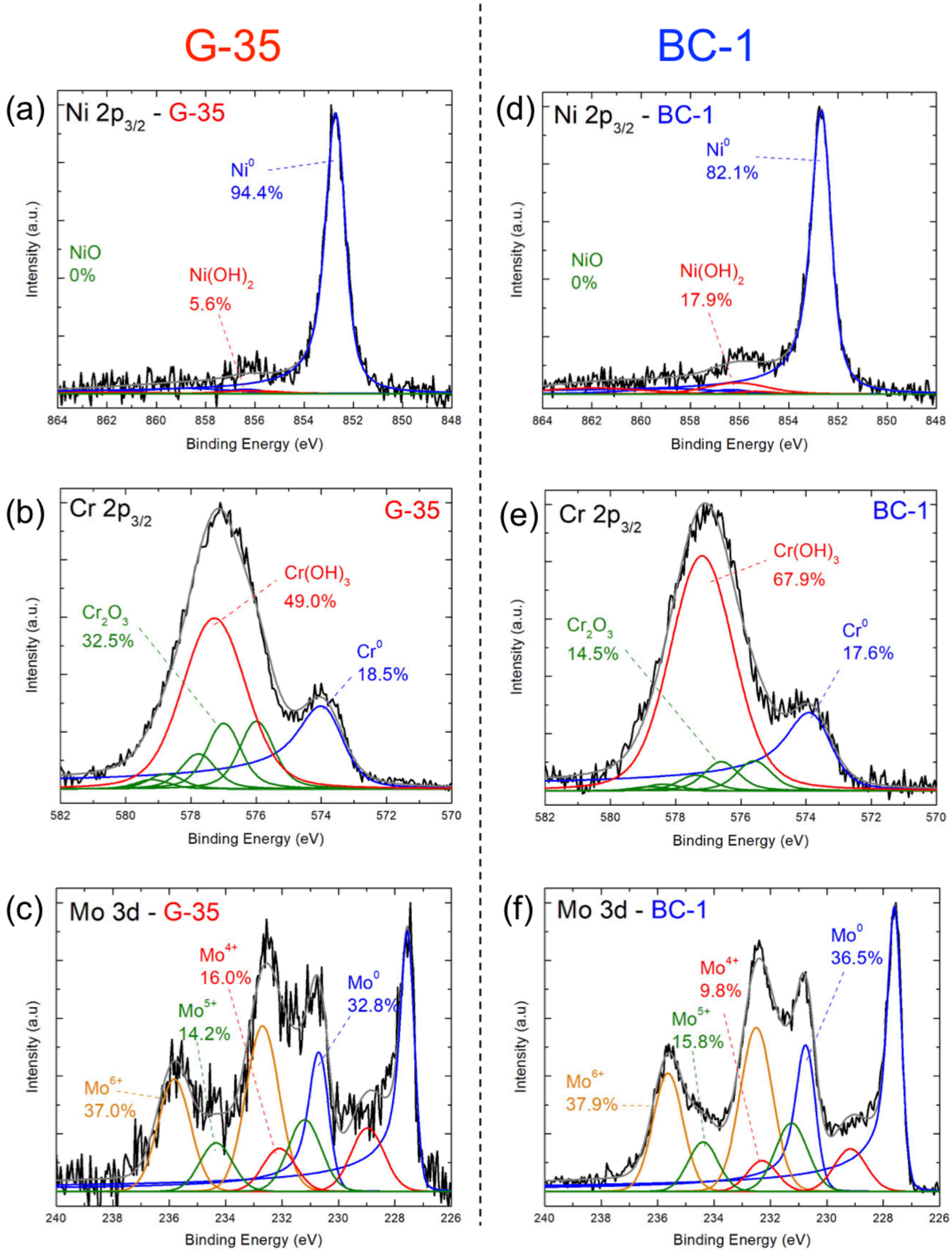

Figure 6.10: XPS high resolution spectra of BC-1 (a-c) and G-35 (d-f) after anodic polarization in ACN/ 0.1 M HCl / 1.0 M H_2O. The black line is the original data; the gray line is the fitting obtained.

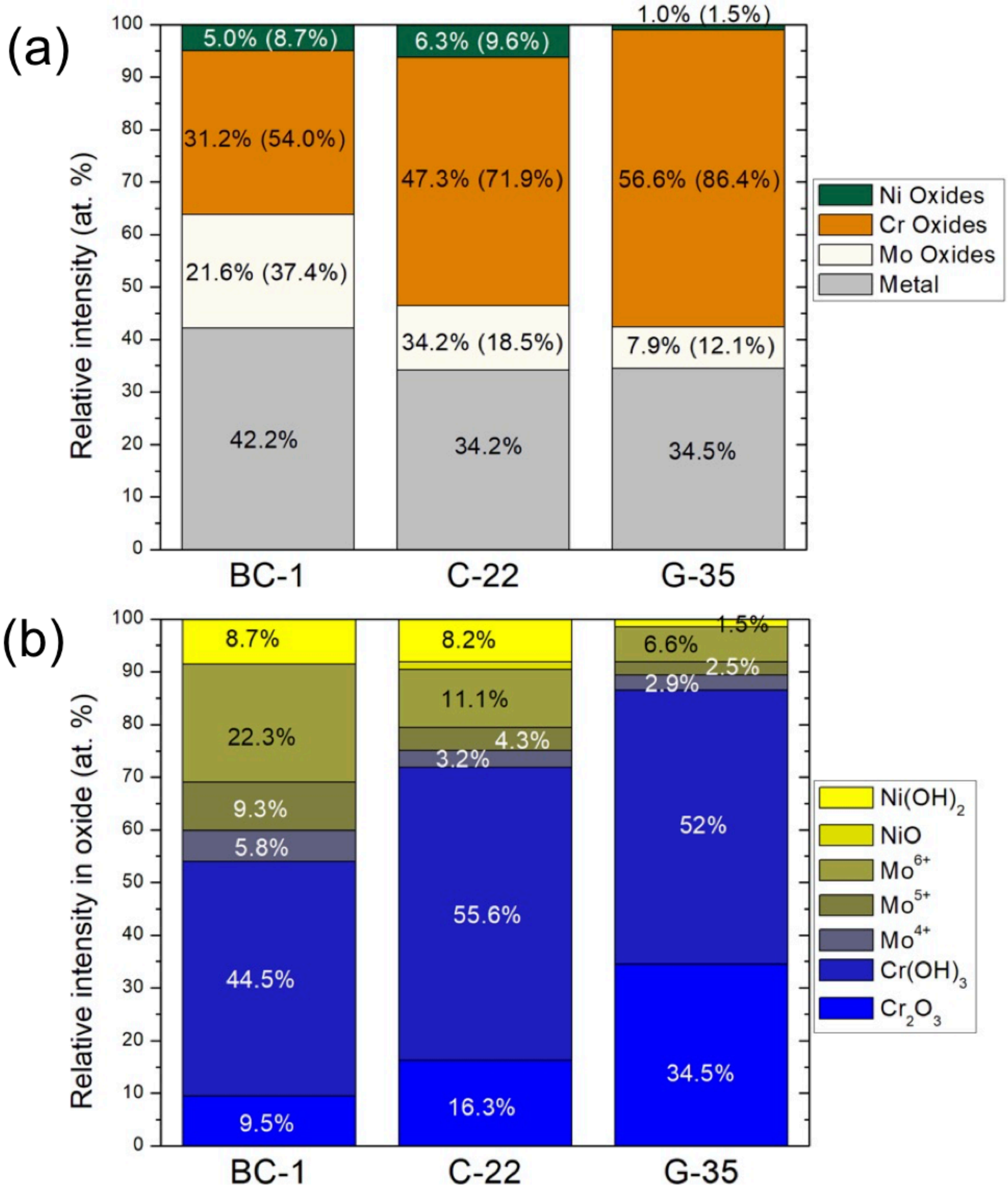

Figure 6.11: Estimation of passive film chemical composition considering the relative ratios from Ni 2p$_{3/2}$, Cr 2p$_{3/2}$, and Mo 3d: (a) Metallic species and oxidized by element. The composition in parenthesis indicates the percentage relative to the oxide signal; (b) Oxidized species only.

Discussion

Effect of water on passivation rate is complex and depends on concentration

As for PDP results in previous chapters, the effect of water on the passivity of Ni-Cr-Mo alloys is often abrupt. The results obtained in this study from potentiostatic holds at the passive region show that transition into passivity is characterized by a critical value ($0.43M < [H_2O]_{crit} < 0.86$ M). When the critical water concentration is surpassed, both the total current density and the passivation rate in scratch tests change drastically for all alloys studied. Although only one HCl concentration was studied, it can be expected that $[H_2O]_{crit}$ will change as a function of the corrosivity of the solution.

Curiously, some results suggest that the net effect of water concentration below and above $[H_2O]_{crit}$ differs. Below $[H_2O]_{crit}$, addition of water appears to lower the passivation rate (m becomes closer to 0; t_{10} increases). This result agrees with the observation that additions of water below circa 1.0 M have a deleterious effect on the corrosion of C-22 at the corrosion potential (Chapter 3). As mentioned previously, the explanation might be linked to water's superior acceptor and donor properties in comparison with ACN. At small concentrations, the effect of water on solvation and facilitation of dissolution of corrosion products (such as metallic cations and protons) might be more significant than its contribution with reagents for oxide formation. Nevertheless, the current density measured after 10 min always decreases with $[H_2O]$. Possibly, the effect of water after long polarizations is different than that on a freshly exposed metallic surface – as shown by XPS, Cr oxides accumulate on the surface of C-22 even at low water concentration during a 2 min polarization at 0.3 V vs Fc/Fc^+. The rate of this accumulation could be a function of $[H_2O]$, and the effects might be noticeable only after longer polarizations.

Above $[H_2O]_{crit}$, passivity is achieved by formation of an oxide film – as confirmed by surface analysis – and repassivation data is compatible with formation of a protective passive layer ($m < -0.8$ or $m < -0.6$, depending on the time scale of the analysis). At these higher water concentrations, further addition of water continues to improve passivity, as observed by a reduction of current density and more negative m. Thus, the Ni-Cr-Mo passive oxides formed with limited availability of H_2O are generally worse than in fully aqueous solutions.

Films formed in low water concentration do not provide a passive condition

Although C-22 is not passive at 0.3V Fc/Fc^+ below $[H_2O]_{crit}$, some results in this study indicate the formation of a surface film: i) C-22 dissolution is not under charge transfer control at that potential, so there is a limitation to the kinetics of oxidation; ii) when the surface is bared by a scratch, current rises rapidly and then decays again; iii) larger amounts of Cr oxidized species (with an increase in %Cr_2O_3) and smaller amounts Mo oxides are found on the surface in comparison with activated samples, which has been associated with the formation of an oxide film on C-22 under AP in aqueous HCl [81]. Because the current density in potentiostatic polarizations with $[H_2O] < [H_2O]_{crit}$ is inversely correlated with bulk Cr concentration (BC-1 has the highest *i(t)*), it can be inferred that the accumulation of Cr oxides is a determining factor in the limitation anodic kinetics, even at low water concentration and high dissolution rates.

Nevertheless, the XPS results after activation and after AP in low water concentration show similar amounts of oxidized signal. Thus, if a solid film forms, it might be very thin and/or partially soluble in solution. It should be pointed that because the decay in current transients shows two different stages, the nature of this phenomenon may also change over time. The first stage obeys a power law with $m > -0.6$, which has been associated with growth of a film with superposed dissolution [77]. The second stage, where i decays almost linearly with time, could be associated with long-time accumulation of species in the film or accumulation of corrosion products in the liquid phase (local change in solution chemistry). Future work using supporting techniques such as EIS will be necessary for a better characterization of film properties in solution.

Composition of passive films formed in ACN-HCl differs from results in aqueous HCl

The composition of the oxide films found in this study show similarities with recent results reported by authors who worked with anodically polarized Ni-Cr-Mo alloys in aqueous H_2SO_4 and aqueous HCl [81,82]. Despite the different activation methods used, the results obtained after the activation step in this work are similar to those obtained by Henderson et al[81] in 1 M HCl: the oxide is enriched with Mo oxides, of which the most prevalent species is Mo^{4+}, associated with the formation of insoluble MoO_2 at low potentials[82]; oxidized Cr is found in higher concentration as $Cr(OH)_3$ than as Cr_2O_3. In this study, the ratio $Cr_2O_3/Cr(OH)_3$ in the activated state is 0.18, whereas Henderson et al. found a 0.4 proportion in aqueous 1M HCl.

The passive films formed by AP with 1.0 M H_2O (2.3 wt%) also have similarities with results in aqueous solutions, such as the enrichment with Cr species and the depletion of Mo species (in comparison with samples activated), as well as the preference for the Mo^{6+} valence (as opposed to Mo^{4+} after activation). In the literature, these changes have been attributed to the oxidation of Mo and MoO_2 to MoO_4^{2-} and other solid molybdate species of higher solubility, as well as the dissolution of Ni species, leaving a Cr-rich oxide. Nevertheless, the passive oxide layer (1.0 M H_2O) obtained in this study shows a much higher concentration of hydroxides: the NiO/Ni(OH)$_2$ ratio is about 0.16 for C-22 (other alloys had no detectable NiO) vs 3.1, 38.5 and 4.9 for BC-1, C-22 and G-35, respectively, found by Henderson et al. in aqueous solutions [81]. The ratios of Cr$_2$O$_3$/Cr(OH)$_3$ found in the present study on BC-1 (0.21), C-22 (0.29) and G-35 (0.66) are also much lower than their results – 0.72, 1.15 and 0.98, respectively. Although the proportion of Ni oxides to Cr oxides found in this study is similar to results in aqueous solutions, the higher valences of Mo are in higher concentrations: Mo^{4+}/Mo^{6+} = 0.26 for BC-1, 0.29 for C-22 and 0.43 for G-35; in aqueous solution Mo^{4+}/Mo^{6+} = 0.66, 0.70 and 0.80, respectively.

It could be argued that these characteristics are partially due to differences in experimental parameters, such as temperature, acidity or applied potential. In this study the applied potential was 0.3V vs Fc/Fc$^+$, which according to reference[30] equals 0.680 V vs SCE ≈ 0.724 V vs Ag/AgCl, whereas in the study by Henderson et al. the applied potential was 0.6 V vs Ag/AgCl. However, both potentials offer a polarization 0.7 V vs OCP and both are circa 300 mV below the transpassive region in the solution of interest, suggesting that they are comparable.

The differences observed might be a consequence of solvent properties. The higher oxidation states of Mo which are partially soluble in water might be less soluble in ACN due to its lower donor strength. Thus, as the oxide layer grows, Mo^{4+} gets further oxidized to Mo^{5+} and Mo^{6+} without necessarily leaving the oxide, resulting in a higher proportion of Mo^{6+}. The higher concentrations of Cr(OH)$_3$ could also be a consequence of solvent properties. The conversion of Cr(OH)$_3$ to Cr$_2$O$_3$ requires the release of protons as a byproduct. However, ACN has protophobic properties (due to its low donor strength), and this process might rely on the solvation offered by other molecules with better donor properties such as H$_2$O, which exists in low concentration in the solutions used. Thus, formation of Cr$_2$O$_3$ and other oxides could be less favorable in ACN. A higher Cr$_2$O$_3$/Cr(OH)$_3$ ratio usually correlates with superior corrosion resistance of the passive film, due to the excellent barrier properties of Cr$_2$O$_3$ [83]. Thus, passive oxides formed in minimal water conditions might be less corrosion resistant. It can be inferred, therefore, that passive oxide films formed in water concentrations higher than 1.0 M will have higher concentrations of Cr$_2$O$_3$. This would be in agreement with the decrease in passive current density associated with higher concentrations of residual water (above [H$_2$O]$_{crit}$), seen in potentiostatic tests.

Effect of alloy composition on passivity

The effects of alloy composition on passive film properties found in this study are in qualitative agreement with results found in the aqueous literature. In potentiostatic holds at 0.3 V vs Fc/Fc$^+$, BC-1 has presented the highest current densities and the slowest kinetics of passivation. This is an indication that, at the potential used, higher concentrations of Cr are desirable as opposed to higher concentrations of Mo. The superior performance of Cr-rich Ni alloys in oxidizing environments has been extensively reported in the literature, and it is mostly attributed to the barrier properties of chromium oxide [2,37]. Despite the higher Cr concentration in G-35 (and higher Cr_2O_3 concentration in its passive oxide), the differences between performance of C-22 and G-35 are not very clear. The current density in long anodic polarizations and the metrics of repassivation rate do not change much between the two alloys, but these results could change for a higher potential.

Conclusions

The passivity of Ni-Cr-Mo alloys BC-1, C-22 and G-35 in ACN / 0.1M HCl and the effect of water were studied by a combination of potentiodynamic and potentiostatic techniques associated with scratching of the electrode surface, and surface analysis by XPS. The main findings can be summarized as follows:

- Water has a marked influence on the passivity of Ni-Cr-Mo alloys, but the effect of water on passivation rate is complex and depends on concentration. The dependence of passive current density and repassivation rate on water is characterized by a critical water concentration ($[H_2O]_{crit}$) between 0.43 and 0.86 M. Below $[H_2O]_{crit}$, Ni-Cr-Mo alloys have a high dissolution rate, and addition of small concentrations of water appears to have a deleterious effect on repassivation kinetics, slowing the current decay after scratching. Above $[H_2O]_{crit}$, a passive oxide layer is formed, the passive current density is low and repassivation kinetics is compatible with the formation of a passive oxide without superposition of dissolution. Further increase in water concentration above $[H_2O]_{crit}$ improves the passive properties.
- Under potentiostatic anodic polarization with water concentration below $[H_2O]_{crit}$, the surface film is not capable of passivating the metal, although some accumulation of Cr_2O_3 is found in subsequent surface analysis, in comparison with the activated condition.
- Under potentiostatic anodic polarization with 1.0 M H_2O (above $[H_2O]_{crit}$), the passive film has similarities in chemical composition with oxides formed in similar conditions in aqueous solutions, such as accumulation of oxidized Cr oxides and depletion of Mo oxides. However, passive films formed in ACN have a higher concentration of higher valence Mo species (Mo^{5+} and Mo^{6+}). The ratio of $Cr_2O_3/Cr(OH)_3$ is significantly lower in passive films formed in ACN-based solutions, which might be the cause of the worse corrosion properties observed.

- At 0.3V vs Fc/Fc$^+$, the dissolution rates of C-22 and G-35 are lower than that of BC-1, for all water concentrations tested. Additionally, the repassivation rate of BC-1 is the slowest between the three alloys. These results indicate that a high Cr bulk concentration ($\geq$ 22 wt%) is desired to ensure higher concentrations of Cr oxides in the passive film.

Concluding remarks

The corrosion of metals in organic solvents is not a new topic, but it is new to most corrosion scientists. Naturally, a much larger portion of the scope of knowledge in corrosion science is focused on aqueous systems, which are more frequently found in this planet. The application of metallic materials in non-aqueous systems remains a challenge because the impact of organic solvents and their solutes on the corrosion behavior is still vastly unknown, despite the contributions from great corrosion scientists since the early 1970s. The process of materials selection for application in organic solvents is still largely based on data from aqueous applications. The scientific studies in each organic solvent are often not translatable to other systems, mostly because of the lack of understanding of the connection between solvent properties and corrosion reactions.

In order to bridge this knowledge gap, the objective of this dissertation was to solve an industrial problem while understanding the underlying mechanisms to the fundamental level, so that these findings can be applied and translated to other systems in the future. The five parts of this study can be summarized as follows:

- The first part of this work investigated the role of each actor in the corrosion of C-22 in ACN solutions. It was learned that C-22 is active in ACN containing HCl and low water concentrations, and that high-potential quinones such as DDQ can act as strong oxidants towards metals. The lessons learned in this part motivated the lines of work followed in the subsequent parts.
- The second part investigated the influence of solvent properties and residual water on the corrosion of C-22. By using solvents with different chemical properties, it was found that C-22 is only active in aprotic solvents where HCl is an undissociated, weak acid. In solvents where HCl dissociates, pitting corrosion occurs. The complicated effects of residual water and of HCl on the corrosion process were discussed using concepts based on the donor-acceptor approach to coordination chemistry.
- The third part of this work was an extension of the methods used in part 2 to neutral, chloride-containing solutions. The hypothesis that the availability of free Cl^- ions would result in pitting even in neutral solutions was confirmed for all solvents studied. The effect of solvent properties, water concentration, and chloride concentration were studied, and the results were compared with the models for pitting in aqueous solutions. Some of the differences encountered were attributed to the effect of solvent properties on Cl^- and to the role of water in passivation, which is often neglected in models for aqueous environments.

- The fourth part of this work studied the application of other Ni-Cr-Mo alloys in ACN solutions of reducing and oxidizing character. The effects of water on anodic passivity and transpassivity were described. It was observed that high-Cr alloys are not suitable for application in ACN-HCl solutions of low water concentrations (<0.65 M) because they cannot form a passive oxide layer and they have a more intense active behavior than alloys with more Mo.

- The fifth and last part of this work was focused on the chemical and electrochemical properties of passive films formed in ACN solutions. The objective was to test the hypothesis that oxide films formed in organic solvents are less protective than those formed in aqueous environments. The kinetics of repassivation in different water concentration was measured for alloys of various Cr and Mo concentrations. The passive films formed in solutions of limited water concentration were analyzed; their chemical composition is different than those formed in aqueous acidic solutions, as reported in the literature. The connection between the passive properties of the films formed in ACN and their chemical composition was discussed.

This work has successfully answered many of the initial questions of the project and has revealed corrosion mechanisms of importance to materials selection in the chemical and pharmaceutical industries. Maybe more importantly, this work has provided many new research questions which can be pursued, some of which are mentioned as suggestions for future work.

Suggestions for future work

- As shown in the second study in this work, the effect of HCl on the uniform corrosion of Ni-Cr-Mo alloys in organic solvents is still not fully understood. The addition of experiments in other halide and non-halide acids would be useful to the understanding of the mechanism by which uniform corrosion takes place, and the relevance of acidity in the process.
- The results obtained in the third part of this work show some peculiar characteristics of pitting in ACN-chloride solutions. This line of study could benefit from single pit experiments by the lead-in-pencil technique, from which kinetic information can be obtained which could help explain some of the behavior observed in this work. Furthermore, the use of aprotic solvents of various properties would allow the tuning of parameters which cannot be altered in aqueous solutions (*i.e.*, water concentration, activity coefficients), potentially allowing the expansion or improvement of existing models of pitting.
- Many of the mechanisms hypothesized in this work were explained using thermodynamics and kinetics concepts which cannot be proved by electrochemical experiments. For these situations, the author believes that modeling methods in the molecular scale could be useful.

Acknowledgements

I would like to acknowledge:

- Dr. Robert G. Kelly, for the scientific discussions, advice, support, and mentorship.
- Lee Kendall, for his collaboration with XPS measurements and analysis.
- Michael Beekwilder, for his experimental contributions.
- Dr. Ajit Mishra, who provided the alloys used in this project.
- Dr. Gary Koenig, for giving me access to his laboratory's KF titrator.

References

1. R. B. Rebak, in *Stress Corrosion Cracking*,, p. 273–306, Elsevier (2011).

2. R. B. Rebak and P. Crook, in *Transportation, Storage, and Disposal of Radioactive Materials*,, vol. 2004, p. 131–136, ASME (2004).

3. P. Marcus, *Corros. Sci.*, **36**, 2155–2158 (1994).

4. K. Hashimoto, K. Asami, and K. Teramoto, *Corros. Sci.*, **19**, 3–14 (1979).

5. C. R. Clayton and Y. C. Lu, *J. Electrochem. Soc.*, **133**, 2465 (1986).

6. A. C. Lloyd, J. J. Noël, S. McIntyre, and D. W. Shoesmith, *Electrochim. Acta*, **49**, 3015–3027 (2004).

7. K. Lutton Cwalina, C. R. Demarest, A. Y. Gerard, and J. R. Scully, *Curr. Opin. Solid State Mater. Sci.*, **23**, 129–141 (2019).

8. P. Marcus and J. Oudar, *Corrosion Mechanisms in Theory and Practice*, M. Dekker, (1995).

9. K. Izutsu, *Electrochemistry in Nonaqueous Solutions*, Wiley-VCH Verlag GmbH & Co. KGaA, Weinheim, FRG, (2002).

10. R. G. Kelly and P. J. Moran, *Corros. Sci.*, **30**, 495–509 (1990).

11. K. Schwabe and M. Berthold, *J. Appl. Electrochem.*, **9**, 171–181 (1979).

12. D. A. Shifler, in *Corrosion science: a retrospective and current status in honor of Robert P Frankenthal*,, vol. 201, p. 218–230 (2002).

13. T. Kikuchi and K. Aramaki, *Corros. Sci.*, **42**, 817–829 (2000).

14. C. Farina, G. Faita, and B. Bazzoni, *Corros. Sci.*, **20**, 1101–1108 (1980).

15. R. G. Kelly, P. J. Moran, and J. Kruger, *J. Electrochem. Soc.*, **136**, 3262 (1989).

16. K. Aramaki, *J. Electrochem. Soc.*, **140**, 1561 (1993).

17. V. A. Safonov and S. Haruyama, *Russ. J. Electrochem.*, **36**, 1108–1116 (2000).

18. F. Bin Li, D. H. Bremner, and A. E. Burgess, *Corros. Sci.*, **41**, 2317–2335 (1999).

19. L. Ercolano, T. Monetta, and F. Bellucci, *Corros. Sci.*, **35**, 161–167 (1993).

20. T. C. Franklin and C. R. Parsons, *J. Electrochem. Soc.*, **109**, 641 (1962).

21. T. Ramgopal, in *Corrosion 2004*, (2004).

22. E. J. Schindelholz, M. A. Christie, S. P. Allwein, and R. G. Kelly, *Corrosion*, **72**, 1292–1299 (2016).

23. D. A. Shifler, P. J. Moran, and J. Kruger, *J. Electrochem. Soc.*, **139**, 54–60 (1992).

24. H.-D. Becker and A. B. Turner, in *The Quinonoid Compounds: Vol. 2 (1988)*, PATAI'S Chemistry of Functional Groups., p. 1351–1384, John Wiley & Sons, Inc., Chichester, UK (1988).

25. A. Stoyanova and E. Slavcheva, *Mater. Corros.*, **62**, 872–877 (2011).

26. A. I. Onuchukwu and F. K. Oppong-Boachie, *Corros. Sci.*, **26**, 919–926 (1986).

27. S. Kannan and R. G. Kelly, *Corros. Sci.*, **38**, 1051–1069 (1996).

28. ASTM International, *Significance*, **90**, 1–9 (1999).

29. ASTM International, *Astm G 102*, **89**, 1–7 (1999).

30. V. V Pavlishchuk and A. W. Addison, *Inorganica Chim. Acta*, **298**, 97–102 (2000).

31. S. Creager, in *Handbook of Electrochemistry*,, p. 57–72, Elsevier (2007).

32. S. P. Harrington and T. M. Devine, *ECS Trans.*, **19**, 131–148 (2019).

33. M. Stern and A. L. Geary, *J. Electrochem. Soc.*, **104**, 56 (1957).

34. N. Ebrahimi, P. Jakupi, J. J. Noël, and D. W. Shoesmith, *CORROSION*, **71**, 1441–1451 (2015).

35. B. A. Kehler, G. O. Ilevbare, and J. R. Scully, *Corrosion*, **57**, 1042–1064 (2001).

36. A. Mishra, D. Shoesmith, and P. Manning, *Corrosion*, **73** (2017).

37. A. Mishra, *Acta Metall. Sin. (English Lett.*, **30**, 306–318 (2017).

38. V. Gutmann, *Coord. Chem. Rev.*, **18**, 225–255 (1976).

39. B. D. McCarthy, D. J. Martin, E. S. Rountree, A. C. Ullman, and J. L. Dempsey, *Inorg. Chem.*, **53**, 8350–8361 (2014).

40. G. A. N. Felton, R. S. Glass, D. L. Lichtenberger, and D. H. Evans, *Inorg. Chem.*, **45**, 9181–9184 (2006).

41. V. Fourmond, P.-A. Jacques, M. Fontecave, and V. Artero, *Inorg. Chem.*, **49**, 10338–10347 (2010).

42. V. Gutmann, *The Donor-Acceptor Approach to Molecular Interactions*, Springer US, Boston, MA,

(1978).

43. M. T. Huynh, C. W. Anson, A. C. Cavell, S. S. Stahl, and S. Hammes-Schiffer, *J. Am. Chem. Soc.*, **138**, 15903–15910 (2016).

44. T. A. Lorenzola, *J. Electrochem. Soc.*, **130**, 1359 (1983).

45. J. Jacq, *J. Electroanal. Chem. Interfacial Electrochem.*, **29**, 149–180 (1971).

46. B. R. Eggins and J. Q. Chambers, *J. Electrochem. Soc.*, **117**, 186 (1970).

47. N. Gupta and H. Linschitz, *J. Am. Chem. Soc.*, **119**, 6384–6391 (1997).

48. K. Takamura and Y. Hayakawa, *J. Electroanal. Chem. Interfacial Electrochem.*, **31**, 225–232 (1971).

49. J. Wang et al., *J. Electrochem. Soc.*, **163**, H201–H204 (2015).

50. B. G. Cox, *Acids and bases: Solvent effects on acid-base strength*, Oxford: Oxford Univ Pr., (2013).

51. R. G. Kelly and P. J. Moran, *Corros. Sci.*, **30**, 495–509 (1990).

52. P. Atz Dick, M. J. Beekwilder, and R. G. Kelly, *J. Electrochem. Soc.*, **167**, 161503 (2020).

53. G. J. Brug, A. L. G. van den Eeden, M. Sluyters-Rehbach, and J. H. Sluyters, *J. Electroanal. Chem. Interfacial Electrochem.*, **176**, 275–295 (1984).

54. M. E. Orazem et al., *J. Electrochem. Soc.*, **160**, C215–C225 (2013).

55. V. Gutmann, *Electrochim. Acta*, **21**, 661–670 (1976).

56. B. Löchel, H. -H. Strehblow, and M. Sakashita, *J. Electrochem. Soc.*, **131**, 522–529 (1984).

57. B. Löchel and H. H. Strehblow, *Electrochim. Acta* (1983).

58. V. Gutmann, in *Nonaqueous Chemistry*,, p. 59–115, Springer-Verlag, Berlin/Heidelberg.

59. A. Mishra, D. Shoesmith, and P. Manning, *NACE Corros. Conf.*, **10675**, 1–15 (2016).

60. D. A. Shifler, P. J. Moran, and J. Kruger, *Corros. Sci.*, **32**, 475–496 (1991).

61. J. Banaś, *Corros. Sci.*, **22**, 1005–1013 (1982).

62. R. Huang, D. J. Horton, F. Bocher, and J. R. Scully, *Corrosion*, **66**, 35003–35015 (2010).

63. G. S. Frankel, T. Li, and J. R. Scully, *J. Electrochem. Soc.*, **164** (2017).

64. T. Li, J. R. Scully, and G. S. Frankel, *J. Electrochem. Soc.*, **165**, C762–C770 (2018).

65. D. D. Macdonald, *J. Electrochem. Soc.*, **139**, 3434–3449 (1992).

66. J. R. Galvele, *J. Electrochem. Soc.*, **123**, 464–474 (1976).

67. H. S. Klapper, N. S. Zadorozne, and R. B. Rebak, *Acta Metall. Sin. (English Lett.*, **30**, 296–305 (2017).

68. J. R. Scully, *Corrosion*, **56**, 199–217 (2000).

69. P. Jakupi, D. Zagidulin, J. J. Noël, and D. W. Shoesmith, *Electrochim. Acta*, **56**, 6251–6259 (2011).

70. P. Lorbeer and W. J. Lorenz, *Corros. Sci.*, **21**, 79–86 (1981).

71. J. Banaś, *Electrochim. Acta*, **27**, 1141–1144 (1982).

72. J. Banaś, *Corros. Sci.*, **22**, 997–1003 (1982).

73. S. Boudin et al., *Surf. Interface Anal.*, **22**, 462–466 (1994).

74. M. Sakashita and N. Sato, *Corros. Sci.*, **17**, 473–486 (1977).

75. K. L. Cwalina et al., *J. Electrochem. Soc.*, **166**, C3241–C3253 (2019).

76. J. Wloka, T. Hack, and S. Virtanen, in *Passivation of Metals and Semiconductors, and Properties of Thin Oxide Layers*, P. Marcus and V. B. T.-P. of M. and S. Maurice and Properties of Thin Oxide Layers, Editors, p. 537–542, Elsevier, Amsterdam (2006).

77. R. Kirchheim, *Electrochim. Acta*, **32**, 1619–1629 (1987).

78. B. Stellwag, *Corros. Sci.*, **40**, 337–370 (1998).

79. M. Barbosa, *Corrosion*, **43**, 309–318 (1987).

80. S. B. Madden, D. J. Moosbauer, and J. R. Scully, *ECS Trans.*, **50**, 57–78 (2013).

81. J. D. Henderson et al., *J. Electrochem. Soc.*, **168**, 021509 (2021).

82. X. Li et al., *Corros. Sci.*, **176** (2020).

83. X. Zhang, D. Zagidulin, and D. W. Shoesmith, *Electrochim. Acta*, **89**, 814–822 (2013).